11-5-2014

On the Improvement of the Capacity of the Heterogeneous Networks with Link-Level and System-Level Approaches

Mehmet Bahadır Çelebi
University of South Florida, bahadir@mail.usf.edu

On the Improvement of the Capacity of Heterogeneous Networks with

Link-Level and System-Level Approaches

by

Mehmet Bahadır Çelebi

A dissertation submitted in partial fulfillment
of the requirements for the degree of
Doctor of Philosophy
Department of Electrical Engineering
College of Engineering
University of South Florida

Major Professor: Hüseyin Arslan, Ph.D.
Richard D. Gitlin, Sc.D.
Ravi Sankar, Ph.D.
Dmitry B. Goldgof, Ph.D.
Mazen Saghir, Ph.D.

Date of Approval:
November 5, 2014

DEDICATION

To my family

ACKNOWLEDGMENTS

TABLE OF CONTENTS

iii

LIST OF TABLES

LIST OF FIGURES

ABSTRACT

Evolution of wireless services enabled the development of the advanced applications and shifted the paradigms of research in this field from voice to data centric. Such services are spreading like wildfire between users and hence, increasing the demand for large bandwidth. However, the frequency spectrum that is suitable for wireless mobile communications is already assigned to particular services from 400 MHz to several GHz. Also, allocating a large chunk of band continuously from the same part of the spectrum may not be possible due to spectral crowd. Therefore, meeting the demand for high data rate requiring wireless services within the accessible spectrum range becomes a challenging problem.

The spectrum allocation policies are discussed by regulatory authorities and academia, and the idea of spectrum sharing systems are addressed as a solution. For instance, heterogeneous networks (HetNets) increase the number of available resources and improve the spectrum accessing capabilities of the wireless communication systems. To achieve this, HetNet nodes are deployed within the coverage of the macrocell regions. Thus, spectral efficiency is boosted via spatial reuse of the same spectral resources. On the contrary, HetNets preclude to fully exploit the resources because of serious interference problems between macrocell and HetNet nodes. Thus, wireless networks of the future will observe interference from even a larger number of sources.

Due to co-channel HetNet deployment and denser frequency reuse, interference cancellation is expected to have significant importance for future wireless communication systems. The occupied resources can also be reused as a solution by conducting advanced signal processing algorithms at the receiver to increase the spectral efficiency. While doing so, the proposed approaches are expected to be easily integrated with the existing complementary approaches to improve the capacity further. Besides, new deployment strategies that allow spectrum access for non-licensed users to achieve larger bandwidth become important to increase the spectral efficiency of the HetNets.

Within the scope of the dissertation, new solutions are developed for the aforementioned problems of the next-generation wireless communication systems. First, an interference cancellation receiver that exploits the unique characteristics of current waveforms is developed in Chapter 2. Also the unknown model of interference is converted to a known model and new algorithms are proposed to recover the desired signal. Then, another perspective is brought into the subject by transforming the interference problem to an interference advantage in Chapter 3. The idea of co-existence of different types of signals are analyzed to bring another degree of freedom as a solution. The proposed approaches are integrated to the existing complementary approaches, such as interference coordination and power control, to improve the capacity further. Finally, a cooperation mechanism is suggested to facilitate the transmission of signal which has a large bandwidth by integrating the idle bands in Chapter 4. By this way, geo-spatially idle bands within the coverage area are utilized and spectral efficiency is increased.

CHAPTER 1

INTRODUCTION

Evolution of mobile communication devices enabled services such as social networking, online gaming, video calls, on-demand video streaming and web browsing. These services became very popular and caused large growth in mobile device industry. However, such services require larger capacity compared to the voice centric services and hence, increase the importance of the usage of limited spectrum efficiently. The spectrum allocation policies are also discussed by regulatory authorities and academia, and the idea of spectrum sharing systems is proposed to keep in step with this large growth. For instance, heterogeneous network (HetNet) nodes such as smallcells and relays are addressed as a solution to increase the number of available resources and improve the spectrum accessing capabilities of the wireless networks. New bands are also expected to be allocated in a non-contiguous manner based on the regulatory agencies. However, the HetNets and allocation of new bands brought new challenges and became attractive for research in academia.

HetNets are designed to increase the spectral efficiency (bit per second per hertz) per unit area. This is achieved by dense deployment of smaller base stations (BSs) within the coverage region of existing macrocell BSs (mBSs) by reusing the same resources [1]. Such a deployment strategy can cause serious interference problems and wireless networks of the future require intelligent approaches to overcome these problems. Also, future applications for mobile devices are expected to require more spectral resources. However, allocating a large chunk of spectrum continuously is an issue due to spectral crowd. Carrier aggregation schemes, which are integrating bands from different parts of the spectrum, are proposed to meet the demand for high throughput requiring services. In HetNets, carrier aggregation becomes challenging especially when providing such advanced services for the unlicensed users of the spectrum. Therefore, wireless networks of future need to provide new deployment strategies and adapt improved algorithms to the changes made by regulatory agencies.

1

Considering the current state of the HetNets, many improvements can be achieved in terms of

- design of new interference cancellation approaches for better management of the interference problems,

- effective resource allocation to reuse the occupied resources more efficiently,

- development of new spectrum access schemes to obtain larger bandwidth,

- successful cooperation of these approaches to integrate them into the existing wireless communication systems.

In the current state of the wireless communication systems, different technologies are supported. For instance, global system for mobile (GSM), wideband-code division multiple access (W-CDMA) and orthogonal frequency domain multiplexing (OFDM) are the waveforms employed in 2G, 3G and 4G standards. All these technologies are co-existing and utilized by the mobile devices. After the introduction of HetNets, co-channel interference (CCI) can occur among same type of technologies, e.g., between long term evolution (LTE) based base station. On the other hand, co-channel deployment of OFDM based macrocells with W-CDMA based smallcells is given as an example scenario where different technologies need to co-exist [2]. Traditional interference management approaches consider the performance metrics such as complexity, latency, cancellation performance and efficient usage of resources. However, design criterion for effective interference management approaches must be revisited for HetNets and new approaches are required to integrate the characteristics of the co-existing waveforms into interference management process.

Alternatively, when the observed interference is strong, non-orthogonal access schemes are even more useful for spectral efficiency. In this case, the co-existing signals are allowed to interfere and are decoded at the receiver by employing multi-user detection (MUD) approaches. For instance, the signal with large signal-to-interference-plus-noise-ratio (SINR) is decoded, regenerated and subtracted from the composite signal. Then, the signal with low SINR is decoded from the remainder. This approach is a.k.a successive interference cancellation (SIC) where many variations of it are proposed in the literature. According to the Shannon's capacity, non-orthogonal access with code-word based SIC achieves the multi-user capacity region and superior to orthogonal access schemes [3]. In other words, non-orthogonal access schemes are

spectrally more efficient compared to orthogonal access schemes with an additional processing in return. The dimensions of the allocated spectral resources must also be analyzed to improve the effectiveness of non-orthogonal access schemes. Mainly, the dimensions of the allocated resources are time, frequency and power. A subset of time slots and frequency bands at a power level are allocated to achieve the required throughput for communication by considering the limiting factors such as thermal noise, wireless channel, device capabilities and interference. In interference scenarios, the resources that are allocated to the co-existing signals can be modified in a controlled manner which allows to exploit interference scenario opportunistically [4, 5]. Further, interference can also be created intentionally for signals whose resources have enough separation to implement MUD schemes effectively. Therefore, new resource allocation approaches considering the characteristics of the co-existing waveforms are required. Eventually, integrating these approaches to the MUD schemes that are designed for interference scenarios is needed in HetNets.

Design of new interference cancellation and MUD approaches for HetNets are not sufficient to provide required capacity for large bandwidth requiring wireless services. Due to current spectrum regulations and spectral crowd, finding a large chunk of spectrum as a single band may not be possible. Also, the new spectrum that is allocated for mobile communications is not reserved from the adjacent bands of the current bands. Therefore, carrier aggregation approaches become a good candidate to integrate the available bands from different parts of the spectrum. To achieve this, the HetNet BSs are required to have cognitive capabilities especially when the HetNet nodes are not allowed to co-exist with the licensed users. Thus, the HetNet nodes senses the spectrum and defines the available bands from different parts of the spectrum. Then, a few relays or smallcells in the system facilitates the transmission of a large bandwidth signal of the source by collectively utilizing the idle bands. In this framework, it is necessary to efficiently disperse and aggregate the source signal to achieve a larger bandwidth.

1.1 Common Interference Issues in Heterogeneous Networks

Earlier cellular planning of wireless networks allowed the use of different frequency bands for adjacent macrocells in order to minimize interference. However, a frequency reuse ratio of one is desired to meet large capacity requirements even for adjacent cells. Also, the power within the macrocell region becomes unevenly distributed due to the geographical characteristics. Thus, smallcell BSs (sBSs) are deployed by
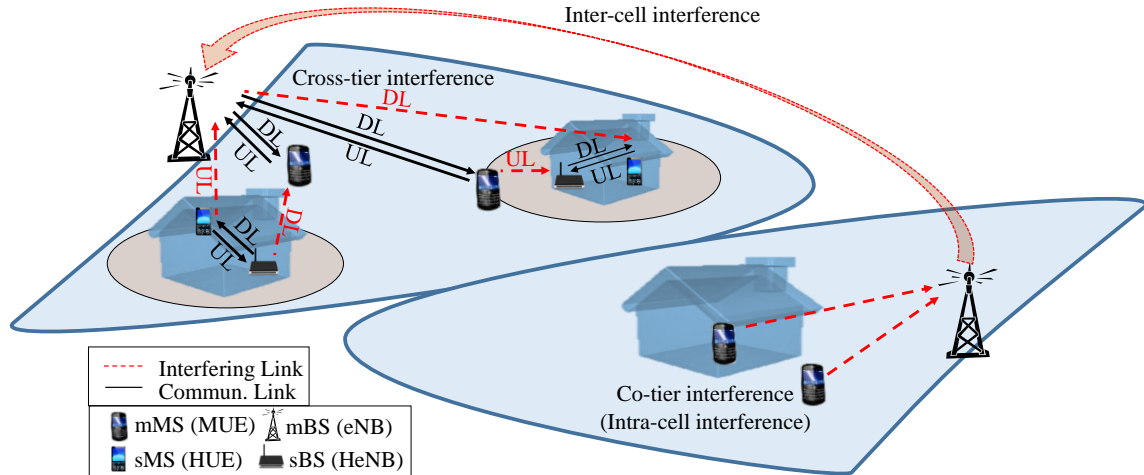
Figure 1.1: Interference scenarios in a cellular network.

reusing the same resources of mBSs with lower transmission powers compared to mBSs to improve the capacity of the wireless network. Such a deployment improves the indoor coverage and cell-edge user performance. On the other hand, this may also cause interference problems between the signals of smallcells and macrocells. Namely, two types of interference scenarios can be defined due to cellular planning which are intra-cell interference and inter-cell interference.

Intra-cell interference is caused by the simultaneous transmissions of nodes within the same cell, i.e. when two MSs of the same macrocell are allocated to the same resources. Inter-cell interference is caused by simultaneous transmissions of BSs or MSs belonging to different cells. In particular, it happens when signals of macrocell MSs (mMSs) and smallcell MSs (sMSs) or mBSs and sBSs within the same mBSs overlap at least partially in a non-orthogonal manner. Since the frequency reuse ratio is one in the current cellular systems, inter-cell interference becomes and important issue.

The interference between the same level of links is called co-tier interference. For instance, interference between two mBS signals is called co-tier interference. The interference between different levels of links, such as interference between a mBS and sBS, is known to be cross-tier interference. In HetNets, two access techniques are defined for the MSs, namely, i) open access and ii) closed access [6]. A mMS can be offloaded to the sBS from the mBS when the received SINR of the signal of mMS at the sBS is larger than the received SINR of the signal of the same mMS at the mBS in open access scheme. In other words, the mMSs are served by mBSs or sBSs based on the observed SINR. In closed access schemes, handover from

mBSs to sBSs is not allowed except for the privileged mMSs only. Obviously, interference problems arise more often when closed access schemes are employed in HetNets. For instance, the observed SINR from the sBS is larger than that of the mBS. This result in inevitable interference scenarios in the uplink (UL) of the smallcell where the sBS is close to the mBS or in the downlink (DL) of macrocell where mMS is at the vicinity of sBS that is placed at the edge of macrocell. As shown in Fig. 1.1, interference scenarios occur especially when a mMS is at the vicinity of a sBS. For instance, sBS and mBSs signals might interfere at a mMS in DL or sMS and mMS signals might interfere at a sBS in UL [7]. Regardless of the access mode of the smallcells, an interface between cross-tiers is required to operate such interference coordination and handover processes. Such an interface can be employed through a backhaul link or over-the-air control signalling [8]. Within the scope of the dissertation, although the inter-cell interference problems are considered mainly, the proposed approaches are also useful for intra-cell interference problems. For the proposed approaches, closed access HetNets are considered to analyze cross-tier interference in Chapter 2 which are compared to the performance of the open access HetNets. In Chapter 3, the proposed techniques employ both closed and open access strategies where the performance of both access schemes are also compared.

Although the main focus of the dissertation is the interference problems due to co-existence of the signals, the interference caused by the wireless channel is worth to explain. Generally speaking, wireless signals are distorted due to multipath and mobility characteristics of the wireless channel. For instance, when an OFDM signal travels through multiple paths, the replicas of the same OFDM signal arrive to the receiver. Some part of the OFDM symbol from the end is cloned and attached to the beginning which is called cyclic prefix (CP). The CP header is removed at the receiver, which simplifies the equalization process. However, when the maximum excess delay of the channel is longer than the duration of the CP header, the replicas of the same OFDM symbol or the previous OFDM symbols cause inter-symbol-interference (ISI). The ISI can be controlled by adaptively changing the CP duration based on the maximum excess delay of the users. Such an approach can be considered as interference management technique which sacrifice the spectral efficiency due to large CP usage and requires scheduling approaches integrated into the processing [9]. Note that, the symbols of OFDM signals are modulated on mutually orthogonal *sinc* functions, namely subcarriers, in frequency domain. Before transmitting the OFDM signal, inverse discrete Fourier transform (IDFT) of the subcarriers map to a set of rectangular windowed sinusoidal functions. Due to mobility,

the sinusoidal shapes of the signals are altered and the orthogonality between the subcarriers in frequency domain is lost. This is a.k.a. inter-carrier interference (ICI). A detailed analysis of ICI and its bounds can be found in [10] and in [11] respectively. Adaptively changing the subcarrier spacing is an interference coordination approach in OFDM systems [12]. Advanced equalization techniques for the same ICI problem can also be found in the literature which can be considered as interference cancellation techniques [13, 14]. Other sources of interference can be given briefly such as the impairments and the non-linearities introduced by the components of the device hardware. For instance, antenna coupling, non-linear response of the power amplifiers, frequency offset in the voltage controlled oscillators and imperfect filtering distort OFDM signals in the form of interference. However, interference due to co-existence is analyzed in this dissertation. Also, different wireless channel models are considered for performance analysis. On the other hand, the interference problems that are caused by impairments are kept out of the scope of the dissertation.

1.2 A Review of Interference Management Approaches

Interference management approaches are proven and well studied in the literature for wireless mobile communication systems [15, 16]. However, approaches dealing with interference in HetNets to increase the capacity in the context of OFDM-based systems are relatively new. Mainly, the approaches that are considered in this dissertation can be divided into two categories, namely, filtering (notch, linear, matched, etc.) and multi-stage (successive, parallel, iterative etc.) approaches.

1.2.1 Filtering Approaches

Filters are designed to suppress a particular band or to meet the spectral mask requirements that are specified by the regulatory agencies. Alternatively, these approaches are also useful for interference cancellation purposes. For instance, considering a narrowband interference scenario for an orthogonal frequency division multiple access (OFDMA) signal, only a fraction of subcarriers are altered due to interference. A notch filter can be designed to suppress those subcarriers. However, the information allocated to those subcarriers cannot be recovered unless complementary techniques such as interleaving and coding are utilized. On the other hand, those subcarriers can be switched-off for transmission to avoid the interference.

6
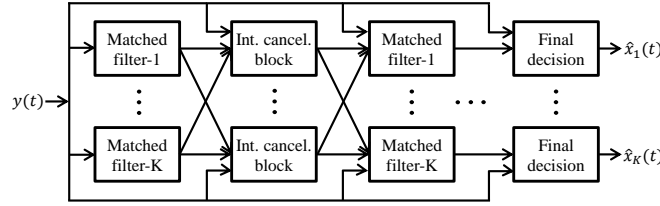
Figure 1.2: Block diagram of parallel interference cancellation scheme.

Note that in the current HetNets, single carrier-frequency division multiple access (SC-FDMA) signals are employed in the UL which is slightly different than the OFDMA signal. An additional IDFT operation is performed to spread the generated symbols in frequency domain. Therefore, filtering can be utilized for interference cancellation purposes when the desired signal is a SC-FDMA signal. Filtering the interference signal out from the SC-FDMA signal distorts the subcarriers. Unlike in OFDMA signal, this does not cause the loss of symbols since the symbols are distributed over all subcarrier. However, the undesired impact caused by the filter is distributed over all symbols. Considering SC-FDMA signals, filtering cause convolution operation in symbol domain and injects error in the form of ISI while suppressing the co-existing interference signal [17, 18]. By this way, the dominant interference is converted to a known ISI model. Same approach can be applied when an OFDMA signal and the interference signal overlap partially in time domain since the symbols of the OFDMA signal is distributed over all samples in time domain. This approach is considered for SC-FDMA signal to cancel narrowband dominant interference in Chapter 2.

Matched filtering is another approach which is employed in CDMA systems. In CDMA systems, orthogonal codes are assigned to the users and the transmitted signals by different users are overlapping simultaneously in time and frequency domains. Then, to decode the signal of a desired user, the signals of the other users are treated as noise after decorrelating the composite signal at the receiver with that user's code. However, this approach is not optimal if the number of interfering signals increase enormously. Also, when the power of the received signals are disparate, employing matched filtering approaches solely is not useful. The performance of the filtering approaches can be improved when other interference cancellation or MUD approaches are introduced into the process. Accordingly, advanced filtering approaches are integrated with iterative interference cancellation techniques in the Chapter 2 of the dissertation.

7
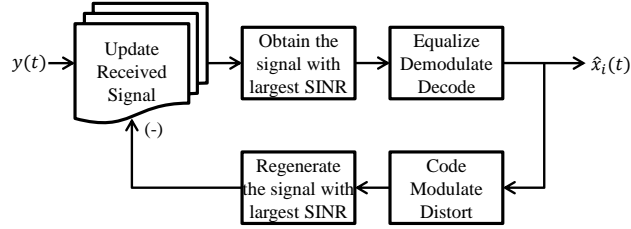
Figure 1.3: Block diagram of successive interference cancellation scheme.

1.2.2 Multi-stage Interference Cancellation for Multi-User Detection

Mainly, interference cancellation approaches divide into two categories for MUD purposes. In parallel interference cancellation (PIC) schemes, demodulation of the composite signal is performed in multiple stages as shown in Fig. 1.2. At each stage, the signals of all users are detected simultaneously. The initial coarse detection at the first stage is used to cancel the interference partially at the next stages. This also causes non-linear behaviour since any error at the output of one stage affects input of the next stage. To reduce the impact of the non-linear behavior, soft interference cancellation approaches can be introduced to the PIC process [19]. Then, better estimates are obtained for all signals at the next stage. The composite signal can also be decoded successfully by repeating this process multiple times [20, 21]. The PIC technique is suitable for the UL interference in the conventional CDMA systems where the received signals have similar power levels at the receiver because of path loss compensation. Thus, the latency of PIC schemes is proportional to the number of stages. On the other hand, symbols of K number of users are coarsely estimated at the end of each of N number of stages. Then, the overall complexity is increased to KN where $K \gg N$ in the current cellular systems [22].

Unlike the PIC approaches, only one user is decoded at every stage of the successive interference cancellation (SIC) technique. Fig. 1.3 shows the block diagram of a conventional SIC receiver where a coding block is adopted into the MUD scheme [23]. After decoding the signal with the largest SINR, that signal is regenerated by modulating the decoded bits and injecting the impact of the channel. Then, the regenerated signal is removed from the received composite signal, which allows to decode the signal with the second largest SINR sequentially. This approach is preferable over PIC when the received power of the co-existing signals are disparate [23–25]. However, SIC the latency increases with the number of co-existing users, K, proportionally.

8
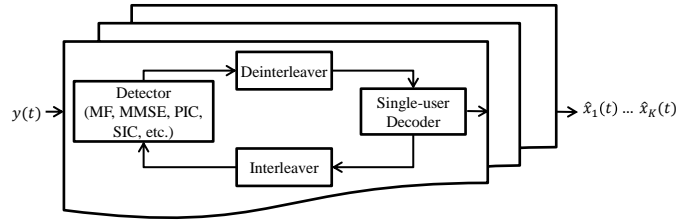
Figure 1.4: Block diagram of iterative interference cancellation scheme.

The SIC technique outperforms the PIC technique when the received power of the co-existing signals are disparate. On the other hand PIC schemes are better as the powers of the received signals are similar. Considering the advantages and the drawbacks of PIC and SIC schemes, multistage SIC schemes are also proposed by processing a subset of the user signals in parallel at each iteration and successively removing their impact from the composite signal [26, 27]. Within the scope of this dissertation, SIC approaches are employed in Chapter 2 and 3 for analysis and present baseline to compare the results of the proposed more advanced approaches.

Alternative to the PIC and SIC approaches, iterative interference cancellation (IIC) approach is introduced after the development of turbo codes [5, 28–31]. Turbo codes allow to decode the signals at low SNR region and becomes attractive for MUD purposes. In CDMA systems, the performance of turbo codes can approach the single-user limit with different system configurations and receiver strategies [28]. Briefly, this is achieved by passing the estimates between two decoders that are connected with the interleaver/deinterleaver blocks as shown in Fig. 1.4. This framework is also suitable to describe the PIC/SIC approaches and well-utilized for IIC techniques [5, 30, 31]. The IIC technique has also non-linear behaviour as PIC and SIC techniques. In general, received composite signal must be decodable at the receiver to fully utilize these techniques and to reduce the non-linear behavior of these algorithms. To achieve this, *a priori* information about the co-existing signals is required and assumptions must be made carefully such as the availability of the ideal carrier frequency and the perfect time/frequency synchronization to the composite signal at the receiver [2]. Although these approaches are well-studied for CDMA systems, advanced receiver algorithms becomes important for OFDM based HetNets which are developed in Chapter 2 and 3. In detail, co-existence scenario specific IIC approaches are developed to improve the capacity of HetNets.

9

1.2.3   Maximum Likelihood Sequence Detection

In the literature, the analysis on broadcast channels in [32] and the development of maximum likelihood sequence detection (MLSD) in [33] lead to the discovery of an optimal multi-user receiver for CDMA in [34]. This maximum likelihood (ML) receiver optimally decodes multiple users in parallel however, it is not practical considering the current capabilities of the mobile devices. The computational needs increase as 2^N for a binary alphabet where N is the number of users. Thus, ML receivers with an acceptable complexity and suboptimal performance are developed for MUD purpose [4, 35]. These receivers can also be utilized for intentionally created interference between signals if the parameters of the co-existing signals are known at the receiver. Eventually the complexity of the ML detector can be reduced by this way. Although MLSD approach is not considered in this dissertation solely, an ML test is integrated to the proposed approaches and introduced in Chapter 2 and Chapter 3.

1.2.4   Complementary Interference Management Approaches

As mentioned in Section 1.2.2, the PIC technique performs best where all the received powers are equal, otherwise the SIC technique performs better. Unequal received power distribution is also preferable for IIC techniques [36]. The performance of these techniques can be improved further by integrating power control approaches into the process. However, power control approaches require information exchange through control channels in CDMA systems to set the optimal power values for the co-existing signals. Although this becomes a problem for the SIC receivers (e.g., [19, 37]), integrating power control approaches is very feasible by introducing a feedback mechanism between interfering nodes [38–41]. Additionally, power control approaches can eliminate the inter-cell interference problems by intentionally allocating disparate powers to users and hence, turn the interference problem into an advantage [42, 43]. In this dissertation, power control approaches are considered in Chapter 3 to improve the performance of the proposed ML based SIC for MUD purposes.

1.2.5   Interference Coordination (Time-Frequency Resource Sharing)

One class of solutions is interference coordination where interfering nodes cooperate to switch-off their transmission at some resources, or sBSs apply range expansion techniques [44, 45]. However,
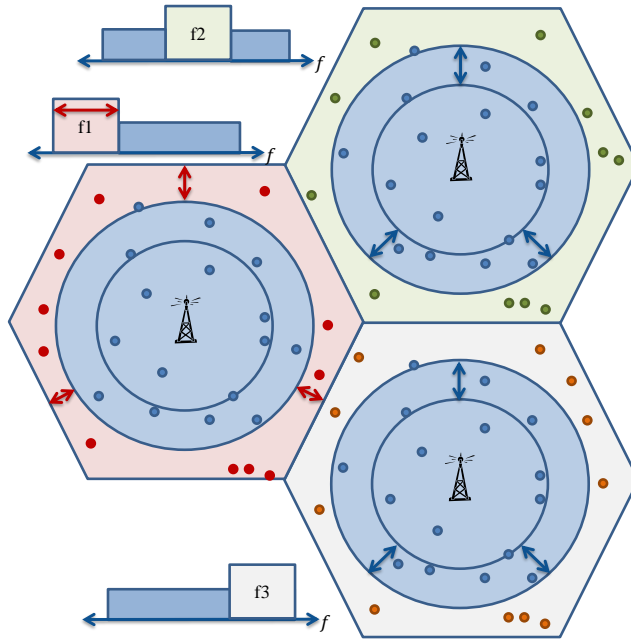
Figure 1.5: Fractional frequency reuse diagram.

such approaches sacrifice throughput and require self-organization by the exchanging information between interfering BSs [46]. Mainly, due to reuse ratio of one in HetNets, interference coordination techniques are proposed to increase capacity. For instance, fractional frequency reuse (FFR), inter-cell interference coordination (ICIC), techniques allocate resources by preventing co-existence between signals [44]. In other words, interference coordination schemes suggest sharing of resources orthogonally to provide access to the nodes [47]. Such schemes are utilized for the cell edge mMSs and also suggested for MSs at the vicinity of HetNet nodes. For instance, various types of FFR technique are also suggested considering the density of the cell edge users. In FFR technique, allocated bands are shared adaptively as shown in Fig. 1.5 [48–50]. However, interference coordination approaches are not useful always when the objective is increasing the capacity. These techniques can be applied when the performance of the interference cancellation or MUD techniques cause worse performance compared to interference coordination. These approaches are integrated to the designed receivers within the rest of of the dissertation. In particular, these approaches are integrated in the proposed MUD approaches Chapter 2 and 3 when the co-existing signals cannot be decoded.

1.3 Challenges

To fully-exploit the interference management approaches the challenges and the implementation issues that are attached with these approaches must be well-understood. First, the common challenges related to interference cancellation, coordination and MUD are explained briefly. Then, the challenges that are tackled within this dissertation are explained in detail.

The complexity of multi-stage interference cancellation approaches increase as number of signals to be distinguished increase. Thus, the additional latency and complexity introduced by these approaches affect the quality of service of some applications. For instance, the delay sensitive applications might fail in case of interference even when the received signal is successfully decoded. Multi-stage interference cancellation approaches have also non-linear behavior where any decoding error at the previous stage of the cancellation process causes error propagation to the next stages [51]. The non-linear behaviour can be reduced by introducing power control approaches into processing. Thus, error propagation can be prevented by providing the sufficient power gap between the co-existing signals. On the other hand, large power gap between signals cause implementation issues during analog-to-digital (A/D) conversion stage. The A/D converters are required to have a very large dynamic range and good resolution at the quantization stage. Otherwise, a very large power gap may cause the low power signal to be lost during A/D conversion stage due to quantization errors. Therefore, it is necessary to overlap the co-existing signals in a controlled manner with an optimal power gap in between. In Chapter 2 and Chapter 3, these issues are pointed out during design process. Also, the proposed power control algorithms force the signals to co-exist with minimal power gap while procuring that the signals can be decoded efficiently.

Estimation of wireless channel parameters is important for MUD approaches to successfully equalize the co-existing signals. However, estimating the channel coefficients is challenging since the reference signals to estimate these coefficients are also overlapping. Generally speaking, the optimal received powers are allocated to the signals where it is assumed that the signal with large SINR is decoded successfully [23, 52]. Unfortunately, this might not be achieved in practice and the residual interference causes error propagation at the later stages of the MUD. This degrades the decoding performance and the overall throughput of the system. The drawback of channel estimation error can be gradually removed by following a similar approach that is employed for interference cancellation schemes [53]. In particular, a multistage channel

estimation scheme can be integrated into the SIC receiver [54]. Although this approach reduces the channel estimation errors, latency and computational complexity increase. On the other hand, power control mechanisms can be modified based on the channel estimation errors [43, 55, 56]. This is achieved by increasing the power of the user signal which has low SINR to decrease the channel estimation errors [43]. Thus, the channel estimation must also be considered while designing power control algorithms [54, 57]. The impact of the wireless channel is analyzed for the proposed approaches in Chapter 2 and Chapter 3.

1.4 Dissertation Outline

1.4.1 Chapter 2 : Interference Suppression by Filtering Approach and Signal Recovery for LTE Uplink

In this chapter, an interference cancellation receiver that utilizes the unique characteristics of SC-FDMA based systems is proposed. The proposed receiver suppresses the co-channel dominant interference by blanking the frequency-domain samples where the desired and interfering signals overlap. In order to improve the performance, demodulation and regeneration stages are introduced and repeated multiple times. Further enhancement is made possible by initially processing a group of reliable symbols at each the iteration. The simulation results indicate that proposed methods work particularly well for low overlap ratios compared to interference coordination and no cancellation schemes.

1.4.2 Chapter 3 : Theoretical Analysis of the Co-existence of LTE-A Signals and Design of an ML-SIC Receiver

In this chapter, the occupied resources are reused as a solution by intentionally overlapping the long term evolution-advanced signals. To achieve this, first, the co-existence of OFDMA and SC-FDMA signals is analyzed. In detail, the signals are aligned in time-domain, and the impact of co-existence in frequency and power domains is analyzed. Then, the average bit-error-rate of each co-existence case is derived based on a conventional SIC (c-SIC) receiver as a baseline. The results of the analysis lead us to design an improved adaptive MUD, which outperforms c-SIC receiver. The proposed MUD, namely maximum likelihood-SIC (ML-SIC), performs iterative likelihood test and a SINR based processing to improve the decoding performance. Additionally, three different power control schemes are proposed for heterogeneous networks

to improve the gain further and observe the performance in the system-level. Our results show that the proposed combination of methods works well in dense mobile communication environments.

1.4.3 Chapter 4 : Idle Band Integration for Cooperative Relaying in a Cognitive Network and Impact of Beam-Forming on the Performance

In a cooperative cognitive network, a methodology is proposed which utilizes multiple relays to facilitate the transmission of a large-bandwidth source signal. This is achieved by integrating the idle bands from different locations and different parts of the spectrum. In this framework, first the probability of finding a particular number of available bands in the system is analyzed based on different beam-forming capabilities of the unlicensed nodes. Then, the maximum achievable capacity of the proposed system is derived under Rayleigh fading channel assumption. Accordingly, the probability of reaching a target capacity is provided. Amplify-and-forward and decode-and-forward relaying approaches are analyzed and the generalized outage probability expressions are derived. Consequently some important trade-offs and interesting results for the performance of the proposed methodology are presented.

CHAPTER 2

INTERFERENCE SUPPRESSION BY FILTERING APPROACH AND SIGNAL RECOVERY

FOR LTE UPLINK

Increasing demand for more bandwidth consuming applications and lack of spectrum availability will lead to denser frequency reuse and coexistence of different technologies in next generation wireless communication systems.[1] The introduction of heterogeneous network (HetNet) nodes such as femtocells, picocells, relays, and remote radio heads, wireless networks of the future will observe co-channel interference (CCI) from even a larger number of sources. Such co-channel interference can occur among same type of technologies, e.g., between long term evolution (LTE) based base station (BS). On the other hand, co-channel deployment of LTE-based macrocells with W-CDMA based femtocells can be given as an example scenario where different technologies need to coexist [2]. The impact of the interference can be removed from the signal of interest in such scenarios by operating interference cancellation methods simultaneously in multiple domains (like in time and frequency).

Interference cancellation methods become effective especially in the uplink (UL) of HetNet deployments, where dominant interference (DI) is observed frequently. A detailed overview of cross-tier interference scenarios for HetNets can be found in [46]. For example, in the context of femtocell networks, such a scenario happens when a macrocell user equipment (MUE) is at the vicinity of a closed-access femtocell network and interferes with the home enhanced node base (HeNB) in the UL [59–61]. While the UL interference from the MUE that are far from the HeNB may be tolerated, such DI scenarios should be detected and mitigated at the HeNB in order to improve the performance. Interference cancellation for the same type of waveforms is well-studied in the literature, and a contemporary overview on interference cancellation for cellular systems can be found in [62]. Iterative CCI cancellation is considered in [63, 64], which focus on

---

[1]The content of this chapter is partially published in [17, 18, 58]. Copyright for these publications can be found in Appendix B, Appendix C, and Appendix D.

narrow-band systems. These studies assume that the interference signal and the desired signal belong to the same technology. The single-carrier and multi-carrier interference scenario is investigated in [2], where narrowband interference (NBI) and orthogonal frequency division multiple access (OFDMA) signals are demodulated iteratively in order to cancel the interference. Moreover, some *a priori* information is required about the NBI signal and assumptions are made such as the availability of the ideal carrier frequency, and the perfect time/frequency synchronization at the OFDMA receiver for desired and interference signals [2]. Interference cancellation in a HetNet scenario where both multi-carrier signals interfere with each other is considered and, macrocell and femtocell user signals are demodulated jointly as an interference cancellation method in [65]. However, this approach requires a power control mechanism to be implemented along with the joint demodulator. Similarly, the information related to the macrocell network may not be available for the femtocell network or vice-verse. On the other hand, impulsive noise cancellation techniques identify the impulsive peaks that are spread within the received time-domain signal and clip/null those samples as a cancellation method (non-iterative approaches) where consecutive samples are not considered for cancellation and processing is performed only in one domain in OFDM-based power line communications and digital TV systems [66–68].

In this chapter, we treat single carrier-frequency domain equalization (SC-FDE) and single carrier-frequency domain multiple access (SC-FDMA) signals as desired signals and our aim is to suppress the impact of narrow-band DI. The proposed methods are independent from the waveform of the interferer (e.g., it may be a W-CDMA or LTE interferer) and only a partial overlap in frequency-domain is assumed between the desired and interferer signals. Suppressing the DI in frequency-domain by using a blanking algorithm causes inter symbol interference (ISI) in time-domain for single-carrier transmissions. Thus, we utilize an iterative algorithm to enhance the performance of the blanking technique and to reduce the ISI. In order to do that, the desired signal is processed in time-domain and in frequency-domain consecutively, and the obtained information, such as frequency coefficients, symbols, etc., in one domain is used in the other domain. The impact of ISI is further reduced by involving the reliable information into the iterations initially. The capacity of the proposed techniques are investigated by overlapping desired signal with narrow-band single-carrier DI signal through link level simulations. Additionally, the DI problem is mapped to the interference scenarios in the UL of LTE network where SC-FDMA scheme is employed. More specifically,

the capacity of the proposed techniques are investigated for the DI scenarios that occur when a MUE is at the vicinity of the HeNB. In this scenario, MUE is the DI signal overlaps with the home user equipment (HUE) signal at the HeNB. The system level capacity of the proposed techniques are compared to those of enhanced intercell interference coordination (eICIC) time and no-eICIC techniques which are recently discussed in [46]. Based on the signal-to-interference-plus-noise-ratio (SINR) level and the overlap ratio with the DI signal, an adaptive receiver can choose the best mode of operation among the candidates. Through simulations, it is shown that the proposed algorithms work particularly well for HetNet deployments, where the desired signal is typically interfered with DI signal only at a small portion of its spectrum.

This chapter is organized as follows: In Section 2.1 we introduce the system model for SC-FDE signal, followed by Section 2.3 which describes the blanking method. The impact of wireless channel and interference on blanking is analyzed in Section 2.4. Bit error rate (BER) of the blanking receiver is analyzed in Section 2.5. Iterative processing by a blanking receiver is examined in Section 2.6, employing iterations based on the reliable information is introduced by iterative likelihood test in Section 2.7. The performances of the proposed methods are demonstrated by computer simulations for SC-FDE and SC-FDMA signals in Section 2.8.

2.1 System Model

Consider that a transmitted SC-FDE signal is modeled as

$$x(t) = \sum_{n=-N_G}^{N-1} a[n]g(t - nT_s), \quad n \in [-N_G, -1], \tag{2.1}$$

where T_s is symbol duration and $a[n]$ represents modulated bits. It is assumed that $a[n]$ are independent and identically distributed (i.i.d) with zero mean and unit variance. Some portion of the generated symbols at the end are copied as cyclic prefix (CP) to the beginning, where $a[n] = a[n + N]$ within $[-N_G, 0)$. Symbols are passed through a root-raised-cosine filter, $g(t)$, with a roll-off factor of α before transmission. It is assumed that perfect time and frequency synchronization to the SC-FDE signal is achieved at the receiver. After
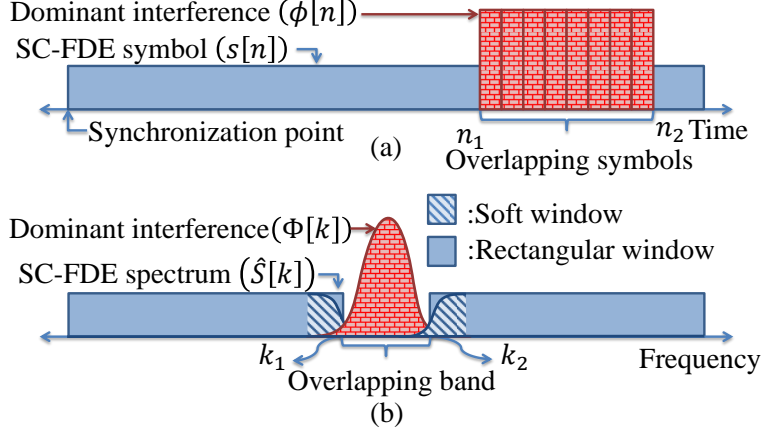
Figure 2.1: (a) Received signal, (b) blanked signal.

removing the CP, the received signal in sample time domain in the absence of noise becomes

$$y[n] = \sum_{l=0}^{L-1} h[l]x[n-l], \tag{2.2}$$

where $y[n]$ is sample of the received SC-FDE signal at the sample time index n which is defined in the interval $[0, N-1]$, L is the length of the impulse response of the channel $h[l]$, and $x[n] = x[n+N]$ for $n \in [-L+1, -1]$. Path loss and shadowing effects are also folded into $h[l]$. It is assumed that the maximum excess delay of the channel does not exceed the CP duration.

In our model, the SC-FDE signal is exposed to DI as shown in Fig. 2.1(a) and the received signal becomes

$$r[n] = y[n] + \phi[n] + \eta[n], \tag{2.3}$$

where $\phi[n]$ is the interference observed by SC-FDE receiver and $\eta[n]$ is the additive white Gaussian noise (AWGN) at sample time index n. The received signal in frequency-domain shown in Fig. 2.1(b) is modeled as

$$R[k] = X[k]H[k] + \Phi[k] + \Omega[k], \tag{2.4}$$

where k is the frequency-domain sample index, and $\Omega[\cdot]$ is the frequency-domain reciprocal of $\eta[\cdot]$.

Information bits of SC-FDE and SC-FDMA schemes are both modulated in time-domain. Assume that M symbols are mapped to M subcarriers after M-point discrete Fourier transform (DFT) pre-coding of

18

the time-domain symbols for SC-FDMA signal. Then N-point inverse-DFT (IDFT) spreads these DFT pre-coded symbols into N-point time-domain samples followed by adding cyclic prefix (CP) as in (2.1) where the impact of the interference becomes as in (2.3). Considering both SC-FDE and SC-FDMA schemes after N-point DFT, the obtained frequency-domain samples are composed of DFT pre-coded symbols of SC-FDE and SC-FDMA signals. However, there are N symbols and for SC-FDMA signal, there are M symbols. Hence, the system model is explained only for the SC-FDE scheme for the simplicity of derivations. However, the simulations are performed for both schemes.

Note that, knowledge of the DI location over the desired signal spectrum and synchronization to the desired signal under the impact of DI becomes important for interference cancellation. Detection of the NBI on wide-band signal is studied in the literature (e.g., [53, 69] and references therein). Additionally, the power of the narrow-band DI signal is distributed over wide-band desired SC-FDE/SC-FDMA signal in time-domain by the ratio of the DI signal bandwidth to the desired signal bandwidth in our model. Therefore, the power of the DI signal has to be large compared to the desired signal power to dominate the desired signal. Therefore, DI signal rises over desired signal in frequency-domain which allows the detection of the DI signal in frequency-domain by employing thresholding techniques. On the other hand synchronization in the presence of narrow-band DI at very low signal-to-interference-ratio (SIR) might be challenging as discussed in [70]. However, there are techniques available in the literature to improve the synchronization accuracy in the presence of NBI (see e.g., [71, 72] and references therein.). For the clearness of the presentation, proposed narrow-band DI cancellation techniques are investigated solely for certain SC-FDE/SC-FDMA schemes while they are overlapping in all possible domains (such as time, frequency, and space).

In order to benefit from the blanking receiver, it is assumed that DI signal have smaller bandwidth when compared to the desired signal or only partial overlap in frequency-domain is considered for the cases where the bandwidth of the DI signal is larger than the bandwidth of the desired signal. However, in time-domain, it is also assumed that the DI signal is overlapping through the frame duration of the SC-FDE signal for now, which will be removed later. The SC-FDE signal is exposed to the DI at frequency sample indices, $[k_1, k_2)$, as illustrated in Fig. 2.1, and can be detected by setting a threshold similar to [2] which is kept out of the scope of this chapter. First, only the impact of blanking some part of the desired signal spectrum is

19

considered in the absence of DI in AWGN channel. Later, in Section 2.4, the impact of DI and multipath channel is considered.

2.1.1 Rectangular Windowing of a Single Band

The DI is removed by blanking the overlapping band through the use of a rectangular window as presented in Fig. 2.1(b) (the DI signal is shown in the frequency-domain after blanking for illustration purposes). After blanking, $k = (k_2 - k_1)$ of N overlapping frequency-domain samples, the remaining $(N - k)$ samples contain the information related to the desired symbols. Because each time-domain sample of SC-FDE signal is spread within its spectrum[2].

The blanked SC-FDE signal without CP in frequency-domain by using a rectangular window can be given by using a piecewise function as (c.f., [58])

$$\widehat{S}[k] = \begin{cases} \sum_{n=0}^{N-1} s[n]e^{-j2\pi kn/N} & ,0 \leq k < k_1, \\ 0 & ,k_1 \leq k < k_2, \\ \sum_{n=0}^{N-1} s[n]e^{-j2\pi kn/N} & ,k_2 \leq k < N, \end{cases} \tag{2.5}$$

where $s[n]$ is the sample time-domain SC-FDE signal and $\widehat{S}[k]$ is the SC-FDE signal blanked in frequency-domain. Then, $\widehat{S}[k]$ in time-domain becomes

$$\hat{s}[m] = \frac{1}{\sqrt{N}} \sum_{k=0}^{N-1} \widehat{S}[k]e^{j2\pi km/N}. \tag{2.6}$$

In order to analyze the impact of ISI in time-domain, $\hat{s}[m]$ can be obtained by replacing $\widehat{S}[k]$ in (2.6) into (2.5) as

$$\hat{s}[m] = \begin{cases} \frac{1}{\sqrt{N}} \sum_{k=0}^{N-1} \frac{1}{\sqrt{N}} \sum_{n=0}^{N-1} s[n]e^{-j2\pi kn/N}e^{j2\pi km/N} & ,0 \leq k < k_1, \\ 0 & ,k_1 \leq k < k_2, \\ \frac{1}{\sqrt{N}} \sum_{k=0}^{N-1} \frac{1}{\sqrt{N}} \sum_{n=0}^{N-1} s[n]e^{-j2\pi kn/N}e^{j2\pi km/N} & ,k_2 \leq k < N. \end{cases} \tag{2.7}$$

[2]Note that as opposed to [2], the DI signal can be modulated either in time-domain or in frequency-domain.

After interchanging the sum terms in (2.7) and arranging the remaining terms, $\hat{s}[m]$ becomes

$$\hat{s}[m] = \frac{1}{N} \sum_{n=0}^{N-1} s[n] \left(\sum_{k=0}^{k_1-1} e^{j2\pi k(m-n)/N} + \sum_{k=k_2}^{N-1} e^{j2\pi k(m-n)/N} \right). \tag{2.8}$$

Considering the cases $(m-n)$ and $(m \neq n)$ separately, (3.11) can be given as

$$\hat{s}[m] = \begin{cases} \frac{1}{N} \sum_{n=0}^{N-1} s[n] \left(\sum_{k=0}^{k_1-1} e^{j2\pi(m-n)k/N} + \sum_{k=k_2}^{N-1} e^{j2\pi(m-n)k/N} \right) & , m \neq n, \\ \frac{1}{N} \sum_{n=0}^{N-1} s[n](k_1 + (N - k_2)) & , m = n. \end{cases} \tag{2.9}$$

The exponential sum terms in (3.13) can be reduced by utilizing the formula, $\sum_{a=0}^{N-1} b^a = \frac{1-b^N}{1-b}$, as

$$\hat{s}[m] = \begin{cases} \frac{1}{N} \sum_{n=0}^{N-1} s[n] \left(\frac{1 - (c_{m,n})^{k_1}}{1 - c_{m,n}} - \frac{1 - (c_{m,n})^{k_2}}{1 - c_{m,n}} \right) & , m \neq n, \\ \frac{1}{N} \sum_{n=0}^{N-1} s[n] (k_1 + (N - k_2)) & , m = n, \end{cases} \tag{2.10}$$

where $c_{m,n} = e^{j2\pi(m-n)/N}$. After some manipulation, (2.10) is derived to its final form given as

$$\hat{s}[m] = \underbrace{s[m] \left[\frac{N - k_2 + k_1}{N} \right]}_{\text{Desired Part } (P_s i[m])} + \underbrace{\frac{1}{N} \sum_{\substack{n=0 \\ n \neq m}}^{N-1} s[n] \frac{c_{m,n}^{k_2} - c_{m,n}^{k_1}}{1 - c_{m,n}}}_{\text{ISI Part}(\xi[m])}, \tag{2.11}$$

which shows that blanking by using a rectangular window scales the amplitude of the desired part of the blanked signal by $(N - k_2 + k_1)/N$ due to energy loss and injects undesirable products in the form of ISI. After blanking the same K samples of SC-FDMA signal as in Fig. 2.1(b), M-point IDFT operation is performed to the DFT spreaded SC-FDMA samples in frequency-domain. This results in ISI of the same form for SC-FDE signal where for SC-FDMA waveform, the N term in (3.14) must be replaced with M. Consequently, considering the same blanking ratios for both SC-FDE and SC-FDMA signals, the impact of blanking blanking is the same and the equations regarding the proposed blanking techniques derived for SC-FDE signal can be applied for SC-FDMA signal. In order to reduce the impact of the ISI, smoother blanking windows might be considered.

2.1.2 Soft Windowing for SC-FDE

Blanking through the use of a rectangular window (and/or brick-wall filter) in frequency-domain introduces high side-lobes which increases the contribution of ISI. Soft windowing, as in Fig. 2.1(b), may reduce this contribution because of the faster decay at the tails of the time domain conjugate of the applied filter. Therefore, we examined raised cosine filter which is composed of two parts

$$W_L[k] = \frac{1}{2}[1 + \cos(\pi k/M)], \tag{2.12}$$

$$W_R[k] = \frac{1}{2}[1 + \cos(\pi k/M)], \tag{2.13}$$

where $W_L[\cdot]$, $W_R[\cdot]$ exemplifies left and right halves of the raised cosine filter and M is the sample size of the each half of the filter. If the blanking region is larger than the filter length, M, the samples between $W_L[\cdot]$ and $W_R[\cdot]$ are padded with zeros and the applied soft window becomes

$$W[k] = \begin{cases} W_R[k - k_1 + \frac{M}{2}] & , k_1 - \frac{M}{2} \leq l < k_1 - \frac{M}{2}L, \\ 0 & , k_1 + \frac{M}{2} \leq k < k_2 - \frac{M}{2}L, \\ W_R[k - k_2 + \frac{M}{2}] & , k_2 - \frac{M}{2} \leq k < k_2 + \frac{M}{2}L, \end{cases} \tag{2.14}$$

where $W[k]$ represents the applied soft window. Thus, the frequency-domain soft filtered signal, $\widehat{S}[k]$, can be written as a piecewise function as

$$\widehat{S}[k] = \begin{cases} \frac{1}{\sqrt{N}} \sum_{n=0}^{N-1} s[n]e_{n,k} & , 0 \leq k < k_1 - \frac{M}{2}L, \\ W[k]\frac{1}{\sqrt{N}} \sum_{n=0}^{N-1} s[n]e_{n,k} & , k_1 + \frac{M}{2} \leq k < k_2 - \frac{M}{2}L, \\ \frac{1}{\sqrt{N}} \sum_{n=0}^{N-1} s[n]e_{n,k} & , k_2 + \frac{M}{2} \leq k < NL, \end{cases} \tag{2.15}$$

where $e_{n,k} = e^{j2\pi kn/N}$ represents the DFT coefficients.

Theorem 1 *The soft filtered signal in time-domain can be obtained after taking the inverse DFT of (2.15). The impact of soft filtering on the desired signal can be given as in (2.16), where the desired part of the*

signal is the same as in the case of blanking with a rectangular window (See Appendix for the proof.).

$$\hat{s}[m] = \frac{N - k_2 + k_1}{N} s[m] + \frac{1}{N} \sum_{\substack{n=0 \\ n \neq m}}^{N-1} s[n] \left[\frac{c_{m,n}^{k_1 - \frac{M}{2}} - c_{m,n}^{k_2 + \frac{M}{2}} - j \sin\left(\frac{\pi(n-m)M}{N}\right)\left[c_{m,n}^{k_1} + c_{m,n}^{k_2}\right]}{1 - c_{m,n}} \right.$$

$$\left. + \frac{1}{4}\left(\frac{1 + e^{j\left(\frac{2\pi\beta M}{N}\right)}}{1 - e^{j\left(\frac{\pi}{M} + \frac{2\pi\beta}{N}\right)}} + \frac{1 + e^{j\left(\frac{2\pi\beta M}{N}\right)}}{1 - e^{-j\left(\frac{\pi}{M} - \frac{2\pi\beta}{N}\right)}}\right)\left[c_{m,n}^{k_1 - \frac{M}{2}} + c_{m,n}^{k_2 - \frac{M}{2}}\right]\right] \tag{2.16}$$

2.1.3 Generalized Case: Blanking From Multiple Bands

In this section, it is assumed that the desired signal is interfered from two or more separate parts of its spectrum. Following the same steps given previously, blanking the desired signal from L different parts by using a rectangular window in frequency-domain can be obtained as

$$\hat{s}[m] = \frac{N - K}{N} s[m] + \frac{1}{N} \sum_{l=1}^{L} \sum_{\substack{n=0 \\ n \neq m}}^{N-1} \left[s[n]\left(\frac{c_{m,n}^{k_2^{(l)}} - c_{m,n}^{k_1^{(l)}}}{1 - c_{m,n}}\right)\right], \tag{2.17}$$

which can be written for blanking with a raised cosine window similarly.

2.1.4 Time-Frequency Analysis of the Blanking Algorithm

In the previous sections, it is assumed that the DI signal is overlapping in time-domain continuously throughout the frame duration of the desired signal. However, there might be cases where the DI signal has a bursty transmission nature as shown in Fig. 2.1(a). Note that blanking in frequency-domain introduces ISI to the symbols that are not overlapped with the DI signal in time-domain. In order to restrain the unnecessary ISI impact to the non-interfered symbols of the desired signal, continuity of the corresponding frequency-domain samples must be preserved after blanking in frequency-domain. Thus, the time-domain blanked

signal can be given as

$$
\bar{s}[n] = \begin{cases} \dfrac{1}{\sqrt{N}} \displaystyle\sum_{k=0}^{N-1} s[n]e^{j2\pi kn/N} & ,0 \le n < n_1, \\[4mm] 0 & ,n_1 \le n < n_2, \\[4mm] \dfrac{1}{\sqrt{N}} \displaystyle\sum_{k=0}^{N-1} s[n]e^{j2\pi kn/N} & ,n_2 \le n < N, \end{cases}
\tag{2.18}
$$

where $\bar{s}[n]$ is the time-domain signal blanked at sample indices $n \in [n_1, n_2)$ as in Fig. 2.1(a). The continuity of the non-interfered symbols can be procured by replacing the blanked samples between the indices $[k_1, k_2)$ given in (2.5) with the sample values of $\bar{s}[k]$ as

$$
\widetilde{S}[k] = \begin{cases} \displaystyle\sum_{n=0}^{N-1} s[n]e^{-j2\pi kn/N} & ,0 \le k < k_1, \\[4mm] \bar{s}[n] & ,k_1 \le k < k_2, \\[4mm] \displaystyle\sum_{n=0}^{N-1} s[n]e^{-j2\pi kn/N} & ,k_2 \le k < N, \end{cases}
\tag{2.19}
$$

where $\widetilde{S}[k]$ is the frequency-domain representation of the desired signal after employing blanking in both domains and replacing the frequency-domain sample values of the non-interfered time-domain samples. Inverse DFT of (2.19) explains the impact of ISI after blanking in both domains as

$$
\tilde{s}[n] = \begin{cases} \dfrac{1}{\sqrt{N}} \displaystyle\sum_{k=0}^{N-1}\left(\dfrac{1}{\sqrt{N}}\displaystyle\sum_{n=0}^{N-1} s[n]e_{n,k}\right)e_{m,k}^{-1} & ,0 \le k < k_1, \\[4mm] \dfrac{1}{\sqrt{N}} \displaystyle\sum_{k=0}^{N-1}\left(\dfrac{1}{\sqrt{N}}\displaystyle\sum_{n=0}^{N-1} s[n]e_{n,k}\right)e_{m,k}^{-1} & ,k_1 \le k < k_2, 0 \le n < n_1, \\[4mm] 0 & ,k_1 \le k < k_2, n_1 \le n < n_2, \\[4mm] \dfrac{1}{\sqrt{N}} \displaystyle\sum_{k=0}^{N-1}\left(\dfrac{1}{\sqrt{N}}\displaystyle\sum_{n=0}^{N-1} s[n]e_{n,k}\right)e_{m,k}^{-1} & ,k_1 \le k < k_2, n_2 \le n < N, \\[4mm] \dfrac{1}{\sqrt{N}} \displaystyle\sum_{k=0}^{N-1}\left(\dfrac{1}{\sqrt{N}}\displaystyle\sum_{n=0}^{N-1} s[n]e_{n,k}\right)e_{m,k}^{-1} & ,k_2 \le k < N. \end{cases}
\tag{2.20}
$$

After some manipulation, we have

$$\tilde{s}[n] = \frac{1}{N}\left(\sum_{n=0}^{N-1}\sum_{k=0}^{k_1-1} c_{m,n}{}^k + \sum_{n=0}^{n_1}\sum_{k=k_1}^{k_2-1} c_{m,n}{}^k + \sum_{n=n_2}^{N-1}\sum_{k=k_1}^{k_2-1} c_{m,n}{}^k + \sum_{n=0}^{N-1}\sum_{k=k_2}^{N-1} c_{m,n}{}^k\right), \tag{2.21}$$

which has the form analogous to (3.11) and subsequently following the similar steps result in the final form as

$$\tilde{s}[n] = s[m]_{\substack{0\leq m<n_1 \\ n_2\leq m<N}} + s[m]_{n_1\leq m<n_2}\left(\frac{N-k_2+k_1}{N}\right) + \frac{1}{N}\sum_{\substack{n=0 \\ n\neq m}}^{N-1} s[n]\frac{c_{m,n}{}^{k_2} - c_{m,n}{}^{k_1}}{c_{m,n}}. \tag{2.22}$$

This shows that when bursty interference overlaps at some of the symbols of the desired signal in time-domain, non-interfered symbols are recovered without any impact of the ISI if non-interfered time-domain samples are included into processing.

2.2   Effects of Wireless Channel and Interference on Blanking

Consider the frequency-domain signal in (2.4) which includes the desired signal and the DI signal. After blanking the DI signal we have the remaining desired signal as

$$\widehat{R}[k] = \widehat{X}[k]\widehat{H}[k] + \widehat{\Omega}[k], \tag{2.23}$$

where $\widehat{\Omega}[.]$ is colored due to blanking. We assume that the channel is perfectly known for the desired signal[3], and zero-forcing (ZF) FDE yields

$$\check{X}[k] = \frac{\widehat{Y}[k] + \widehat{\Omega}[k]}{\widehat{H}[k]}, \tag{2.24}$$

where $\check{X}[\cdot]$ represents the equalized symbols in frequency-domain. In time-domain $\check{x}[\cdot]$ can be expressed in terms of transmitted symbols, $x[\cdot]$, similar to (3.14) as follows

$$\check{x}[m] = \underbrace{x[m]\left(\frac{N-k}{N}\right)}_{\text{Desired Part } (P_s i[m])} + \underbrace{\frac{1}{N}\sum_{\substack{n=0 \\ n\neq m}}^{N-1} x[m]\frac{c_{m,n}{}^{k_2} - c_{m,n}{}^{k_1}}{1 - c_{m,n}}}_{\text{ISI Part } (\xi[m])} + \check{\eta}[m], \tag{2.25}$$

---

[3]The channel can be estimated by using pilots in frequency-domain or by transmitting preambles prior to the desired signal.

where $\breve{\eta}[m] = \mathcal{F}^{-1}\{\widehat{\Omega}[m]/\widehat{H}[m]\}$ and the undesired term becomes $\xi[m] + \breve{\eta}[m]$. Additionally, the impact of DI on blanking and the effects of the undesired terms caused by blanking must be investigated.

2.2.1 Trade-off Between DI and ISI

In order to suppress the DI signal through the use of blanking methods, the overlapping DI signal location must be detected over the desired signal in time and frequency-domains. Errors in the estimation of the overlapping band of the DI signal over the desired signal and/or performing incorrect blanking can cause some interference to leak into the desired signal. This residue of the interference has a negative impact on the desired signal recovery apart from the ISI contributed by blanking. In order to evaluate the performance of blanking algorithms, all these drawbacks should be investigated clearly.

Blanking solely leads to loss in the signal power. If k of N frequency samples are blanked through the use of a rectangular window, the power of the blanked signal, $P_{\hat{s}}$, decreases with the ratio of k/N and becomes $P_{\hat{s}} = P_s \frac{N-k}{N}$ where P_s is the power of $s[\cdot]$. Note that the variance of a zero mean i.i.d sequence equals to its power. Since the desired part of the blanked signal, $P_s i[\cdot]$, given in (3.14) and (2.16) is assumed to be i.i.d. with zero mean and unit variance, $P_{P_s i}$ can be defined as $P_{P_s i} = P_s \left(\frac{N-k}{N}\right)^2$. Therefore, ISI power, P_ξ, can be given as

$$P_\xi = P_{\hat{s}} - P_{P_s i} = P_s \left(\frac{N-k}{N}\right) - P_s \left(\frac{N-k}{N}\right)^2$$
$$= P_s \frac{k(N-k)}{N^2}. \tag{2.26}$$

The relationship of $P_{\hat{s}}$, P_ξ, and $P_{P_s i}$ as a function of the number of blanked samples, k, is presented in Fig. 2.2. In case of blanking with a raised cosine window, the desired part ,$P_s i[\cdot]$, given in (2.16) is the same as blanking with a rectangular window given in (3.14) so the power of the desired part remains the same and P_ξ can be calculated in the same way as in (2.26). However, the power of the $\hat{s}[\cdot]$, $P_{\hat{s}}$, is more complicated to calculate. The raised cosine window, $W[\cdot]$, given in (2.14) is applied only to the interfered band of the desired signal as seen in (2.15) and $P_{\hat{s}}$ is can be calculated by integrating the squared samples in frequency-domain. Since the filter in (2.14) is symmetric, the sum of the squared samples can be obtained
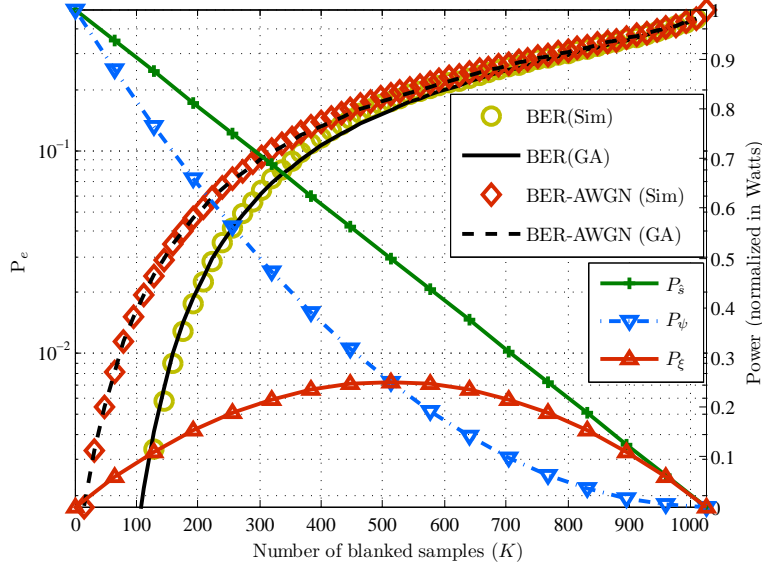
Figure 2.2: Impact of blanking on QPSK modulated noisy and noiseless SC-FDE signal with 1024 symbols (SNR = 10 dB in AWGN - left axis), and theoretical relation between $P_{\hat{s}}$, $P_{P_s i}$ and P_ξ (right axis).

for half of the filter as

$$\int_0^M W_{\mathrm{L}}(t)^2 \mathrm{d}t = \int_0^M \left(\frac{1}{2} \left[1 + \cos\left(\pi t / M\right) \right] \right)^2 \mathrm{d}t = \frac{3M}{8}. \tag{2.27}$$

Therefore $P_{\hat{s}}$ becomes the superposition of the powers of each part of the piecewise function given in (2.16)

as

$$P_{\hat{s}} = \frac{\left[\left(k_1 - \frac{M}{2} \right) + \left(N - k_2 - \frac{M}{2} \right) + 2 \left(\frac{3M}{8} \right) \right]}{N} = \frac{N - k}{N} - \frac{M}{4N}, \tag{2.28}$$

$$P_\xi = P_{\hat{s}} - P_{P_s i} = \frac{k(N - k)}{N^2} - \frac{M}{4N}. \tag{2.29}$$

This shows that for $M = 0$, the raised cosine window merges to the rectangular window. Moreover, as M

increases, ISI decreases, which is presented in Fig. 3.3(a) to show the impact of the ISI for three different

raised cosine filters. It should also be noted that, there is a trade-off between the suppressed DI power and

the introduced ISI power in case of applying a soft filter. Although the raised cosine window reduces the

impact of the ISI, the DI can be introduced from the excess band of the applied filter as shown in Fig. 2.1(b).

This can be compensated by applying blanking in a wider band without changing the roll-off to remove the

impact of the DI signal which is leaking from the excess bands of the applied window. However, this results

in sacrifice from the desired signal power. Thus, the generalized form for the power of the received signal,

$P_{\breve{x}}$, in AWGN channel can be given as,

$$P_{\breve{x}} = P_{P_s i} + P_\xi + P_\vartheta + P_{\breve{\eta}} = \left(\frac{N-k}{N} - \frac{M}{4N} \right) + \frac{\left(\mathbf{W} \cdot \boldsymbol{\Phi}^{\mathsf{T}} \right)^2}{k+M} + \sigma_\eta^2 \left(\frac{N-k}{N} \right), \tag{2.30}$$

where P_ϑ appears as the residue of the interference from the excess bands of the window, $\mathbf{W}$ is a vector
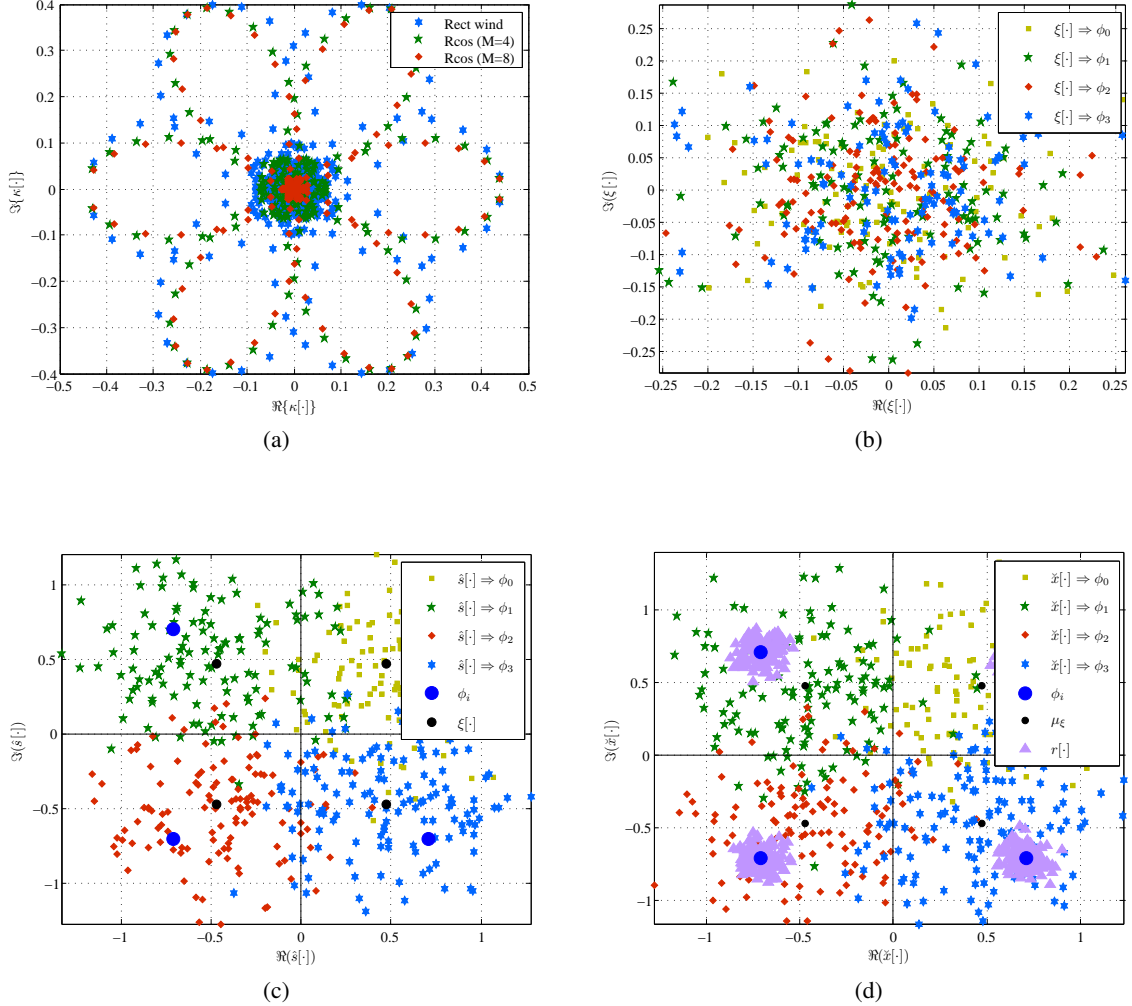
Figure 2.1: Constellation representations of: (a) $\kappa[\cdot]$ term for $m = 30, n = [0, 511], k_1 = 80, k_2 = 90$, for rectangular window given in (2.39) and raised cosine window with filter lengths of 4 and 8 samples (b) injected $\xi[\cdot]$ for all symbols, (c) $\hat{s}[\cdot]$ for $m = 30, n = [0, 511], k_1 = 80, k_2 = 250$, (d) blanked signal, $\breve{x}[\cdot]$ in AWGN channel, and received signal in the absence of interference, $r[\cdot]$, where SNR = 20 dB.

composed of zeros for rectangular windowing or

$$\mathbf{W} = [W[1] \, W[2] \, \cdots \, W[M]] \tag{2.31}$$

for raised cosine windowing and

$$\mathbf{\Phi} = [\Phi[1] \, \Phi[2] \ldots \Phi[M]] \tag{2.32}$$

is the DI signal observed by the blanking receiver. In case of rectangular windowing, $k \neq 0$ and the DI signal is removed. If it is assumed that DI signal has a rectangular shape in frequency-domain, P_ϑ can be derived similar to (2.27) in the interval $\left[\frac{M}{2}, M\right]$ and becomes

$$P_\vartheta = P_\xi \frac{(k - M)}{k} M \left(\frac{3\pi - 18}{16N}\right). \tag{2.33}$$

Otherwise, the spectral shape of the DI signal from both sides of its band should be taken into account. In AWGN channel, $P_{\check{\eta}} = P_{\widehat{\eta}}$ and the noise power is scaled due to blanking. However, in case of no-cancellation as in (2.4), $\{k, P_\vartheta\} = 0$ and $P_{\check{x}}$ becomes P_r.

2.2.2 Optimum Blanking for Interference Suppression

Choosing the optimum blanking window parameters is important because of the trade-off between the desired signal power, the ISI power and the residue of the interference. For instance, the use of blanking window with a larger roll-off factor reduces ISI but increases the leakage from the DI power. On the contrary, decreasing the roll-off factor of the applied filter for the same size of blanking window causes larger ISI and decreases the residue of the DI signal. Therefore, the optimum filter can be designed in order to maximize SINR as

$$\{\widehat{k}, \widehat{M}\} = \arg \max_{k \in [0,N), M \in \left[0, \frac{N-k}{2}\right)} \left\{\frac{P_{P_s i}}{P_\xi + P_\vartheta + P_{\widehat{\eta}}}\right\}. \tag{2.34}$$

The noise term can be neglected at high SINR region where a reliable communication link is assumed to be established for the choice of the optimum filter in case of no-interference and (2.34) can be rewritten as

$$\{\widehat{k}, \widehat{M}\} = \arg\max_{k\in[0,N), M\in\left[0, \frac{N-k}{2}\right)} \left\{ \frac{\left(\frac{N-k}{N}\right)^2}{\frac{k(N-k)}{N^2} - \frac{M}{4N} + P_\vartheta} \right\},$$ (2.35)

where $\widehat{k}$ and $\widehat{M}$ are the blanking size and the filter length for the choice of the optimum filter respectively. The spectral shape of the DI signal affects the design of the optimum raised cosine filter and the residue of the DI signal can be calculated by integrating the blanking window and spectral shape of the DI signal as

$$P_\vartheta = \frac{2}{N} \int_0^{N-1} \left(W_\text{L}\left(t - k_1 + {}^M/_2\right) W_\vartheta\left(t\right)\right)^2 \mathrm{d}t,$$ (2.36)

where the power is calculated within the desired signal band for one-side of the blanking window and multiplied by two because of symmetry, and $W_\vartheta\left(t\right)$ is the spectral shape of the DI signal[4]. Although it might be complex to model the spectral shape of the DI signal mathematically, a sub-optimal solution can be proposed to simplify (2.36). The spectral shape of the DI signal can be assumed rectangular if DI power is larger than the power of the desired part ($P_\phi \gg P_{P_s i}$) or the rise of the DI signal spectral shape is sharp. On the other hand, blanking can be applied to the k samples of the desired signal where k can also be larger than the bandwidth of the DI signal at a value of $\Delta k \geq 0$ samples. In this case, the formulation of the powers for desired and ISI parts ($P_{P_s i}$ and P_{ξ}) is the same as given before. Thus, the residue interference power, P_ϑ, is calculated by the integral given in (2.27) within the interval $[{}^{(M + \Delta k)}/_2, M]$ and yields

$$P_\vartheta = \frac{3\left(M - \Delta k\right)}{8N} - \frac{9M}{\pi 8N} \cos\left(\frac{\pi\Delta k}{2M}\right).$$ (2.37)

Since both nominator and denominator in (2.35) have positive values, the maximization of (2.35) based on (2.37) can be simplified to the maximization of the following

$$\left(N - 2k\right)\left(N - k\right) + N\left(\frac{3\Delta k - M}{8} + \frac{9M}{8\pi} \cos\left(\frac{\pi\Delta k}{2M}\right)\right).$$ (2.38)

[4]We investigated the impact of raised cosine filter. Similar steps can be followed for any kind of filter which may give the optimum solution based on the spectral shape of the DI signal to maximize the SINR.

However, the optimum filter parameters $\{\widehat{k}, \widehat{M}\}$ based on the assumptions might not give the optimum solution if those assumptions do not hold. Therefore we apply all possible blanking windows by changing the blanking size and the filter length parameters based on the power formulas given above considering the expected value of the DI signal spectral shape and we chose the blanking window parameters giving the largest SINR of the desired signal.

2.3 BER Analysis of the Blanking Receiver

2.3.1 Statistics of ISI

For a better understanding of the impact of ISI to the statistics (distribution, mean and variance) of the blanked signal, ISI part might be further analyzed. Considering the rectangular window, $\xi[\cdot]$ given in (3.14) as

$$\xi[m] = \frac{1}{N} \sum_{\substack{n=0 \\ n \neq m}}^{N-1} s[n] \underbrace{\frac{c_{m,n}{}^{k_2} - c_{m,n}{}^{k_1}}{1 - c_{m,n}}}_{\kappa[m-n]}, \tag{2.39}$$

is composed of the sum of the product of other symbols $((m-n)eqn)$ with a sinc function which is not defined at m (the value of the sinc function at m defines the value of the desired part.). As m changes, $\xi[m]$ is exposed to a circular shift where the peak of the sinc function is placed at m. Only $\text{Re}\{\xi[m]\}$ will be effective for real-valued modulations (such as BPSK). Otherwise, both in-phase and quadrature branches are distorted. The impact of ISI is illustrated in Fig. 3.3(a) where the differences between constellation plots of $\kappa[\cdot]$ for a rectangular window and two raised cosine windows can be observed.

Mean, μ_ξ, and variance, σ_ξ^2, of the ISI in (2.39) can be given as

$$\mu_\xi = E\left[\xi[m]\right] = \frac{1}{N} \sum_{\substack{n=0 \\ n \neq m}}^{N-1} \mu_s \kappa[m-n], \tag{2.40}$$

$$\sigma_\xi^2 = E\left[\xi[m]^2\right] - \mu_\xi{}^2 = \frac{1}{N} \sum_{\substack{n=0 \\ n \neq m}}^{N-1} \sigma_s^2 \kappa[m-n], \tag{2.41}$$

where μ_s and σ_s^2 are mean and variance of $s[\cdot]$ respectively for rectangular windowing case. Assume that the blanked signal is employing a complex $\mathcal{M}$-ary modulation, where symbols have discrete uniform distribution

31

with probabilities $\Pr(s[n] = \phi_i) = 1/M$ and ϕ_i, $i \in [0, M-1)$ are possible symbols with the mean and variance of $\{0, 1\}$. Accordingly, $\{\mu_s, \sigma_s^2\} \cong \{0, 1\}$ for large number of symbols and (2.40) and (2.41) can be simplified as

$$\{\mu_\xi, \sigma_\xi^2\} \cong \{\mu_\xi Cong, \sigma_\xi^2 Cong\}, \tag{2.42}$$

where the additive $\xi[\cdot]$ for every symbol is shown in Fig. 3.3(b)[5]. The mean value of the desired part, $P_s i[m]$, of the blanked signal, $\hat{s}[m]$, is scaled due to blanking which can be fixed later.[6] Consequently, the mean and the variance of the blanked signal become

$$\{\mu_{\hat{s}}, \sigma_{\hat{s}}^2\} = \left\{\mu_\xi + \frac{(N-k)\phi_i}{N}, \sigma_\xi^2\right\}. \tag{2.43}$$

The distribution of $\hat{s}[\cdot]$ around each constellation point is shown in Fig. 3.3(c).

In AWGN channel, the received symbols, $r[\cdot]$, in the absence of the interference are distributed around each ϕ_i based on the statistics of the noise. Assume that the statistical distribution of complex AWGN is $\mathcal{N}_c\left(0, \sigma_\eta^2\right)$. Thus, $r[\cdot]$ is distributed around each ϕ_i with statistics $\mathcal{N}_c\left(\phi_i, \sigma_\eta^2\right)$. Due to blanking (as in (3.14)), σ_η^2 is scaled and the noise power becomes $\sigma_{\hat{\eta}}^2 = \sigma_\eta^2 \frac{N-k}{N}$. Although the noise ($\widehat{\eta}[\cdot]$) is colored and/or correlated due to blanking, the distribution of $\widehat{\eta}[\cdot]$ remains Gaussian (caused by the linear combination of Gaussian random variables) with statistics as $\widehat{\eta}[\cdot] \sim \mathcal{N}_c\left(0, \sigma_\eta^2\left(\frac{N-k}{N}\right)\right)$. Consequently, the mean, $\mu_{\hat{r}}$, and the variance, $\sigma_{\hat{r}}^2$, of $\hat{r}[\cdot]$ in AWGN channel become

$$\{\mu_{\hat{r}}, \sigma_{\hat{r}}^2\} = \left\{\frac{(N-k)\phi_i}{N}, \sigma_\eta^2\frac{(N-k)}{N} + \frac{1}{N}\sum_{\substack{n=0 \\ n \neq m}}^{N-1} \kappa[m-n]\right\}. \tag{2.44}$$

The distribution of $\hat{r}[\cdot]$ around each constellation point is shown in Fig. 3.3(d). In case of multipath and Doppler channels, the distribution of the symbols around constellation points after equalization may vary based on the preferred equalization method. Thus, undesired terms such as residues of the blanked interfer-

---

[5]Different markers show the symbols belonging to different ϕ_i, which are multiplied by $\kappa[m-n]$ then its superposition is contributed as ISI to the mth symbol, $\hat{s}[m]$.

[6]Considering PSK modulation schemes BPSK and QPSK, the change in the $\mu_{\hat{s}}$ does not cause erroneous demodulation in case of windowing. However, AM modulation schemes such as 16QAM, 64QAM, the mean is required to be shifted back to ϕ_i by multiplying symbols with $\left(\frac{N}{N-k}\right)$.

ence, noise and equalization errors can be combined under the term, $\varepsilon[\cdot]$. Finally, the mean and the variance of $\check{x}$ can be obtained by including the mean and variance of $\varepsilon[\cdot]$.

Blanking with a rectangular window can be considered as a special case of blanking with a raised cosine window in which the roll-off factor is equal to zero (or $M = 0$). Thus, the impact of ISI for the raised cosine window can be nested from rectangular window.

Deriving the exact and/or approximate distribution of the symbols around the ideal constellation points can be used to reduce the outcomes of blanking. Hence, a receiver can be proposed based on the statistical distribution of the symbols to reduce the impact of blanking.

2.3.2 BER Analysis with Gaussian Approximation

In OFDM based systems, Gaussian approximation to the symbol distribution for error rate derivation is frequently referred in the literature [58, 73–75]. Due to the central limit theorem, the distribution of the AWGN in the reciprocal domain (after DFT or inverse DFT) can be estimated as Gaussian as well [73, 75]. In case of blanking, some part of the desired signal in frequency-domain has non-linear impact on the time-domain symbols. For instance, analogous to this approach, nulling/clipping in OFDM based waveforms in time-domain, which has non-linear impact on symbols in frequency-domain verifies this assumption for large number of symbols ([73–76] and the references therein). On the other hand, if few number of samples are affected in reciprocal domain, this assumption loses its validity even for large number of symbols [74, 77]. In our case, DI signal affects a sufficiently large number of samples in frequency-domain considering the bandwidth of the DI signal.

For simplicity, BPSK and QPSK modulated SC-FDE and DI signals are considered for BER analysis. The bit error probability of the BPSK and QPSK modulated bits can be given as $\mathrm{Pr}_e = Q\left(\sqrt{2\gamma_b}\right)$ in AWGN channel, where γ_b is the ratio of bit energy to the noise variance (which equals to SNR per bit as well). We can analyze the impact of blanking on the BER solely, by discarding the impact of the AWGN channel. We assume the Gaussian approximation of the ISI contribution for bit error probability calculation. In case of blanking with a rectangular window, the bit error probability of the desired signal, $\mathrm{Pr}_{\hat{s}}$, can be given theoretically for BPSK modulation as $Q\left(\sqrt{P_{P,i}/P_\xi}\right)$. In AWGN channel, the variance of the noise can be neglected if $P_\xi \gg \sigma_\eta^2$. This allows to approximate the error floor caused by blanking with a rectangu-

lar window as $\approx Q\left(\sqrt{(N-k)/k}\right)$, which is a monotonically increasing function of k as shown in Fig. 2.2. Because of this error floor, blanking the desired signal for DI mitigation may not be useful in some cases (e.g. if injected ISI power is larger than the DI power, P_ϕ and P_ξ.). The BER curves of the blanking with a rectangular window and the received signal with no-cancellation intersect at an SINR value as seen in the simulation section which can be defined as cross-point SINR (e.g. Received and Rect. BER curves in Fig. 2.4). For interference cancellation, we expect the noise floor to be much lower than the P_ϕ. Thus, cross-point can be approximated as the point where $P_{P_s i}/P_\xi = P_s/P_\phi$ (i.e., SIR after blanking is equivalent to no-cancellation SIR). Hence, an adaptive receiver can use the blanking algorithm if the SINR (P_s/P_ϕ) is smaller than this cross-point SINR ($P_{P_s i}/P_\xi$), and use no-cancellation otherwise. Furthermore, the BER of the desired signal blanked with a rectangular window, $\check{x}[\cdot]$, in AWGN channel can be generalized based on the power values given in (2.30) as

$$\mathrm{Pr}_e = Q\left(\sqrt{\frac{P_{P_s i}}{P_\xi + P_\vartheta + P_{\check{\eta}}}}\right) = Q\left(\sqrt{\frac{P_s\left(\frac{N-k}{N}\right)^2}{P_s\left(\frac{k(N-k)}{N^2} - \frac{M}{4N}\right) + \frac{(\mathbf{W}\cdot\boldsymbol{\Phi}^{\mathrm{T}})^2}{k+M} + \sigma_\eta^2\left(\frac{N-k}{N}\right)}}\right). \tag{2.45}$$

2.4   Iterative Blanking Method

In order to reduce the drawbacks of blanking, symbols can be processed further. In this section, we propose an iterative technique to reconstruct the desired signal by processing the desired signal both in time and frequency-domains.

The samples of the blanked signal, $\check{x}[\cdot]$, are demodulated to obtain information bits at the output of the decision device. Due to the impact of impairing factors, which are folded into $\varepsilon[\cdot]$ (such as ISI, noise, equalization errors etc.), erroneous bits are expected at the output of the decision device. Based on the symbol decisions the desired signal is regenerated and represented as $\ddot{x}_1[\cdot]$ (without CP). Note that some frequency components arise within the blank spectrum after the Fourier transform of $\ddot{x}_1[\cdot]$ which is represented as $\ddot{X}_1[\cdot]$. Blanked spectrum of $\check{X}[\cdot]$, is replaced with those corresponding frequency components of $\ddot{X}_1[\cdot]$, as

$$\check{X}_1[k] = \begin{cases} \ddot{X}_1[k] & \text{, if } k_1 \le k < k_2, \\ \check{X}[k] & \text{, otherwise.} \end{cases} \tag{2.46}$$

Therefore, the desired signal is obtained in time-domain as $\ddot{x}_1[\cdot] = \mathcal{F}^{-1}\left\{\ddot{X}_1[\cdot]\right\}$. This replacement procures the continuity of the desired signal in frequency domain for correctly detected symbols. Thus, the ISI, which is caused by discontinuities and/or blanking, is reduced by dropping the terms for correctly detected symbols from $\xi[\cdot]$ given in (2.25). On the contrary, false decision of symbols distort the other symbols in the form of $\xi[\cdot]$. To further analyze the effects of iteration, the replaced signal can be considered as the sum of two blanked signal as seen in (2.46). Thus, $\check{x}_1[\cdot]$ can be rewritten as

$$
\begin{aligned}
\check{x}_1[m] = & x[m]\left(\frac{N-k}{N}\right) + \frac{1}{N}\sum_{\substack{n=0 \\ n \neq m}}^{N-1} x[m]\frac{c_{m,n}{}^{k_2} - c_{m,n}{}^{k_1}}{1 - c_{m,n}} + \check{\eta}[m] \\
& + \ddot{x}_1[m]\left(\frac{k}{N}\right) + \frac{1}{N}\sum_{\substack{n=0 \\ n \neq m}}^{N-1} \ddot{x}_1[m]\frac{c_{m,n}{}^{k_1} - c_{m,n}{}^{k_2}}{1 - c_{m,n}},
\end{aligned}
\tag{2.47}
$$

where the ISI parts for $\ddot{x}_1[m]$ and $x[m]$ cancels each other in case $\ddot{x}_1[n] = x[n]$, for $\forall n$. If all of the symbols are correctly detected, (2.48) becomes,

$$
\check{x}_1[m] = x[m] + \check{\eta}[m].
\tag{2.48}
$$

However, the impact becomes destructive where $\ddot{x}_1[\cdot] \neq x[\cdot]$ for desired and ISI parts. Consequently, $\ddot{x}_\rho[\cdot]$ is regenerated based on the symbol decisions of $\check{x}_{\rho-1}[\cdot]$ at $(\rho - 1)$th iteration which is used to obtain $\check{x}_\rho[\cdot]$. As more symbols are correctly detected at the end of each iteration, the BER is reduced and bounded by the remaining undesired terms.

2.5   Iterative Likelihood Test

The iterative processing mentioned in the previous section demodulates all symbols together and reconstructs the blanked signal consecutively at each iteration. However, considering $\check{x}[\cdot]$, the impact of the impairing effects, $\varepsilon[\cdot]$, to each symbol may vary. For instance, the contribution of ISI, $\xi[\cdot]$, for each symbol is different in case of blanking. Also the impact of the noise and the channel equalization errors may not be the same for each symbol. Thus, it is useful to process reliable symbols initially based on their likelihoods.

Probability of error for the nth symbol can be defined as $\text{Pr}_e\{\check{x}[n]\} \triangleq \text{Pr}\{\check{x}[n] \neq x[n]\}$. Therefore, an optimum detector chooses $\check{x}[n]$ to minimize the $\text{Pr}_e\{\check{x}[\cdot]\}$. When the statistical distribution of the transmitted symbols is uniform, a maximum likelihood (ML) detector can be employed to minimize the Pr_e and choose the optimum ideal symbol value, ϕ_i, from the constellation map for each $\hat{s}[n]$. Notwithstanding, when the distribution is not known, uniform assumption can be made based on the Minimax Theorem [3]. Therefore, the decision rule becomes

$$\Gamma_i \triangleq \check{x}[n] \Rightarrow \phi_i, \text{ if } p_{\check{x}|\phi_i}(\check{x}[n]) \geq p_{\check{x}|\phi_i}j(\check{x}[n]), \forall i \neq j, \tag{2.49}$$

where Γ_i is the decision rule for symbol value, ϕ_i, $\{i, j\} \in [1, \mathcal{M}]$ and $p_{\check{x}|\phi_i}$ is defined as symbol transition probability density function of ϕ_i caused by impairing effects. A symbol $\check{x}[n]$ belongs to the decision region of an ideal symbol value, ϕ_i, if $p_{\check{x}|\phi_i}j(\check{x}[p]) < p_{\check{x}|\phi_i}j(\check{x}[q])$. From (2.49), the likelihood of each $\check{x}[n]$ for every ϕ_i can be calculated. However, the reliability of two symbols belonging to the decision region of ϕ_i, $\{\check{x}[p], \check{x}[q]\} \in \Gamma_i$, for two point constellation map can be defined comparing their likelihoods of belonging to $\phi_i j$ as

$$\mathcal{L}(\phi_i j \mid \check{x}[p]) > \mathcal{L}(\phi_i j \mid \check{x}[q]) \Leftrightarrow p_{\check{x}|\phi_i}j(\check{x}[p]) < p_{\check{x}|\phi_i}j(\check{x}[q]), \tag{2.50}$$

where $\mathcal{L}(\cdot)$ represents likelihood. Under the Gaussian assumption of the symbol distribution around each constellation point, (2.50) can be written based on log-likelihood ratios as

$$\log\left\{\frac{\mathcal{L}(\phi_i j \mid \check{x}[p])}{\mathcal{L}(\phi_i j \mid \check{x}[q])}\right\} > 1. \tag{2.51}$$

Therefore, the reliability of $\check{x}[p] \in \Gamma_i$ for $\mathcal{M}$-ary modulation scheme yields

$$\mathcal{L}_{\text{R}}\{\check{x}[q]\} = \log\left\{\frac{\mathcal{L}(\phi_i \mid \check{x}[p])}{\sum_{\substack{j=1 \\ j\neq i}}^{\mathcal{M}} \mathcal{L}(\phi_i j \mid \check{x}[p])}\right\}, \tag{2.52}$$

where $\mathcal{L}_{\text{R}}$ represents reliability based on log-likelihood ratios.

Based on the symbol reliabilities calculated above, the impact of the ISI can be reduced by initially accommodating the reliable symbols into iterations. We proposed two methods in this concept. The first

36

technique replaces the blanked part of the waveform with the reliable symbols in frequency-domain only. The second technique performs replacement both in time and frequency-domains. For both techniques, $\mathcal{L}_R \{\cdot\}$ of symbols ($\check{x}[\cdot]$) for all ϕ_i are calculated and collected in a vector

$$\mathcal{L}_R = [\mathcal{L}_R \{\check{x}[0]\} \mathcal{L}_R \{\check{x}[1]\} \cdots \mathcal{L}_R \{\check{x}[N-1]\}].$$

(2.53)

Thus, the most reliable symbol, $\check{x}[q] = \max\{\mathcal{L}_R\}$ is demodulated and regenerated as $\ddot{x}_1[q]$ first. For the second technique, the processing continues by replacing the obtained symbol in time-domain from the received equalized signal as

$$\hat{r}_1[n] = \begin{cases} \ddot{x}_1[q] & \text{, if } n = q, \\ \hat{r}[n] & \text{, otherwise,} \end{cases}$$

(2.54)

followed by DFT and blanking the interference to obtain $\check{X}_1[k]$. In the meantime, $\mathcal{F} \{\ddot{x}_1[\cdot]\}$ is taken after padding sample indexes with zero where $n \neq q$. This is followed by replacing the blanked samples of $\check{X}_1[k]$ as

$$\ddot{X}_2[k] = \begin{cases} \ddot{X}_1[k] & \text{, if } k_1 \leq k < k_2, \\ \check{X}_1[k] & \text{, otherwise,} \end{cases}$$

(2.55)

to satisfy the continuity. Consequently, the ISI caused by $\ddot{x}_1[q]$ and the contribution of the ISI to $\check{x}_1[q]$ is removed similar to (2.47). The signal in time-domain at the second iteration is obtained after inverse DFT of (2.55) and the remaining symbols accommodated into process subsequently.

Obviously, this technique increases the number of iterations compared to the non-reliable iterative process implemented in the previous section. However, it removes the impact of ISI and allows the reconstruction of the desired signal in a more controlled manner by beginning the processing from the most reliable symbols. In an iterative process convergence speed is analyzed for ICI removal in OFDM based systems where all symbols are considered together [78]. However, in our case symbol-by-symbol detection and ISI removal is performed. Thus, this technique can be further investigated to reduce the number of iterations by defining reliable symbol groups and process them initially.

2.6 Simulation and Results

Computer simulations are performed to investigate the performance of the proposed blanking algorithms. First, the impact of blanking some part of the SC-FDE and SC-FDMA signal spectrum is presented under AWGN and ITU Vehicular A (Veh.A) multipath channels. Then, the desired signals are overlapped with a narrow-band single-carrier DI signal with a roll-off factor of 0.35 and interference suppression performance of the of the proposed blanking algorithms are presented through link level simulations. Moreover, the capacity of the proposed techniques are investigated in the UL of LTE network by system level simulations for the DI scenarios when co-channel MUEs employing SC-FDMA scheme are at the vicinity of the HeNBs and overlapping with the HUEs employing SC-FDMA scheme. For all simulations, FFT size is 512, CP size is 40 samples (subcarriers), and ZF-FDE is performed. The spectrum to be blanked on the desired signal is set randomly for all cases (with or without interference).

2.6.1 Effects of Blanking on SC-FDE and SC-FDMA Schemes

Blanking bandwidth is set to be 1/4th of the bandwidth of the desired signal which is quiet large but necessary to compare the BER results of proposed blanking techniques. After extensive Monte Carlo simulations, the BER of the BPSK modulated SC-FDE signal under AWGN channel and the BER of the QPSK modulated SC-FDMA signal under multipath channel are shown in Fig. 2.2 and Fig. 2.3, respectively. For both signals, the BER of not performing any blanking on the SC-FDE signal is presented as a lower bound (No Blank. in figures). Also the BER of blanking with a rectangular window, and the performance of the first and the second iterations after repeating the demodulation and the regeneration steps based on all symbols are presented for various SNRs (Rect., Rect. It-1, Rect. It-2 in figures respectively). The improvement of the proposed rectangular windowing can be observed at low to medium SINR regions where interference cancellation methods operate usually. Better gains are observed at the first iteration and small enhancements are observed at the second iteration.

Optimum raised cosine filter is observed for blanking as well. In order to obtain optimum window, every possible raised cosine window is applied to the desired signal by changing the blanking bandwidth and the roll-off factor of the applied window. Finally, filter parameters are chosen based on the maximum SINR condition after filtering based on the power formulas derived previously. BER of the optimum raised
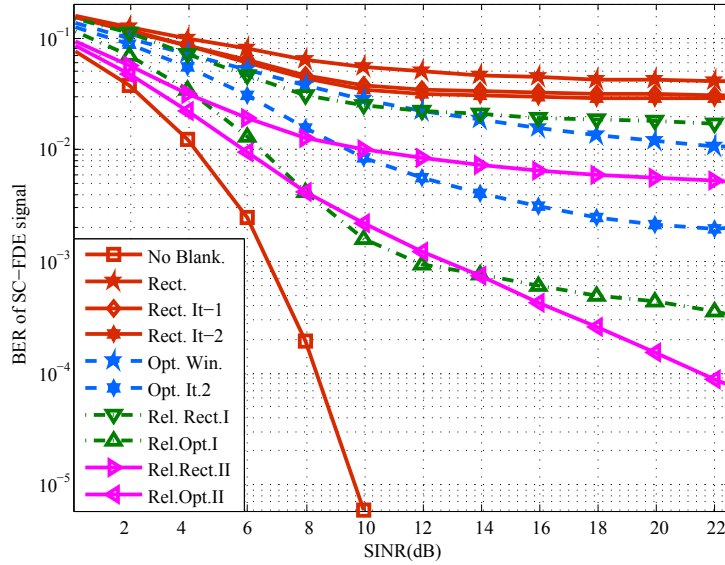
Figure 2.2: BER of SC-FDE - only blanking 1/4th of its spectrum (AWGN Channel, BPSK).
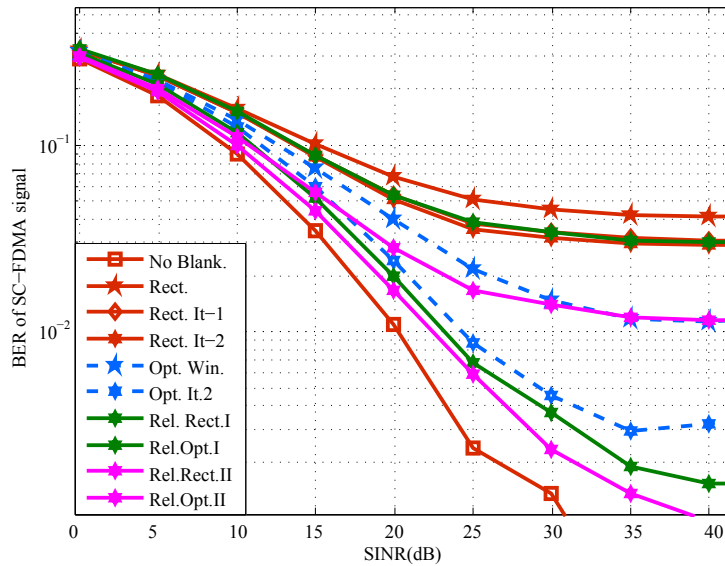
Figure 2.3: BER of SC-FDMA - only blanking 1/4th of its spectrum (ITU Veh.A Channel, QPSK).

cosine filter is less than the iterative rectangular blanking even without iterations (Opt. Win. on figures). Moreover, performance of the optimum window after second iteration reduced the BER remarkably. These results show the importance of the proper filtering.

All the previous results belonging to the proposed iterative receivers accommodate all symbols into iteration by regenerating and replacing the symbols after blanking. However, the iterations can be

performed based on the symbol reliabilities (Rel.Rect.I-II and Rel.Opt.I-II in figures). The first two results (Rel.Rect.I and Rel.Opt.I in Fig. 2.2 and in Fig. 2.3) are for blanking algorithms that are based on symbol reliabilities where the most reliable symbols are regenerated and replaced within the blanked spectrum only in frequency-domain. At each iteration, the most reliable 10 symbols are demodulated and replaced to reduce the iteration count. The BER of the iterative receiver with rectangular blanking approaches the BER of blanking with the optimum window without iterations. Secondly, iterative processing is performed based on symbol reliabilities by accommodating most reliable symbols into processing both in time and frequency-domains (Rel.Rect.II and Rel.Opt.II in Fig. 2.2 and Fig. 2.3). In this case the most reliable symbols are regenerated and replaced from the desired time-domain signal then the blanked band of the desired signal is replaced by the corresponding band of the reliable symbols. The results show that the BER curves of the iterative receivers based on symbol reliabilities are close to each other at low SNR region for optimum windowing case. As SNR increases, performing replacement both in time-domain and in frequency-domain (Rel.Rect.II, Rel.Opt.II) is better in terms of BERs, however, these techniques require more processing.

The performance of the proposed techniques are the same for BPSK modulated SC-FDMA signal under AWGN channel. Therefore BER curves of QPSK modulated SC-FDMA signal under multipath channel is analyzed as given in Fig. 2.3. The results are quiet interesting in this case. The comparative gains of the proposed algorithms are similar to the case for BPSK modulated SC-FDE signal under AWGN channel. However, the BER curve for the lower bound where no blanking is performed is closer to the BER curves obtained by the iterative receiver based on symbol reliabilities when optimum window is employed. Thus, we can conclude that the degradation of the BER under multipath channels are dominated by the channel itself.

In addition to the above, the performance of the proposed techniques are investigated including a convolutional coder/decoder to the simulation setup where various rate LTE based coding schemes are employed including higher order modulations such as 16QAM and 64QAM. Frequency-domain MMSE equalization is performed other than zero forcing as well. The results show that coding and MMSE equalization do not have hidden negative impact on the proposed techniques and similar relative gains are obtained for the proposed techniques shown in the figures.
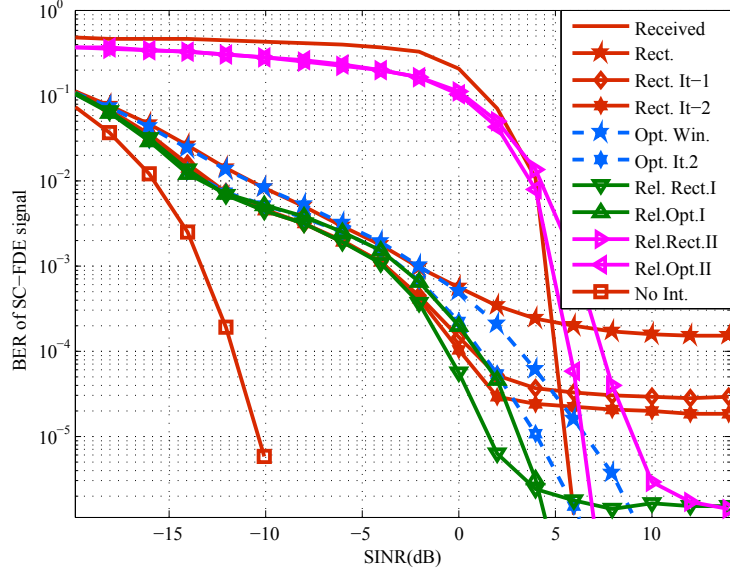
Figure 2.4: BER of SC-FDE under DI (AWGN Channel, BPSK).

2.6.2 Interference Cancellation Performance of the Blanking Algorithms

In this section interference cancellation performance of the proposed blanking algorithms are investigated for both SC-FDE and SC-FDMA signals in Fig. 2.4 and Fig. 2.5, respectively. A single-carrier signal with a roll-off factor of 0.35 is generated as an interference source and overlaps at 1/16th of the desired signal bandwidth. DI power is kept constant at 20 dB above the noise level, and the desired signal power is changed to modify the SINR. For comparison purposes, uncoded BERs of SC-FDE and SC-FDMA signals are plotted in case of no-interference and no-cancellation ("No Int." and "Received" in figures) with the same simulation parameters.

For all proposed blanking algorithms, interference has a negative impact on the BER performance because of the residue of the interference injected to the desired signal after blanking. No gain is observed for the reliable receivers where replacement is performed in time and frequency-domains (Rel.Rect.II, Rel.Opt.II) as shown in Fig. 2.4 and Fig. 2.5. The reason is that when replacing the most reliable symbols in time-domain, discontinuities and/or sharp changes in the interference signal cause the shape of the DI signal to be deformed in frequency-domain, out of band components arise and alters the desired signal. This can be verified by the reliable receiver results when replacement is performed only in frequency-domain (Rel.Rect.I, Rel.Opt.I). Best BER curves are obtained for iterative receiver where blanked part of the re-
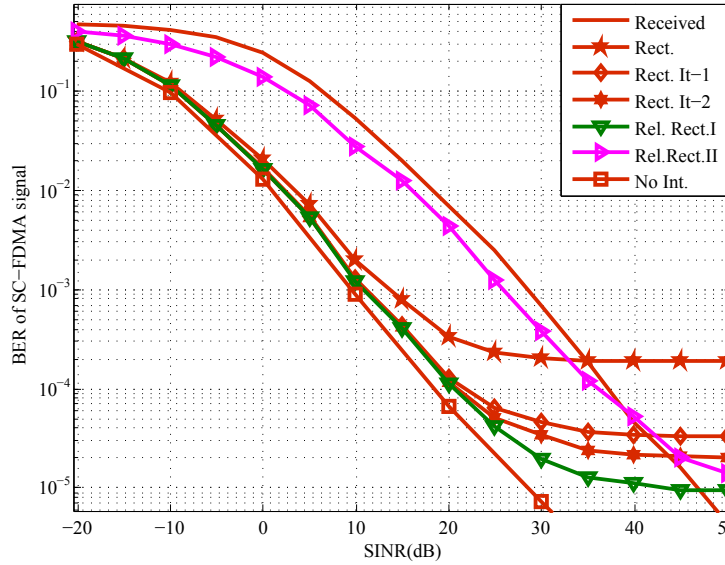
Figure 2.5: BER of SC-FDMA under DI (ITU Veh.A (6 taps) Channel, QPSK).

liable symbols are replaced only in frequency-domain. This is because, there is no discontinuity in the time-domain signal caused by symbol replacement. Additionally, performing blanking based on rectangular window causes an error floor for all cases at high SINR regions. However, the BER of blanking with an optimum window approaches the BER of received signal for high SNR region where the impact of interference can be neglected under AWGN channel.

In Fig. 2.5, we should note that optimum raised cosine windowing for all proposed blanking methods does not improve the BER of the received signal. After regenerating the desired signal from the symbol decisions, regenerated symbols are added to the raised cosine windowed desired signal which is performed in frequency-domain. Note that the regenerated symbols are multiplied by inverse of the blanking filter before adding to the desired signal. However, this causes the residue interference to be deformed and degrades the BER performance of the receiver. Thus, the best BER curve is obtained for the iterative receiver where reliable symbols are processed first and blanking is performed with a rectangular window. In this case BER curve is close to the no-interference case up to BERs $10^{-4} - 10^{-5}$.

2.6.3 Effects of DI on SC-FDMA Scheme

The SC-FDMA signal is generated based on the LTE UL specifications for 512 point FFT [79]. The minimum resource allocation unit is the resource block (RB) composed of 12 consecutive subcarriers for 5 SC-FDMA signal. 300 (25 RB) subcarriers are allocated in each SC-FDMA signal and remaining 106 subcarriers are left blank as guard band from both ends of SC-FDMA spectrum. On the other hand, a proactive indicator known as high interference indicator (HII) is planned to be exchanged between macrocell enhanced node base (MeNBs) that prevents users to be scheduled to the interfered RBs in LTE standard [79, p.298]. This interference coordination (IC) technique sacrifices from bandwidth utilization in order to avoid any overlap with the RBs of the DI signal which is simulated to compare the capacity of the proposed blanking techniques.

The capacity of each subcarrier can be calculated under the binary symmetric channel (BSC) assumption as ([80], p. 381)

$$C_{\text{BSC}} = \text{Pr}_e \log_2 (2\text{Pr}_e) + (1 - \text{Pr}_e) \log_2 2(1 - \text{Pr}_e), \tag{2.56}$$

where C_{BSC} is the capacity of BSC channel and Pr_e is as in (2.45). This assumption is valid with sufficient interleaving of symbols. Thus, the capacity of SC-FDMA signal yields

$$C_{\text{SC-FDMA}} = C_{\text{BSC}} \times n_{\text{M}} \times s_{\text{RB}} \times n_{\text{RB}} \times R, \tag{2.57}$$

where n_{M} is the modulation order, s_{RB} is the number of symbols in each RB, n_{RB} is the number of assigned RBs and R is the number of SC-FDMA signals per second. Capacity of BPSK modulated SC-FDMA signal in AWGN channel and QPSK modulated SC-FDMA signal in multipath channels, where different number of RBs are interfered is represented in Fig. 2.6 and Fig. 2.7. The blanking algorithms are chosen based on the best results obtained in the previous figures. The capacity of blanking algorithm is higher than the capacity of no-cancellation cases at various blanking rates and SINRs.
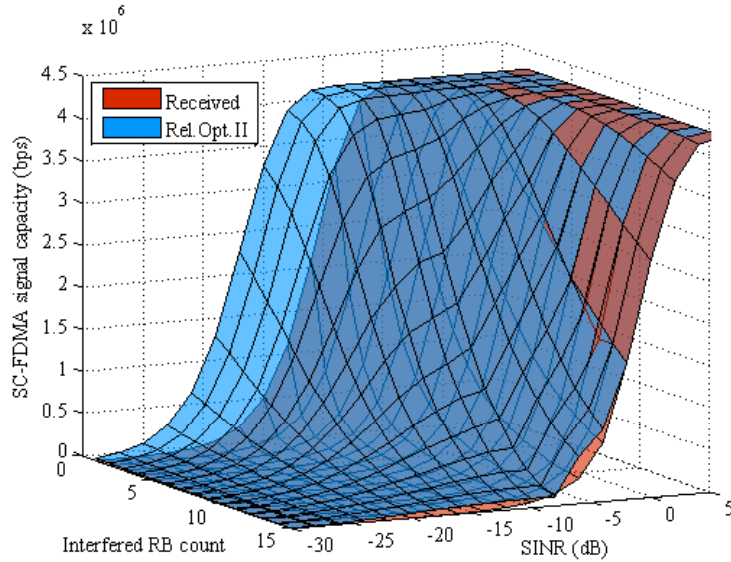
Figure 2.6: BSC capacity of SC-FDMA signal for different numbers of interfered RBs (1 to 15) and SINR levels in AWGN channel (BPSK).
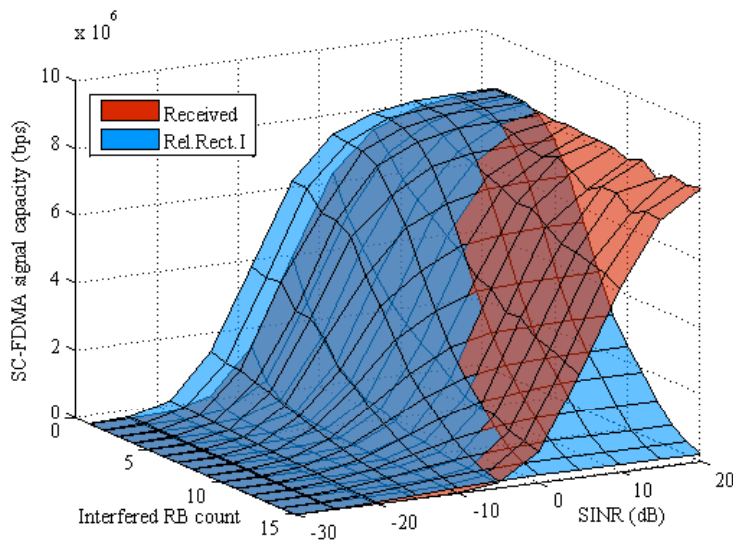
Figure 2.7: BSC capacity of SC-FDMA signal for different numbers of interfered RBs (1 to 15) and SINR levels (ITU Veh.A Channel, QPSK).

2.6.4 HetNet Scenario Example of the Blanking Algorithm

State-of-the-art interference avoidance/management techniques can be grouped under three major categories discussed in third generation partnership projec (3GPP) LTE standard as i) time-domain techniques, ii) frequency-domain techniques, iii) power control techniques [81]. Time-domain techniques are

based on no data transmission except reference signals at the interfered subframes which are known as almost blank subframe (ABSF). frequency-domain techniques schedule control channels and physical channels of different cells in reduced bandwidths for orthogonal transmissions. Power control techniques reduce the transmit power of the femtocell to improve the performance of the victim MUEs while sacrificing from femtocell throughput. As a baseline metric for comparison, we selected two techniques given in [46] which are no-eICIC and eICIC time. There is no action taken against the interference for no-eICIC technique. Time-domain eICIC technique is modified by turning off the transmission at the RBs below the target SINRs including reference signals. Thus, eICIC time sacrifices from bandwidth utilization in order to avoid any overlap with the RBs of the DI signal. In our link level physical layer simulations for the UL LTE network performance of the capacity cumulative distribution functions (CDF) of the proposed iterative blanking techniques are compared with no-eICIC and eICIC techniques in [46].

In a more practical system level scenario as shown in Fig. 2.8 macrocell eNode-B (MeNB), picocell eNode-B (PeNB) and femtocell eNode-Bs (HeNB) are distributed on a layout with user equipments of each eNode-B as MUE, PUE and HUE, respectively. HeNBs and HUEs are allocated indoor. Two stripe model is considered for apartments. Some other considered parameters are losses (wall loss, path loss, etc.), antenna radiation patterns, shadowing, minimum distances between nodes, etc. Only one HUE is connected to the HeNB which is scheduled to all RBs. Round-robin scheduling and fractional power control are implemented for MUEs and PUEs. Since frequency reuse ratio is one, all PUEs and MUEs are interfering at HeNB. For further details of the simulation assumptions, the reader is referred to [82].

Since the proposed techniques work well for small blanking ratios, we applied our proposed interference cancellation techniques to narrow-band DI scenarios in the UL of LTE system. Therefore, we simulated UL of an LTE network where SC-FDMA waveform is employed. For SC-FDMA waveform, 300 of 512 subcarriers are employed and the remaining subcarriers are left as guard bands. The macrocell is divided into three sectors where at each sector 25 RBs are shared between randomly distributed 20 users by assigning one or two RBs to each user within that sector. On the other hand, there is also one co-channel indoor HeNB is placed inside a building at each sector where one or two HUE is exploiting all resources of the HeNB. In other words, 12 up to 25 RBs are allocated for each HUE. Since MUEs are allocated to one or two RBs and HUEs are allocated to 12 up to 25 RBs, DI scenarios might occur at the HeNB especially when

45
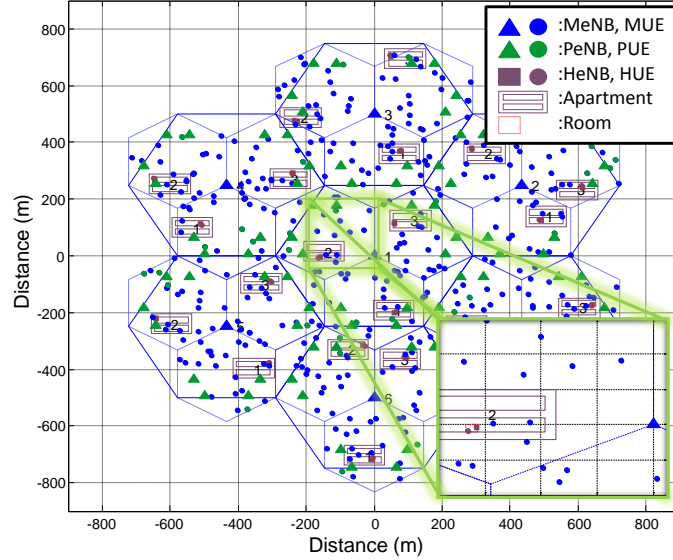
Figure 2.8: System level LTE HetNet simulation scenario.

MUEs are at the vicinity of HeNB. Therefore, interference caused by MUE signal is narrow-band relative to the HUE signal. At each run of the simulation scenario, interfered RBs are defined based on the target SINR values for HUEs and different number of RBs are interfered. In this context, we can assume that there is an interface between femtocell and macrocell networks to exchange information. This can be provided by a connection from backbone between networks which is discussed to be implemented between LTE macrocell base stations [79, p. 298]. For instance, HII message is exchanged with neighboring macrocell base stations to inform that a cell-edge user will be scheduled to certain RBs. Therefore, we consider this to define interfered RBs. Accordingly, proposed blanking techniques are applied and compared with the techniques mentioned as eICIC-time and no-eICIC techniques.

The capacity CDF of the HUE at the first sector of the center MeNB is investigated. Target received power of HUEs is set as -40 dBm and a threshold is used by the HeNB to decide existence of the DI. The difference between the target received HUE power and the DI power is compared to the threshold. If this is above the threshold, corresponding RBs are decided to be interfered by the DI. The capacity of proposed algorithms are higher than the capacity of the IC as shown in Fig. 2.9 and Fig. 2.10 because the number of the interfered RBs are small for HetNet scenarios, where blanking algorithm works effectively. In Fig. 2.9, the capacity CDF of two different deployments are investigated. In the first deployment scenario,
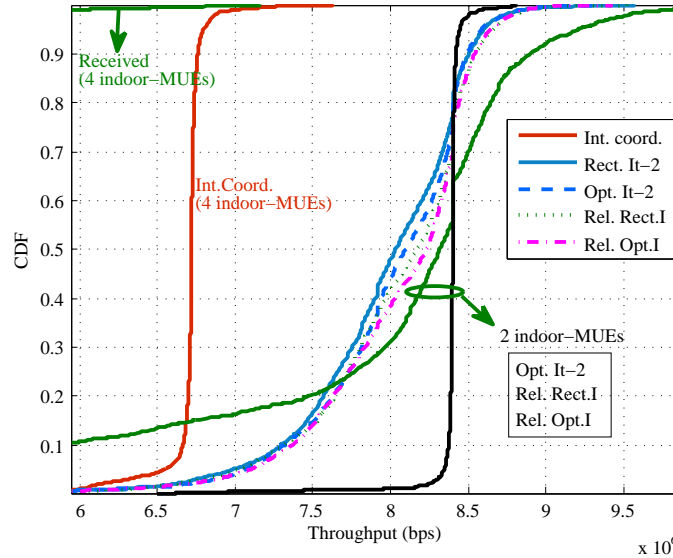
Figure 2.9: BSC CDF of HUEs for different receiver types (4 indoor-MUEs, Veh.A channel for HeNB.).
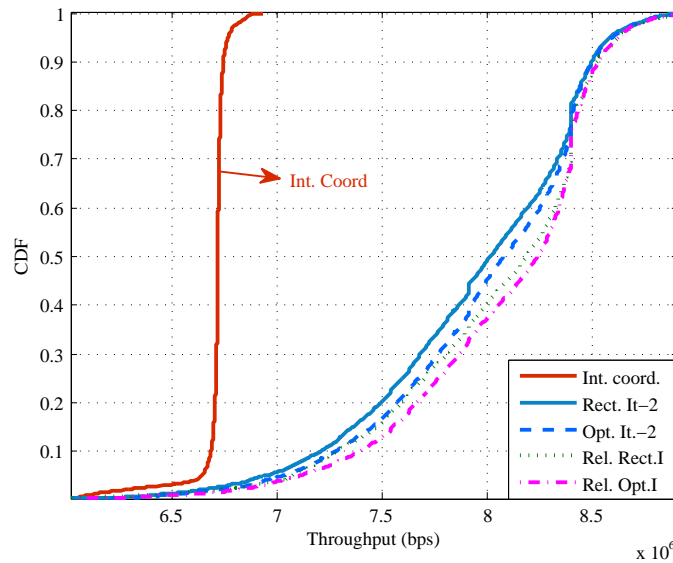
Figure 2.10: BSC CDF of HUEs for different receiver types (4 indoor-MUEs, AWGN channel for HeNB.).

2 indoor-MUEs are placed at each building (the right-most curves indicated with a circle). In the second, 4 indoor-MUEs are placed in average in the vicinity of HeNB. For the former, applied techniques have similar CDF because the proposed blanking methods (Opt. It-2, Rel. Rect.I, Rel. Opt.I) are capable of handling the interference (IC CDF, which rises to its peak between 7.5 Mbps and 8 Mbps, is not presented to observe other CDF curves clearly.). In the latter, interfered RBs increase so the received signal is dominated by

the interference and the difference in the capacity CDF of the proposed methods can be observed where the gains are ordered similar to the BER curves of the proposed methods given previously. In Fig. 2.10, the performance is investigated in case where the received signal at HeNB is exposed to AWGN channel to observe the increase in the comparative gains of the proposed techniques towards IC. Performance of all the proposed techniques are better than the IC where the amount of the gain varies based on the interference scenario.

CHAPTER 3

THEORETICAL ANALYSIS OF THE CO-EXISTENCE OF LTE-A SIGNALS AND DESIGN OF AN ML-SIC RECEIVER

Evolution of wireless services enabled advanced applications and shifted the paradigms of research in this field from voice to data centric.[1] Such services spreading like wildfire between users hence, increasing the demand for large capacity. Heterogeneous networks (HetNets) are addressed as a solution to increase the available resources and offload the macrocell traffic. Thus, spectral efficiency is boosted per unit area via spatial reuse of resources. On the contrary, HetNets may preclude to fully exploit the universal reuse of spectrum due to inevitable interference scenarios between macrocell and HetNet signals. Consequently, the capacity of the current wireless systems is interference-limited and spectrum access schemes become very important to exploit the spectrum efficiently.

Mainly, there are orthogonal and non-orthogonal access schemes in HetNets. For orthogonal access schemes, as more mobile stations (MSs) request access to the network, the existing resources are shared among all MSs with some sacrifice from their resources. Alternatively, the MSs that are claiming access to the network can wait until the resources become available. Interference coordination is one of the solutions where interfering nodes cooperate to switch-off their transmission at some resources. Base stations (BSs) can also apply range expansion techniques in the same context [46]. Obviously, these approaches sacrifice from throughput for orthogonalization and require self-organization (i.e. exchange of information between macrocell and HetNet nodes through backhaul link) to increase the overall throughput of the system.

Non-orthogonal access schemes are also studied as another class of solution. In this case, the signals are non-orthogonally allocated to the resources and multi-user detection (MUD) approaches are employed to distinguish these signals at the receiver. For instance, the signal with large signal-to-noise-ratio is decoded, regenerated and subtracted from the composite signal. Then, the signal with low SNR is

---

[1]The content of this chapter is partially submitted to [83]. Copyright of the publication can be found in Appendix E.
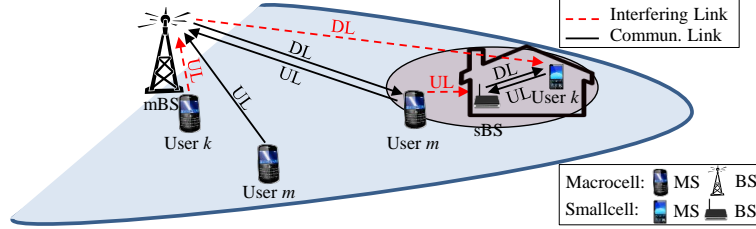
Figure 3.1: System level scenario.

decoded from the remainder. This approach is a.k.a c-SIC where many variations of it are proposed in the literature. According to the Shannon's capacity, non-orthogonal access with code-word based SIC achieves the multi-user capacity region and superior to orthogonal access [3]. Thus, non-orthogonal access schemes are superior to orthogonal access schemes in terms of spectral efficiency with additional processing in return.

The SIC approaches are studied for the code division multiple access (CDMA) systems since orthogonality is altered between the signals due to near-far effect and/or wireless channel [62]. Besides, inevitable interference scenarios can be handled in a controlled manner to improve the performance of these systems [84, 85]. The SIC approaches in orthogonal frequency division multiple access (OFDMA) systems is also very important. For instance, the MSs closer to the BS can exploit the resources more efficiently compared to the MSs far from the BS due to the limitations in the transmit power of the MSs. To provide access to all users for fairness and spectral efficiency, the same resources are allocated to these users non-orthogonally [86]. Then, a conventional-successive interference cancellation (c-SIC) approach is employed as an MUD receiver in the UL. The same approach is also useful in the uplink (UL) of the HetNet to offload the macrocell MSs (mMSs) from macrocell to smallcell by sharing the common resources with the smallcell MSs (sMSs) (see right side of Fig. 3.1) [65]. However, the theoretical analysis of the co-existence of OFDMA signals is important and not provided in [86] and [65]. On the other hand, allocating different types of signals to the co-existing users (i.e. OFDMA and SC-FDMA) for non-orthogonal accessing can be an alternative approach. In this case, the interference observed by the signals of co-existing users have different impact on the received symbols. Therefore, a design of an MUD receiver that adapts itself to the co-existence scenario becomes necessary.

In this chapter, the co-existence of OFDMA and single carrier-frequency domain multiple access (SC-FDMA) signals are analyzed to bring another degree of freedom to the MUD processing. To reveal

the characteristics of co-existence, the frequency and power domains are employed. First, the co-existence of SC-FDMA and OFDMA signals are analyzed based on the overlap ratio and the received power of the corresponding signals for a c-SIC in the link-level. Then, the closed form expressions of the average BER are derived as a baseline. The statistical distribution of the interference in different cases of co-existence lead us to design a new SIC based MUD receiver, namely maximum likelihood-SIC (ML-SIC) receiver, which outperforms the c-SIC approach.

In general, SIC schemes are usually integrated with power control approaches to improve the throughput performance of the network in the system-level [84, 85]. For instance, the power of the co-existing signals are modified to ensure that these signals can be distinguished at the receiver. In the meantime, the allocation of a very large power for the co-existing signals is avoided to prevent the interference to the surrounding macrocells. In this context, we proposed three different power control schemes which are integrated to the ML-SIC receiver for the HetNet deployment model. Then, the impact of the power control schemes on the throughput of the proposed co-existence approach and the ML-SIC receiver is presented in a practical system-level scenario. As a baseline, the performance of the proposed combination of methods (co-existence of different types of signals, ML-SIC receiver and power control) is compared to the c-SIC receiver and the interference coordination approaches.

This chapter is organized as follows: Section 3.2 introduces the system model and the common interference issues in the current systems. Then, the co-existence scenarios are analyzed in Section 3.3 followed by the average bit-error-rate (BER) analysis for the c-SIC in Section 3.4.[2] The impact of frequency offset between co-existing signals are analyzed in Section 3.5 and the ML-SIC receiver is proposed in Section 3.6. Then, the power allocation schemes are explained in Section 3.7. Simulation results are presented in Section 3.8.

3.1 System Model

In a multi-carrier multiple access wireless mobile network, assume that N number of subcarriers of an OFDMA (or SC-FDMA) signal in a set $\mathcal{N} = \{0 \leq n < N-1 | n \in \mathbb{Z}\}$ are shared by two MSs, namely user m and user k. The subcarrier sets of user m and user k are $\mathcal{N}_m$ and $\mathcal{N}_k$, where user m's and user k's subcarriers,

---

[2]The term "BER" is used for "average BER" at the remainder of the chapter.

$x_{m,n} \in \mathcal{N}_m$ and $x_{k,n} \in \mathcal{N}_k$, are allocated at the indices $n \in [m_1, m_2]$ and $n \in [k_1, k_2]$ respectively as shown in Fig. 3.2(a). After inverse discrete Fourier transform (IDFT) of subcarriers and cyclic prefix (CP) attachment, the signals are transmitted through the wireless channel. It is assumed that the maximum excess delay of the channel is smaller than the cyclic prefix duration, and time/frequency synchronization is achieved at the receiver. Note that, this co-existence model is valid for homogeneous and HetNet deployment schemes and the rest of the model is explained for each scheme separately. For clarity, common interference scenarios in cellular networks based on path-loss is summarized in Table 3.1. For the homogeneous deployment model (the first row in Table 3.1), the near and far MS signals can co-exist at the BS in the UL. The signals of different BSs can also be overlapped for non-orthogonal access for the cell-edge MSs in the DL. In HetNets, (second and third rows in Table 3.1) the useful co-existence scenarios depend on the distance between the MSs and the BSs. For both models, the UL case is considered at the rest of the chapter for analysis.

Table 3.1: Common scenarios for non-orthogonal accessing.

Scenario	Uplink	Downlink
Near & far MSs	near MS & far MS @BS	BS_1 & BS_2 @MS
mMS near to far sBS	mMS & sMS @sBS	sBS & mBS @mMS
mMS far to near sBS	sMS & mMS @mBS	mBS & sBS @sMS

3.1.1 Homogeneous Deployment Model

The nth subcarrier ($n \in [n_1, n_2]$) of the received composite signal of user m and user k at the BS is

$$y_n = \sqrt{p_{m,n}} x_{m,n} h_{m,n} + \sqrt{p_{k,n}} x_{k,n} h_{k,n} + \eta_n, \qquad (3.1)$$

where $p_{m,n}$ and $p_{k,n}$ are received powers, $h_{m,n}$ and $h_{k,n}$ are the channel frequency responses of the signals of user m and user k at the nth subcarrier, and η_n is the independent and identically distributed complex additional white Gaussian noise (AWGN) with σ_η^2 variance at the nth subcarrier. To overlap the subcarriers at their optimum sampling points as in (3.1), the propagation delay is compensated by timing advance in

52
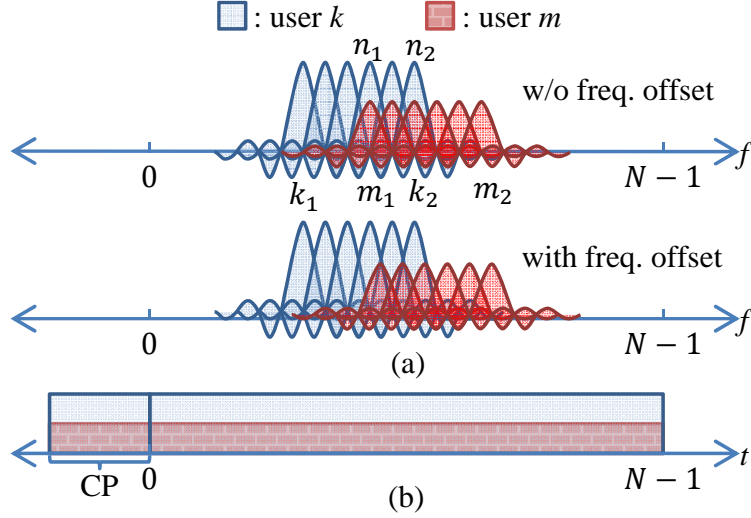
Figure 3.2: Overlapping in (a) frequency and (b) in time domains.

the UL (for MSs shown in the left side of Fig. 3.1) [87]. Hence, both signals arrive to the BS as shown in Fig. 3.2(b). On the other hand, a power gap between the co-existing signals is required at the receiver to achieve non-orthogonal access by successive processing. Thus, transmit powers can be tuned for the MSs considering the characteristics of the wireless channel.

3.1.2 Heterogeneous Deployment Model

In HetNets, timing advance becomes complicated for the co-existing signals of different tiers (i.e. for the mMS and sMS signals received at the sBS at right side of Fig. 3.1). However, reception without interference due to misalignment is possible if the sBS seeks for a synchronization point for nearby interfering mMS. For instance, consider the the UL case given at the second row of Table 3.1. A mMS is at the vicinity of the sBS and, mMS and sMS signals co-exist at the sBS. Thus, the sBS seeks for a synchronization point for the sMS to receive the composite signal aligned at the sBS. In the rest of the chapter, the CP duration is assumed to be large enough to provide that the the co-existing signals are aligned in time domain after removing the CP.[3]

---

[3]It is worth to note that OFDMA and SC-FDMA schemes are employed in the DL and UL of the LTE-A systems respectively. In the following sections, both schemes are assumed to be applicable in the UL for our analysis.

3.2 Analysis of Co-Existence Under c-SIC

In Fig. 3.2(a) the signals of user m and user k are co-existing at the indices $n \in [n_1, n_2]$ either at the optimum sampling points of their subcarriers or with a frequency offset between the signals of user k and user m. First, the co-existance without frequency offset is analyzed for the c-SIC processing.

3.2.1 Impact of Co-existentce without Frequency Offset

In this framework, since the signal-to-interference-plus-noise-ratio (SINR) of user k is larger than the SINR of user m, $\gamma_k > \gamma_m$, the signal of user k is decoded first. Thus, (3.1) is equalized for user k in a zero-forcing fashion

$$\beta_{k,n} = x_{k,n} + x_{m,n}\phi_{m,n} + \hat{\eta}_{k,n}, \tag{3.2}$$

where $\phi_{m,n} = \sqrt{\frac{p_{m,n}}{p_{k,n}}} \frac{h_{m,n}}{h_{k,n}}$ and $\hat{\eta}_{k,n} = \frac{\eta_n}{\sqrt{p_{k,n}}h_{k,n}}$. The subcarriers of user k are obtained at the output of the demodulator from (3.2). After decoding (3.2) for user k, the subcarrier of user k is regenerated as $\hat{y}_{k,n}$. Then, the subcarrier of user m is obtained by subtracting $\hat{y}_{k,n}$ from (3.1) and equalizing the remainder for user m as

$$\beta_{m,n} = \frac{y_n - \hat{y}_{k,n}}{\sqrt{p_{m,n}}h_{m,n}} = x_{m,n} + \overbrace{\left(x_{k,n} - \hat{x}_{k,n}\right)\phi_{k,n}}^{\mathcal{I}_{m,n}} + \hat{\eta}_{m,n}, \tag{3.3}$$

where the second term, $\mathcal{I}_{m,n}$, represents the interference due to an error at the symbol decision on $\beta_{k,n}$ and $\phi_{k,n} = \phi_{m,n}^{-1}$. Obviously, the BER of user k's signal is affected by the user m's subcarrier in (3.2), and (3.3) shows that the BER of user m's signal is affected by the user k's decoding errors in c-SIC processing. However, this analysis is independent of the type of co-existing pairs. Thus, the analysis is extended to four possible pairs of the signals of user k / user m such as OFDMA/OFDMA, OFDMA/SC-FDMA, SC-FDMA/OFDMA and SC-FDMA/SC-FDMA for further analysis.

3.2.2 Analysis of Interference on OFDMA Symbols

Analysis of overlapping two OFDMA signals is quite straightforward since the subcarriers $x_{k,n}$ and $x_{m,n}$ in (3.2) and (3.3) are the symbols $s_{k,n}$ and $s_{m,n}$ respectively. Thus, the error term at the nth symbol of user k due to the nth symbol of user m is

$$\xi_{k,n} = s_{m,n}\phi_{m,n}. \tag{3.4}$$

Likewise, the error term at the user m's symbol due to user k's symbol decision error is

$$\xi_{m,n} = \left(s_{k,n} - \hat{s}_{k,n}\right)\phi_{k,n}, \tag{3.5}$$

where $\xi_{m,n}$ vanishes for the correct decision of user m's symbol. In AWGN channel, $h_{k,n}$ and $h_{m,n}$ drops from $\phi_{k,n}$ and $\phi_{m,n}$. Thus, the error terms in (3.4) and (3.5) are affected by the received power and the modulation scheme of the paired signal. Note that the transmitted symbols are assumed to be uniformly distributed and AWGN noise is added at the receiver. Therefore, the interference has Gaussian mixture uniform distribution. Also, if the SNRs of the signals are large, $(p_{k,n}, p_{m,n}) \gg \sigma_\eta^2$, uniform distribution becomes dominant.

In the second scenario, the user k employs OFDMA scheme and the user m employs SC-FDMA scheme. Due to additional DFT operation in SC-FDMA signal, an overlapping subcarrier of user k is affected by all symbols of the user m. The error term on user k's symbol is

$$\xi_{k,n} = x_{m,n}\phi_{m,n} = \frac{\phi_{m,n}}{\sqrt{N_m}}\sum_{l=0}^{N_m-1} s_{m,l}e^{-j2\pi l(n-m_1)/N_m}, \tag{3.6}$$

where l is user m's symbol index and the exponential coefficient is shifted by m_1 to observe the impact on the nth symbol of user k. In other words, the user m's symbols are allocated to the sinc($\cdot$) functions for each symbol index and followed by DFT operation. This results in N_m number of rectangular windowed orthogonal sinusoids in frequency domain which are multiplied by the complex symbol values. Thus, the error term at the nth symbol of user k, $\xi_{k,n}$, is sum of the value of sinusoids at the nth subcarrier index. Therefore, Gaussian approximation (GA) for the distribution of $\xi_{k,n}$ becomes valid for large N_m. In AWGN channel, the impact of error term and noise together is Gaussian with the variance of $(\sigma_\eta^2 + p_{m,n})$.

Similar to the previous case, user m's signal is obtained by c-SIC processing. Then, the impact of user k's symbol decision error on user m's symbols is

$$\xi_{m,l} = \frac{1}{\sqrt{N_m}}\sum_{n=n_1}^{n_2} \left(s_{k,n} - \hat{s}_{k,n}\right)\phi_{k,n}e^{j2\pi l(n-m_1)/N_m}. \tag{3.7}$$

In this case, GA also holds for the distribution of (3.7) and the variance of error with noise is $(\sigma_\eta^2 + (s_{k,n} - \hat{s}_{k,n})p_{k,n})$.

3.2.3 Analysis of Interference on SC-FDMA Symbols

Analysis of co-existing SC-FDMA signals is a bit devious due to additional DFT operation. Considering SC-FDMA/SC-FDMA overlapping scenario, user k's symbols are obtained after N_k point IDFT of $\beta_{k,n}$ given in (3.2) for subcarriers, $\forall n \in [k_1, k_2]$, which is

$$
\begin{aligned}
\alpha_{k,r} &= \frac{1}{\sqrt{N_k}} \sum_{n=k_1}^{k_2} (x_{k,n} + x_{m,n}\phi_{m,n} + \hat{\eta}_{k,n}) e^{j2\pi r(n-k_1)/N_k} \\
&= s_{k,r} + \xi_{k,r} + \hat{\omega}_{k,r},
\end{aligned}
\tag{3.8}
$$

where r is user k's symbol index, $\xi_{k,r}$ is the error term caused by the symbols of user m and $\hat{\omega}_{k,r}$ is the IDFT of noise term. The error term, $\xi_{k,r}$, in (3.8) can be expressed in terms of user m's symbols, which is

$$
\begin{aligned}
\xi_{k,r} &= \frac{1}{\sqrt{N_k}} \sum_{n=n_1}^{n_2} x_{m,n}\phi_{m,n} e^{j2\pi r(n-k_1)/N_k} \\
&= \frac{1}{\sqrt{N_k N_m}} \sum_{n=n_1}^{n_2} \sum_{l=0}^{N_m-1} s_{m,l}\phi_{m,n} e^{j2\pi \left(\frac{r(n-k_1)}{N_k} - \frac{l(n-m_1)}{N_m} \right)},
\end{aligned}
\tag{3.9}
$$

where l is user m's symbol index. All symbols of user m affect all symbols of user k in the form of error. The statistical distribution of $\xi_{k,r}$ in AWGN channel can be thought as Gaussian due to DFT/IDFT operation. However, if all subcarriers of user k and user m are overlapping and $N_k = N_m$, (3.9) reduces to

$$
\xi_{k,r} = s_{m,r} \otimes \Phi_{m,r},
\tag{3.10}
$$

where $\otimes$ is the circular convolution operator and $\Phi_{m,r}$ is the time domain reciprocal of $\phi_{m,n}$. The error on user k's symbol is contributed by the symbol of user m at the same index. In this case, (3.9) is equal to (3.4), which is given for OFDMA/OFDMA co-existence in AWGN channel. Moving ahead from (3.9) by interchanging the sum terms and rearranging the equation for AWGN channel, the error term becomes

$$
\xi_{k,r} = \frac{1}{\sqrt{N_k N_m}} \sum_{l=0}^{N_m-1} s_{m,l} \sum_{n=m_1}^{k_2} e^{j2\pi \left(\frac{r(n-k_1)}{N_k} - \frac{l(n-m_1)}{N_m} \right)}.
\tag{3.11}
$$

A particular scenario helps to provide a compact form of (3.11) by assuming $N_k = N_m$. The overlapping subcarriers of user m, $\forall n \in [m_1, k_2]$, is further assumed to be shifted to the indices $n \in [k_1, k_1 + k_2 - m_1]$. This shifting operation in frequency domain causes multiplication of user m's subcarriers by an exponential. Therefore, (3.11) is simplified to

$$\xi_{k,r} = \frac{1}{N_k} \sum_{l=0}^{N_k-1} s_{m,l} \sum_{n=k_1}^{k_1+k_2-m_1} e^{j2\pi \left(\frac{(n-k_1)}{N_k}(r-l) \right)}. \tag{3.12}$$

Considering the cases $r \neq l$ and $r = l$ separately, (3.12) becomes

$$\xi_{k,r} = \begin{cases} \frac{1}{N_k} \sum\limits_{l=0}^{N_k-1} s_{m,l} \sum\limits_{n=k_1}^{k_1+k_2-m_1} e^{j2\pi \left(\frac{(n-k_1)}{N_k}(r-l) \right)} & , r \neq l, \\[2mm] \frac{1}{N_k} \sum\limits_{n=0}^{N-1} s_{m,l} \dfrac{k_2 - m_1}{N_k} & , r = l. \end{cases} \tag{3.13}$$

The exponential sum terms in (3.13) can be reduced by utilizing the formula, $\sum_{a=0}^{N-1} b^a = \frac{1-b^N}{1-b}$, and a compact form is

$$\xi_{k,r} = s_{m,l} \frac{N_o}{N_k} + \frac{1}{N_k} \sum_{\substack{l=0 \\ l \neq r}}^{N-1} s_{m,l} \frac{c^{k_2-m_1} - c^{k_1}}{1-c}, \tag{3.14}$$

where N_o is number of overlapping subcarriers and $c = e^{j2\pi(r-l)/N_k}$. A careful observation of (3.14) shows that $\xi_{k,r}$ is composed of user m's symbols multiplied by a sinc-like function. The first term in (3.14) is uniformly distributed which represents the peak of the sinc-like function scaled by the overlapping ratio of the user m's signal. The second term is contributed by the symbols of user m ($r \neq l$) which are scaled by complex coefficients that are following the side-lobes of the sinc-like function. Therefore, the distribution of the second term can assumed to be Gaussian. Moreover, the interference power is N_o/N_k of the power of user m's signal. Accordingly, the power of the uniform distributed term in (3.14) is $(N_o/N_k)^2$. Hence, the power of the Gaussian distributed term in (3.14) is $N_o/N_k - (N_o/N_k)^2 = N_o(N_k - N_o)/N_k^2$. Consequently, as the overlap ratio between the signals of user k and user m increase, the impact of user m's signal is dominated by the uniform distributed term where GA becomes dominant vice-versa. Although this analysis is for the case when ($N_k = N_m$), the results can be generalized. For instance, if $N_k \neq N_m$ the impact of uniformly

57

distributed term decreases. Accordingly, when $N_k \ll N_m$ or $N_k \gg N_m$, the distribution is assumed to be Gaussian only.

Next, the subcarriers of user m are obtained by c-SIC processing as in (3.3) followed by N_m-point IDFT operation. The symbols of user m at the input of the decision device is similar to (3.8). The error term on user m's signal due to user k's symbol decision error is also similar to (3.9).[4] Then, the final form of the error term on user m's symbol due to user k's symbol decision error is

$$\xi_{m,l} = \left(s_{k,r} - \hat{s}_{k,r}\right) \frac{N_o}{N_k} + \frac{1}{N_k} \sum_{\substack{l=0 \\ l \neq r}}^{N-1} \left(s_{k,r} - \hat{s}_{k,r}\right) \frac{c^{k_2 - m_1} - c^{k_1}}{1 - c}. \tag{3.15}$$

When ($N_k = N_m$), (3.15) reduces to

$$\xi_{m,l} = \left(s_{k,l} - \hat{s}_{k,l}\right). \tag{3.16}$$

In the last scenario user k employs SC-FDMA scheme and user m employs OFDMA scheme. This is similar to the OFDMA/SC-FDMA overlapping scenario given before. Thus, the error term on the symbols of users can be written as in (3.6) and (3.7). However, the SC-FDMA user's signal is decoded first in this case. Accordingly, the distribution of the paired signal on the desired signal becomes Gaussian. The variance of the error term plus noise on the SC-FDMA and OFDMA signals are $(\sigma_\eta^2 + p_{m,n})$ and $(\sigma_\eta^2 + (s_{k,n} - \hat{s}_{k,n}) p_{k,n})$ respectively.

3.3   Analysis of BER for c-SIC

In this section, the statistics of the error terms and the SINRs of the co-existing signals are employed to derive the BER. Although the SINR is defined for each subcarrier traditionally, the average SINR can also be defined considering all subcarriers that are assigned to a user. Thus, the SINR of user k's signal in AWGN channel is obtained by considering non-overlapping and co-existing subcarriers, which is

$$\gamma_k = \sum_{\substack{n=k_1 \\ n \notin [n_1, n_2]}}^{k_2} \frac{p_{k,n}}{\sigma_\eta^2} + \sum_{n=n_1}^{n_2} \frac{p_{k,n}}{p_{m,n} + \sigma_\eta^2}. \tag{3.17}$$

[4]Note that the indices are modified while re-writing the equations. The intermediate steps are ignored to reduce the repetitions.

58

Similarly, the SINR of user m's signal is

$$\gamma_m = \sum_{\substack{n=m_1 \\ n \notin [n_1, n_2]}}^{m_2} \frac{p_{m,n}}{\sigma_\eta^2} + \sum_{n=n_1}^{n_2} \frac{p_{m,n}}{p_{k,n} \left| x_{k,n} - \hat{x}_{k,n} \right|^2 + \sigma_\eta^2}. \tag{3.18}$$

Note that if all subcarriers overlap, the first terms disappear in (3.17) and (3.18).[5] Accordingly, considering the co-existence scenario w/o frequency offset given in Fig. 3.2(a), a generalized form of the BER based on the SINR of a user can be given by the weighted sum of the BER of non-overlapping and co-existing subcarriers as

$$\text{Pr}_u = \frac{N_{\mathcal{D},u}}{N_u} \text{Pr}_{\mathcal{D},u} + \frac{N_{\mathcal{I},u}}{N_u} \text{Pr}_{\mathcal{I},u}, \tag{3.19}$$

where N_u is the number subcarriers of user u, $N_{\mathcal{D},u}$ and $N_{\mathcal{I},u}$ are the numbers of co-existing and non-overlapping subcarriers, $\text{Pr}_{\mathcal{D},u}$ and $\text{Pr}_{\mathcal{I},u}$ are the BERs of co-existing and non-overlapping subcarriers of user u respectively.

3.3.1 Co-existence of OFDMA Signals

In AWGN channel, a co-existing symbol of user k is altered by the ratio of the received power of overlapping subcarriers, $p_{m,n}/p_{k,n}$, the variance of the noise, σ_η^2, and the symbol value of the paired symbol, $s_{m,n}$, in (3.4). These terms contribute into the error probability and integrated into Marcum Q-function to derive the BER of user k's signal. Since $p_{m,n}$, $p_{k,n}$ and σ_η^2 are assumed to be known, the average error that is introduced by symbols of user m is calculated. Assume that the co-existing symbol pair is defined as (c_m, c_k). For instance, the combination of symbols for BPSK modulation is $\forall (c_m, c_k) \in C = \{(-1, -1), (-1, 1), (1, -1), (1, 1)\}$. Thus, the BER of user k's signal in the form of (3.19) is

$$\text{Pr}_k = \frac{N_k - N_o}{N_k} \underbrace{Q\left(\sqrt{\frac{p_k}{\sigma_\eta^2}} \right)}_{\text{Pr}_{\mathcal{D},k}} + \frac{N_o}{N_k} \underbrace{\frac{1}{N_c} \sum_C Q\left(\sqrt{\frac{|p_k c_k + p_m c_m|}{\sigma_\eta^2}} \right)}_{\text{Pr}_{\mathcal{I},k}}, \tag{3.20}$$

where N_o is the number of co-existing subcarriers, $\text{Pr}_{\mathcal{D},k}$ and $\text{Pr}_{\mathcal{I},k}$ are the average BER of the co-existing and non-overlapping subcarriers of user k respectively.

---

[5]The variance of the noise is normalized within the user's band hence, has subcarrier index is removed from the noise term.

Next, the subcarriers of user m are obtained by c-SIC processing. Since $p_k > p_m$, the BER of the overlapping subcarriers of user m, $\text{Pr}_{\mathcal{I},m}$, is bounded by $\text{Pr}_{\mathcal{I},k}$ given in (3.20) due to the wrong decision of the user k's co-existing symbols. Otherwise, the noise term defines the BER which is $\text{Pr}_{\mathcal{D},m}$. Thus, the BER of user m's signal is

$$\text{Pr}_m = \frac{N_o}{N_m}\left(\text{Pr}_{\mathcal{I},k} + (1 - \text{Pr}_{\mathcal{I},k})\,\text{Pr}_{\mathcal{D},m}\right) + \frac{N_m - N_o}{N_m}\text{Pr}_{\mathcal{D},m}, \tag{3.21}$$

where $\text{Pr}_{\mathcal{D},m}$ is $Q(\sqrt{P_m/\sigma_\eta^2})$.

3.3.2 Co-existence of SC-FDMA Signals

The error terms in (3.14) and (3.15) shows that the distribution of the error is uniform mixture Gaussian. For the cases where Gaussian distribution is dominant the BER expression reduces to a single Q-function. The error power caused by user m is scaled by N_o/N_k and distributed over the symbols of user k. In this case, the average BER of user k is

$$\text{Pr}_k = Q\left(\sqrt{\frac{p_k}{p_m\frac{N_o}{N_k} + \sigma_\eta^2}}\right) = \text{Pr}_{\mathcal{I},k}. \tag{3.22}$$

The average BER of user m's signal is limited by the interference caused by user k's signal regeneration errors and the noise. The power of regeneration error is obtained by multiplying the normalized expected power of a symbol decision error, P_ψ, user k's signal power, p_k, and overlap ratio, N_o/N_k. The power of a single symbol decision error is $|\psi_i - \psi_j|^2$ where ψ_i is the value of the correct symbol and ψ_j is the value of the misdetected symbol. Then, P_ψ can be calculated by averaging for all symbols of the employed modulation scheme based on the symbol transition probabilities which is

$$P_\psi = \frac{1}{\mathcal{M}(\mathcal{M}-1)}\sum_{i=0}^{\mathcal{M}-1}\sum_{\substack{j=0\\j\neq i}}^{\mathcal{M}-1} p(\psi_j|\psi_i)\,|\psi_i - \psi_j|^2, \tag{3.23}$$

where $\mathcal{M}$ is the number of symbols and ψ_i is the ith symbol value of the corresponding modulation scheme. Thus, the average BER of user m is

$$\mathrm{Pr}_m = Q\left(\sqrt{\frac{p_m}{P_\psi \mathrm{Pr}_{\mathcal{I},k} p_k \frac{N_\mathcal{I}}{N_m} + \sigma_\eta^2}}\right). \tag{3.24}$$

On the other hand, when the uniform distributed components are dominant in (3.14) and (3.15), the BER of user k and user m is same as OFDMA/OFDMA co-existence in (3.20) and (3.21) respectively. Note that when both uniform and Gaussian distributed components of the error terms in (3.14) and (3.15) are effective, the BER of users can be obtained by introducing the BER expressions for uniform and Gaussian components after scaling.

3.3.3 Co-existence of OFDMA and SC-FDMA Signals

Since the user m employs SC-FDMA, the impact of user m is modeled by GA. Thus, the BER of the co-existing symbols of user k in (3.20) is simplified and the BER is

$$\mathrm{Pr}_k = \frac{N_k - N_o}{N_k}\underbrace{Q\left(\sqrt{\frac{p_k}{\sigma_\eta^2}}\right)}_{\mathrm{Pr}_{\mathcal{D},k}} + \frac{N_o}{N_k}\underbrace{Q\left(\sqrt{\frac{p_k}{p_m + \sigma_\eta^2}}\right)}_{\mathrm{Pr}_{\mathcal{I},k}}, \tag{3.25}$$

The BER of user m is defined by the average symbol decision error of user k, P_ψ, which is distributed over all symbols of user m. There are N_o number of overlapping regenerated subcarriers of user k with power of p_k. These subcarriers cause interference with probability of $\mathrm{Pr}_{\mathcal{I},k}$ based on the average power of symbol decision error. Therefore, the average BER of user m is same as in (3.24).

The last scenario for BER analysis is the co-existence of SC-FDMA/OFDMA signals for user k/user m respectively. The BER of user k is obtained as in (3.22) by following the same steps. On the other hand, the average BER of user m's signal is obtained as follows

$$\mathrm{Pr}_m = \frac{N_m - N_o}{N_m}\mathrm{Pr}_{\mathcal{D},m} + \frac{N_o}{N_m}Q\left(\sqrt{\frac{p_m}{P_\psi \mathrm{Pr}_{\mathcal{I},k} p_k + \sigma_\eta^2}}\right). \tag{3.26}$$

As a result, the error term on the SC-FDMA signal is distributed on all symbols. The distribution of the error term has Gaussian statistics if the co-existing pair is an OFDMA signal. However, if the co-existing pair is another SC-FDMA signal, the error term has a uniform mixture Gaussian statistics. Also, the uniform or Gaussian distribution becomes dominant based on the co-existence scenario. If the co-existing pairs are both OFDMA signals, the error term has uniform distributed statistics. Based on these observations in this section, ML-SIC receiver is proposed in Section 3.6.

3.4   Impact of Frequency Offset on Co-Existence

The analysis of error term and the derived BER expressions in Section 3.3 and 3.4 assume that the co-existing subcarriers are overlapping at their optimum sampling point as shown in Fig 3.2(a). As an alternative, a frequency offset of f_o can be introduced between the co-existing signals as also shown in Fig. 3.2(a). The possible values of f_o is normalized by subcarrier spacing and can take values $f_o \in [0, 1]$ to keep the overlap ratio similar compared to the co-existence scenarios without f_o to observe the impact of offset solely. Moreover, the c-SIC is modified to be synchronized to the user k's signal from the composite signal first. In this case, the interference on a subcarrier of user k is contributed from all subcarriers of the user m. Thus, the nth ($n \in [k_1, k_2]$) subcarrier of user k after equalization is

$$\beta_{k,n} = x_{k,n} + \sum_{n'=m_1}^{m_2} x_{m,n'} \phi_{m,n'} \, \text{sinc}(n' - n + f_o) + \hat{\eta}_{k,n}, \qquad (3.27)$$

where $\text{sinc}(\cdot)$ is the normalized sinc function as $\text{sinc}(x) \triangleq \sin(\pi x)/\pi x$. After decoding (3.27), user k's signal is regenerated and frequency offset of $(-f_o)$ is applied. Then, the c-SIC synchronizes to the user m's signal from the composite signal and subtracts the regenerated signal of user k. After equalizing the remainder, the nth subcarrier of the user m becomes

$$\beta_{m,n} = x_{m,n} + \sum_{n'=k_1}^{k_2} (x_{k,n'} - \hat{x}_{k,n'}) \phi_{k,n'} \, \text{sinc}(n - n' - f_o) + \hat{\eta}_{m,n}. \qquad (3.28)$$

62

It is straightforward to see from (3.27) and (3.28) that the power of the observed interference at a subcarrier depends on its distance to the co-existing subcarriers in frequency domain. Therefore, SINR is calculated for each subcarrier separately.[6]

3.4.1 Impact of Frequency Offset on OFDMA Signal

All symbols of the OFDMA signal are affected when frequency offset is introduced to the co-existence scenarios. However, for a very small frequency offset, $f_o \approx 0$, the error terms, $\xi_{k,n}$ and $\xi_{m,n}$, can be neglected for the non-overlapping symbols of user k. As f_o increases up to 0.5, the interference becomes dominant and GA holds for the distribution of the error term for all symbols. Thus, the variance of the error term at the nth symbol of co-existing users are

$$\sigma^2_{\mathcal{I}_{k,n}} = p_m \sum_{n'=m_1}^{m_2} \text{sinc}^2(n' - n + f_o), \tag{3.29}$$

$$\sigma^2_{\mathcal{I}_{m,n}} = p_k P_\psi \sum_{n'=k_1}^{k_2} \text{sinc}^2(n - n' - f_o), \tag{3.30}$$

where $\sigma^2_{\mathcal{I}_{k,n}}$ and $\sigma^2_{\mathcal{I}_{m,n}}$ are the variance of the user k and user m respectively, and P_ψ is as in (3.23).

In OFDMA/SC-FDMA co-existence scenario of user k/user m pair, the impact of error on user k's signal in (3.6) is shifted by a frequency offset of f_o. This operation does not introduce any uniformity to the statistics which remains Gaussian. However, the error term is distributed over all symbols and affects the SINR of each symbol based on (3.29). Thus, GA for OFDMA signal. After c-SIC processing, the user m's subcarriers are obtained as in (3.28) where the interference is observed due to the incorrectly regenerated subcarriers of user k. The additional IDFT distributes the interference on all symbols of SC-FDMA signal and allows GA for the statistics of error on each symbol of user m. Therefore, the variance of the error term on user m's signal is $(s_{k,n} - \hat{s}_{k,n}) p_{k,n}$.

---

[6]The impact of overlapping w/o frequency offset is analyzed in Section 3.2 and Section 3.3. For the simplicity and avoid repetition of the already provided analysis, the impact of the frequency offset is analyzed briefly.

3.4.2   Impact of Frequency Offset on SC-FDMA Signal

The error terms for SC-FDMA/SC-FDMA co-existence without frequency offset have uniform and Gaussian distributed terms as given in (3.14) and (3.15). In case of frequency offset, the uniform distributed terms are altered as

$$\xi_{k,n}^{\text{uniform}} = \frac{N_o}{N_k} \sum_{n'=m_1}^{m_2} s_{m,n'} \, \text{sinc}(n' - n + f_o), \tag{3.31}$$

$$\xi_{m,l}^{\text{uniform}} = \frac{N_o}{N_k} \sum_{n'=m_1}^{m_2} (s_{k,r} - \hat{s}_{k,r}) \, \text{sinc}(n' - n + f_o). \tag{3.32}$$

On the other hand, the Gaussian distributed terms (w/o frequency offset) is composed of sinc-like functions. Introducing frequency offset to the co-existence scenario accumulates the Gaussian distributed components after weighting by coefficients obtained by the sinc function similar to (3.31) and (3.32). Thus, the Gaussian distributed terms in (3.14) and (3.15) remain Gaussian in case of f_o. Consequently, the uniform distributed terms becomes dominant when overlap ratio is large and frequency offset is small. In all other cases, when both overlap ratio and frequency offset are large or small, and when overlap ratio is small and frequency offset is large, the distribution of the error term is Gaussian.

For SC-FDMA/OFDMA co-existence scenario of user k/user m pair, the impact of user m's signal on user k's signal is assumed to be Gaussian similar to OFDMA/SC-FDMA co-existence. Hence, the variance of the error term for user k is $(\sigma_\eta^2 + p_{m,n})$ and for user m as in (3.30). Moreover, although the subcarriers of SC-FDMA signal observe different SINR, the impact of interference are assumed to be distributed homogeneously on each symbol due to DFT spreading.

3.5   Design of an ML-SIC Receiver

In the previous sections the co-existence scenarios with and w/o frequency offset are analyzed based on a c-SIC. Mainly, the error term is distributed over all symbols for SC-FDMA signal and the GA is valid for the distribution of the error term in many cases where the distribution becomes uniform mixture Gaussian distribution for some other cases. On the other hand, the SINR of symbols far from the overlapping subcarriers is larger compared to the symbols close to the overlapping region in frequency domain for

OFDMA signal. Moreover, the interference has no impact on the symbols that are not overlapping for OFDMA signal when there is no frequency offset. However, c-SIC receiver does not consider these and decodes the symbols belonging to the signal with larger SINR first. Thus, c-SIC approach is modified to improve the performance based on the characteristics of each co-existence scenario in this section. For instance, the symbol likelihoods are considered for SC-FDMA signal and the SINR of each symbol is considered for OFDMA signal for processing.

3.5.1 Iterative Likelihood Test for SC-FDMA Signal

Considering the co-existence of SC-FDMA signal with another signal (SC-FDMA or OFDMA), the error term is distributed on all symbols of SC-FDMA signal. In this case, the symbols of the SCFDMA signal which are most likely to be correct are processed initially. As a fact, decoding a fraction of the symbols belonging to the signal with large SINR from the composite signal increases the SINR of the paired signal. Moreover, the probability of error of the nth symbol is defined as $\Pr_e\{\hat{\psi}_n\} \triangleq \Pr\{\hat{\psi}_n \neq \psi_n\}$ where $\hat{\psi}_n$ is the decoded symbol and ψ_n is the exact symbol value. A maximum likelihood decoder compares the likelihood of the received symbol to the decision regions of all symbol to minimize the $\Pr_e$. Then, the reliability of based on the symbol likelihoods for an $\mathcal{M}$-ary modulation scheme is

$$\mathcal{L}_R\left\{\hat{\psi}_n\right\} = \log\left\{\frac{p_{\hat{\psi}_n|\psi_i}(\hat{\psi}_n)}{\sum_{\substack{j=1 \\ j\neq i}}^{\mathcal{M}} p_{\hat{\psi}_n|\psi_j}(\hat{\psi}_n)}\right\}, \tag{3.33}$$

where $\mathcal{L}_R$ is the reliability metric based on log-likelihood ratios, $p_{\hat{\psi}_n|\psi_i}(\hat{\psi}_n)$ is defined as symbol transition probability density function of ψ_i and $\{i, j\} \in [1, \mathcal{M}]$. Then, $\mathcal{L}_R\{\cdot\}$ of all symbols for all ψ_i are calculated and collected in a vector $\mathcal{L}_R$. The most reliable SC-FDMA symbol, $\hat{\psi}_n = \max\{\mathcal{L}_R\}$ is decoded first and the interference on the paired signal is reduced gradually. This approach is called ML-SIC. The number of iterations is larger for ML-SIC compared to the c-SIC. However, ML-SIC can be improved by processing multiple symbols at each iteration based on an SINR criterion.

The SINR of user k's signal is larger than the SINR of user m's signal, $\gamma_k > \gamma_m$. Then, the SINR criterion is defined as $\gamma_k < \gamma'_m$, where γ'_m is the updated SINR of user m, which is obtained after decoding a number of symbols from user k's signal. For SC-FDMA/SC-FDMA co-existence scenario w/o frequency

65

offset, the SINR of user k's signal is

$$\gamma_k = \frac{p_k}{\sigma_\eta^2 + p_m \frac{N_o}{N_k}}. \tag{3.34}$$

The SINR of user m, γ_m, is also obtained after replacing the user indices in (3.34). Correctly decoding one symbol from user k's signal decreases $1/N_k$ of its power. Also, the power of interference on a symbol of user m decreases by the ratio of $N_o/(N_k N_m)$. Thus, the SINR criterion is obtained by decoding α number of symbols from user k's signal, which is

$$\gamma_m' = \frac{p_m}{\sigma_\eta^2 + p_k \left(\frac{N_k - \alpha}{N_k}\right) \frac{N_o}{N_m}} > \gamma_k. \tag{3.35}$$

Then, the number of symbols to be decoded is

$$\alpha = \left\lceil N_m - \left(\frac{p_k}{\gamma_k} - \sigma_\eta^2\right) \frac{N_k N_m}{p_m N_o} \right\rceil, \tag{3.36}$$

where a ceiling integer value is chosen for α. Then, the most reliable α number of symbols of user k are processed by the ML-SIC. After decoding, γ_m' is larger than γ_k at the current stage of the iteration. Next, the most reliable symbols of user m are processed by following (3.33) and (3.36). Note that the reliability information is outdated at the end of each iteration and recalculated for the remaining symbols. Consequently, the iterations are repeated until all symbols are decoded.

For the SC-FDMA/OFDMA co-existence of the signals of user k/user m, the conditions to define the number of symbols to be decoded are

$$\gamma_m' = \frac{p_m}{\sigma_\eta^2 + p_k^{(N_k - \alpha)}/N_k} > \gamma_k, \tag{3.37}$$

$$\gamma_k' = \frac{p_k}{\sigma_\eta^2 + p_m^{(N_o - \alpha)}/N_k} > \gamma_m, \tag{3.38}$$

respectively. Note that only N_o number of symbols of user m cause interference to the user k's signal. However, all symbols of user k cause interference to the overlapping symbols of user m. Therefore, correctly decoding one symbol from the signal of user m decreases $1/N_k$ of the interference power on all symbols of the user k. On the other hand, decoding one symbol of user k decreases $1/N_m$ of the interference power on

one symbol of user m. Thus, the number of user k's symbols to be decoded is

$$\alpha = \left\lceil N_k - \left(\frac{p_m}{\gamma_m} - \sigma_\eta^2 \right) \frac{N_k}{p_k} \right\rceil. \tag{3.39}$$

The number of the symbols of user m to be decoded can be obtained similarly. For OFDMA/SC-FDMA co-existence, α is derived as in SC-FDMA/OFDMA co-exsitence. Moreover, the co-existence of OFDMA/OFDMA signals, there is no additional DFT operation hence, a symbol of user k affect only their paired symbol. In this case, introducing reliability information into ML-SIC processing is not useful.

3.5.2 SINR Based ML-SIC Processing in Case of Frequency Offset

The reliability information is not useful when OFDMA signal is paired in the co-existence scenarios without frequency offset. However, when frequency offset is introduced, the SINR of the symbols of OFDMA signal is exponentially distributed as explained in Section 3.5. In this case, the decoding performance of the ML-SIC is improved for the OFDMA signal. This is achieved by processing the symbols of OFDMA signal which has large SINR initially. Also, the expressions that are used to calculate the number of symbols to be decoded at each iteration based on the SINR criterion is calculated for SC-FDMA and OFDMA signals in case of the frequency offset. A generalized form of the interference power observed by a symbol of the co-existing signals (either OFDMA or SC-FDMA) is

$$
\begin{aligned}
P_{\mathcal{I}_k} = \lambda & \sum_{\substack{n=k_1 \\ n \in \mathcal{N}_k'}}^{k_2} \sum_{\substack{n'=m_1 \\ n' \in \mathcal{N}_m'}}^{m_2} p_m \, \mathrm{sinc}(n' - n + f_o)^2 \\
+ \lambda & \sum_{\substack{n=k_1 \\ n \notin \mathcal{N}_k'}}^{k_2} \sum_{\substack{n'=m_1 \\ n' \notin \mathcal{N}_m'}}^{m_2} P_\psi \, \mathrm{sinc}(n' - n + f_o)^2,
\end{aligned}
\tag{3.40}
$$

where λ is a multiplier, $\mathcal{N}_k'$ and $\mathcal{N}_m'$ are the set of the user's remaining subcarriers at the current iteration, N_d is the number of decoded subcarriers until the current iteration and the interference power due to the sidelobes of the subcarriers is expressed by the square of the $\mathrm{sinc}(\cdot)$. Note that the second term in (3.40) appears for the symbols that are decoded incorrectly. However, ML-SIC assumes that the symbols of the

co-existing pairs are decoded correctly while calculating the number of symbols to be processed at each iteration to satisfy the SINR criterion. Thus, the second term in (3.40) is discarded.

For the co-existence of OFDMA signals, $\lambda = 1$ and there is only one sum term in (3.40). Then, (3.40) is employed to compare the SINR of each remaining symbols by iterating the number of symbols to be decoded (α) in a loop. When the SINR criterion is satisfied, the current value of α is selected. For instance, at least one of the symbols of the paired signal must have larger SINR compared to all symbols of the signal that is processed. For OFDMA/SC-FDMA co-existence scenario, the SINR of each symbol of OFDMA signal is obtained same as in OFDMA/OFDMA co-existence. Also, α is calculated similarly. However, the interference observed by the SC-FDMA signal is scaled by $\lambda = 1/N_k$ and distributed over all symbols equally due to DFT spreading in (3.40).

When SC-FDMA signals are co-existing, the interference is observed from all subcarriers of the paired signal at all iterations due to DFT spreading. However, as symbols are decoded, the interference power is scaled by $\lambda = \frac{N_k - N_d - \alpha}{N_k N_m}$. Also, the interference is assumed to be distributed equally over the symbols of the paired signal equally. Thus, the most reliable symbols of the SC-FDMA signal is decoded in case of frequency offset. For all co-existence scenarios with frequency offset, the minimum value of α that satisfies the SINR criterion is calculated in a loop by varying its value.

3.6   Integration of Power Control to the ML-SIC for HetNet Performance Analysis

Generally speaking, the performance of the SIC receivers are usually improved by integrating power control schemes to the system. Therefore, the performance of the proposed ML-SIC approach is improved by integrating three different approaches, which are a combination of power control and spectrum access schemes. In this system, the macrocell is the primary user and smallcell is the secondary user of the spectrum. Thus, the sMSs are not allowed to interfere to the macrocell network in the UL. The sBS is also assumed to have cognitive capabilities and adapts itself to the interference scenario. This is performed by power allocation which enables ML-SIC processing at the sBS. If ML-SIC processing is not possible, the sMS transmission is terminated to prevent interference to the macrocell network. The interference scenarios for the UL of HetNet in Table 1 are exploited by the proposed power control schemes. Accordingly, both OFDMA and SC-FDMA signals are assigned to the mMSs and sMSs. Namely, the proposed schemes

are sBS-power back-off (sBS-PBO), sBS-power control (sBS-PC) and paired-access with power control (PAPC).[7]

3.6.1 sBS-PBO Scheme

In this scheme, co-existence is only allowed at the sBS. The sMSs can only decrease their transmit power to exploit the resource blocks (RBs) occupied by the mMSs based on successive processing. The rules of this approach is as follows:

- The received power of the mMS signal has to be larger than the received power of the sMS signal at the sBS,

- the SINR of the mMS signal at the sBS has to be at least equal the SINR of that mMS signal at the mBS,

- the SINR of the sMS signal has to be large enough to allow at least the lowest order of modulation after decoding the mMS signal from the composite signal by successive processing at the sBS.

The pseudo algorithm of the sBS-PBO scheme for successive processing is given in Algorithm I. The sBS-PBO scheme sets the transmit power of the sMSs and selects the RBs that are suitable for ML-SIC processing. Then, the OFDMA and the SC-FDMA signals are assigned to the selected RBs to obtain co-existence between different types of signals. The following methodology is followed while assigning signals to the sMSs:

- The unoccupied RBs and the RBs that are available for ML-SIC at the sBS are combined to generate a single SC-FDMA signal and assigned to the sMS to perform ML-SIC.[8] Then, the proper modulation scheme is assigned to the sMS signal based on the observed SINR.

- The same RBs are are allocated for OFDMA signal. The sMS transmits with a different modulation order at each RB based on the observed SINR.

Note that, if a separate SC-FDMA signal is generated for each RB, the observed SINR becomes the same compared to the SINR of the OFDMA signal that is generated for those RBs. However, the observed

---

[7]Similar power control schemes can be found in the literature. The aim of proposing these schemes is to observe the performance of the ML-SIC for the analyzed co-existence approaches, which is the main goal of this work.

[8]Instead of performing DFT spreading at each resource block, a single DFT spreading is performed over the allocated RBs.

Algorithm 1 Pseudo algorithm of the sBS-PBO scheme
___
Define available/occupied RBs
Get modulation type of mMS
Define the required minimum SINR for mMS at the sBS
if mMS signal is decodable at the sBS by ML-SIC **then**
    Mark RB to be processed by ML-SIC
else
    Reduce the sMS transmit power
    if mMS signal is decodable **then**
        Calculate the new SINR of the RB
        if the SINR allows a communication link for sMS **then**
            Mark the RB to be processed by ML-SIC
        else
            Deactivate sMS
        end if
    end if
end if
___

interference from surrounding cells is different at each RB and hence, the SINR of the SC-FDMA signal is different than the SINR of the OFDMA signal. The RB assignment and the transmit power of the mMSs are not modified in case of successive processing. The mMS signals are assumed to generate OFDMA and SC-FDMA signals. This allows to observe the performance the co-existence of different types of signals in the system-level.

3.6.2 sBS-PC Algorithm

The sBS-PC scheme allows the sMSs to increase their transmit powers to enable ML-SIC at the mBS for the co-existing RBs. Obviously, increasing the transmit power of the sMS creates a larger interference to the mMS signal at the mBS. Accordingly, the SINR of the mMS signal at the sBS decreases and error probability increases during the decoding process of the mMS signal. This also increases the error probability of the sMS signal. Thus, sBS-PC scheme does not improve the capacity of the sBS for the co-existence scenarios at the sBS. On the other hand, increasing the transmit power of sMSs is useful for the co-existence scenarios at the mBS for UL in Table 1. In this case, the sMS signal has a larger SINR at the mBS compared to the mMS signal. The sMS signal must be decodable at the mBS to obtain the mMS signal by ML-SIC. Hence, the sMS signals allocated to the corresponding RBs can increase their transmit power to use the occupied RBs without increasing the probability of error for the mMS signals. Since the sMSs are

the secondary users, the lowest modulation order is assigned to the sMSs to minimally increase the overall interference in the system. The conditions that allow to increase the transmit power of the sMSs is included to the Algorithm 1 for the co-existence scenarios at the mBS in sBS-PC scheme. The signal assignment algorithm that is explained for sBS-PB scheme is same as in sBS-PC scheme.

3.6.3 PAPC Scheme

In the PAPC scheme, the sBS is assumed to offload the mMS signals different than the sBS-PB and the sBS-PC schemes. The received SINR of the mMS signal at the sBS has to be larger than its SINR at the mBS as a required condition. On the other hand, sMS signals are not allowed to be paired with mMS signals at the mBS as in sBS-PB scheme. The pseudo-algorithm of this scheme is given in Algorithm 2. Following the PAPC scheme, the OFDMA and the SC-FDMA signals are assigned to the mMSs same as in the previous schemes. Note that, either the mMS signal or the sMS signal is decoded first by ML-SIC in PAPC scheme. Thus, while combining the RBs to assign the SC-FDMA signal to the sMS, there is a possibility that some of the RBs of the sMS have to be decoded first and the other RBs have to be decoded after subtracting the mMS signal from the composite signal. However, the SC-FDMA signal cannot be decoded at some of its allocated RBs due to DFT spreading. Thus, for a sMS two SC-FDMA signal is generated. The active RBs of the sMS that have to be decoded first by ML-SIC are combined. Similarly, the rest of the RBs of the sMS are combined to be decoded by ML-SIC after successive processing of the mMS signals that are overlapping at those RBs. The OFDMA signal is assigned to the sMS RBs similar to the previous schemes since the symbols that are allocated to each RB can be decoded individually.

3.7 Simulations

3.7.1 Link-Level Performance Results

First, the BER performance of the proposed co-existence approaches are analyzed based on the c-SIC and ML-SIC in the link-level. The signals of user m and user k are allocated to 512 of total 1024 subcarriers. These signals are co-existing with different overlap ratios and can employ OFDMA (MC) and SC-FDMA (SC) schemes for comparison. The SNR of the signal of user m is fixed at 5 dB and the SNR of user k's signal is varied. Then, the BER of the co-existing signals for all scenarios are compared.

Algorithm 2 Pseudo algorithm of the PAPC scheme

Chose the best serving node for mMSs
if the mMS and the sMS are active at the sBS **then**
   Get modulation type of mMS
   Calculate the $\gamma_{\text{threshold}}$ for mMS at the sBS
   if $(\gamma_{\text{mMS}} > \gamma_{\text{sMS}}) \wedge (\gamma_{\text{mMS}} > \gamma_{\text{threshold}})$ **then**
      Mark RB to be processed by ML-SIC
   else if $(\gamma_{\text{mMS}} > \gamma_{\text{sMS}}) \wedge (\gamma_{\text{mMS}} \leq \gamma_{\text{threshold}})$ **then**
      sBS backs-off the sMS TX power
      Calculate $\gamma_{\text{sMS}}^{\text{back-off}}$
      sBS increases the sMS TX power minimally
      Calculate $\gamma_{\text{sMS}}^{\text{increased}}$
      if $\gamma_{\text{sMS}}^{\text{back-off}} > \gamma_{\text{sMS}}^{\text{increased}}$ **then**
         Mark RB to be processed by ML-SIC
         mMS signal marked to be decoded first by ML-SIC
      else
         Mark RB to be processed by ML-SIC
         sMS signal marked to be decoded first by ML-SIC
      else
         Deactivate sMS
      end if
   else if $(\gamma_{\text{mMS}} < \gamma_{\text{sMS}}) \wedge (\gamma_{\text{mMS}} > \gamma_{\text{threshold}})$ **then**
      if sMS signal is decodable **then**
         Mark RB to be processed by ML-SIC
      else
         sBS backs-off the sMS TX power
         Mark RB to be processed by ML-SIC
      end if
   else
      Deactivate sMS
   end if
else
   if mMS is active at mBS **then**
      Deactivate sMS
   end if
end if

3.7.1.1 BER Performance of c-SIC Processing on Co-existence

In Fig. 3.3, the BER performance of the c-SIC approach is presented for an overlap ratio of 1/8 without frequency offset. The best and the worst BER results are obtained for SC/SC and MC/MC co-existence respectively. Additionally, the BER performance of SC/MC co-existence is better than MC/SC
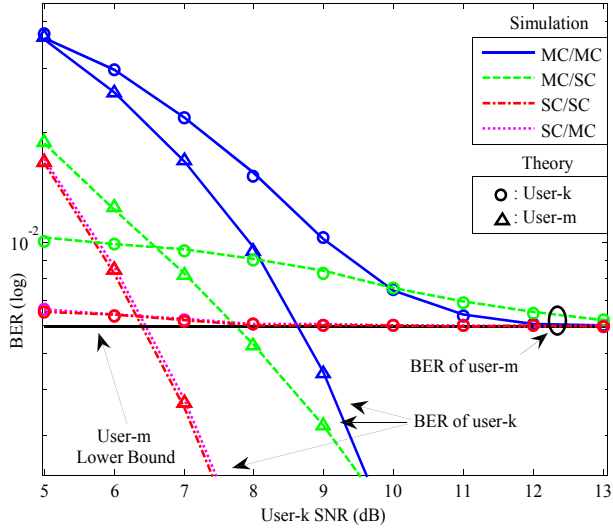
Figure 3.3: BER performance of c-SIC, BPSK, AWGN channel, 1/8 overlap, no frequency offset.
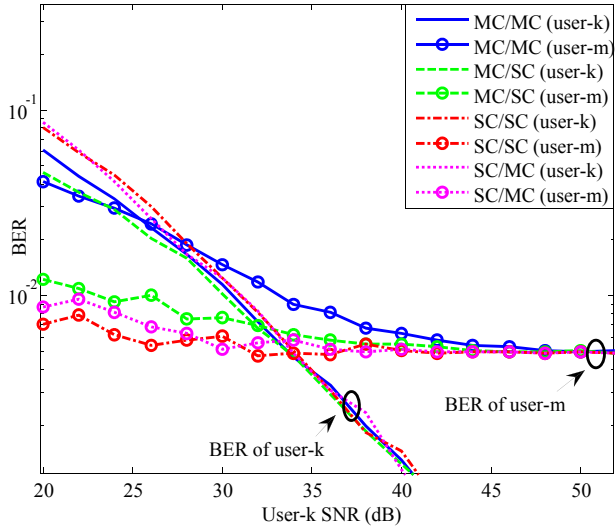
Figure 3.4: BER performance of c-SIC, QPSK, Rayleigh fading channel, 1/4 overlap

co-existence. This is due to employing SC-FDMA signal for user k (the signal with larger SNR) which can compensate the error due to interference introduced by user m's signal in this particular case. On the other hand, as SNR increases, the BER of user m's signal merges to the BER bound of AWGN channel for all co-existence scenarios and simulations validate theoretical results. The BER performance of c-SIC for co-existence without frequency offset is presented in Rayleigh fading channels in Fig. 3.4. In this case, the SNR of user m is set to 20 dB and the SNR of user k is varied. The BER curves for user k are similar. However,
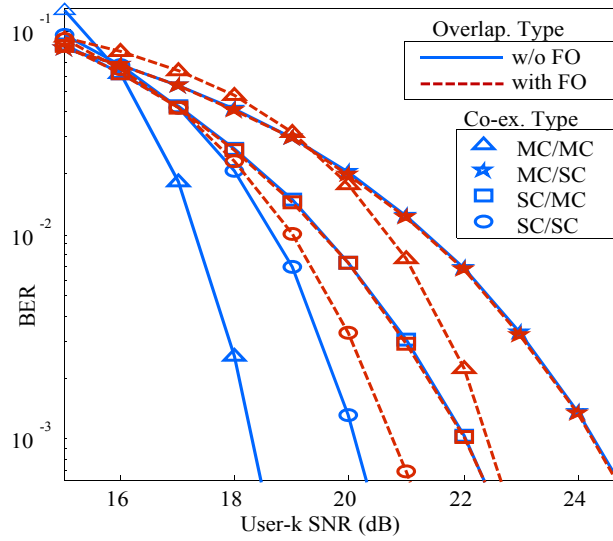
Figure 3.5: Impact of f_o on the BER performance c-SIC (QPSK, AWGN channel, 1/2 overlap, $f_o = 0.5$)
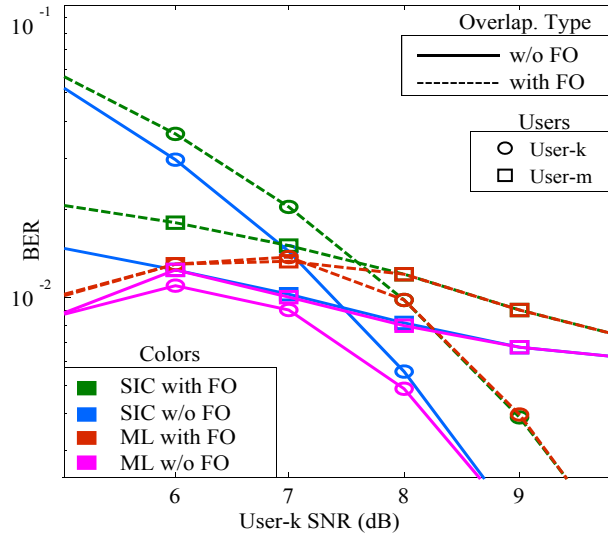
Figure 3.6: BER comparison of c-SIC and ML-SIC for SC/SC co-existence case (BPSK, AWGN channel, 1/2 overlap, $f_o = 0.5$)

the BER of SC/SC co-existence for user m is slightly better in Fig. 3.4. The co-existence of different types of signals does not bring an identical advantage in Rayleigh fading channels. However, multi-user diversity approaches can be developed to exploit the fading characteristics of the channel and ML-SIC receiver can be improved accordingly. Then, the performance of the proposed co-existence schemes can be analyzed for co-existence.

3.7.1.2 The Impact of Frequency Offset on Co-existence

In Fig. 3.5, the impact of frequency offset on the BER performance is presented for c-SIC processing. A frequency offset of $f_o = 0.5$ is introduced and the overlaping ratio is set to $1/2$ between the co-existing signals. The BER performance of the user k's signal with f_o is compared to user k's signal without f_o. Mainly, the co-existence of same types of signals (SC/SC or MC/MC) have worse BER compared to the co-existence without frequency offset case. The main reason is that the interference has uniform distribution for co-existence w/o f_o for MC/MC. However, intreference is observed from all subcarriers and has Gaussian distribution in case of f_o. This results in worse BER performance. Note that, for SC/SC scenario, the interference has uniform mixture Gaussian distribution even if there is a frequency offset and the degradation in BER is not as worse as MC/MC co-existence. On the other hand, the BER performance for SC/MC and MC/SC co-existence scenarios are same for the cases with and without frequency offset. This is due to the error term which has Gaussian distribution for co-existence without frequency offset. Also, introducing frequency offset still has the same impact with similar variance. Same conclusion is also valid for ML-SIC for with and w/o f_o comparisons and not presented.

3.7.1.3 The Advantage of ML-SIC Processing on Co-Existence

The ML-SIC processing that is designed for co-existence of different types of signals is compared to c-SIC processing. In Fig. 3.6, the BER curves of c-SIC and ML-SIC for SC/SC co-existence in case of f_o and without f_o are presented. The overlap ratio is set to $1/2$ and BPSK modulation is employed for both users. The BER performance of the ML-SIC is better at low SNR region compared to the c-SIC for all co-existence scenarios. Moreover, the BER performance of both receivers in case of f_o is worse compared to co-existence without f_o. The overall best performance is obtained for ML-SIC processing when f_o is not introduced. Additionally, the BER of ML-SIC and c-SIC receivers for co-existence without f_o merge to their BER curves that are obtained for co-existence without f_o at high SNRs. Although the c-SIC receiver appears to be more useful at high SNR region due to its low complexity, the ML-SIC receiver calculates the number of symbols to be processed and demodulates all symbols at high SNRs as in c-SIC processing. The complexity of this calculation is negligible when the number of symbols to be decoded are calculated without a loop.
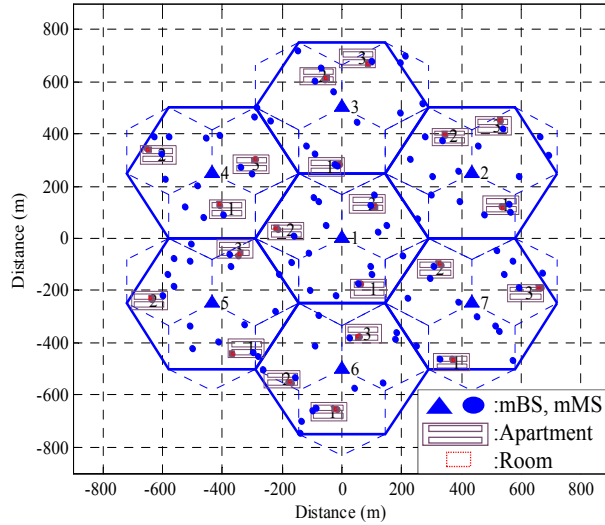
Figure 3.7: Plot of the system level multi-cell grid model.
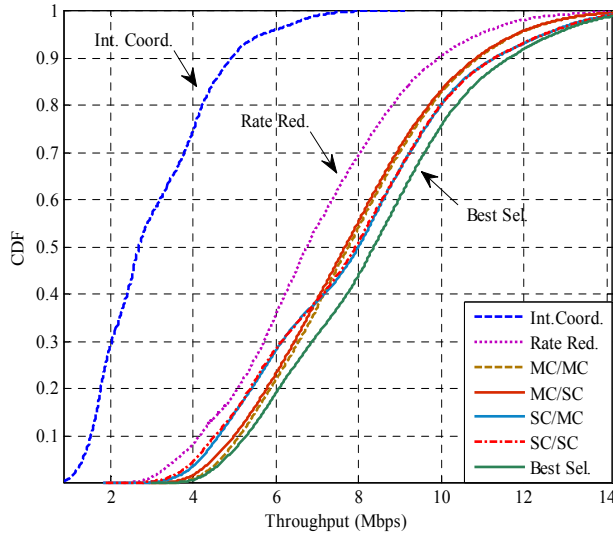
Figure 3.8: Throughput CDFs for homogeneous deployment.

3.7.2 System-Level Performance Results

The performance of co-existence and ML-SIC are also presented for homogeneous and HetNet deployment models. For this purpose, hexagonal grid model is implemented as shown in Fig. 3.7. There are 7 macrocells each having 3 sectors. Also, 5 mMSs and an apartment are placed at each sector to represent the indoor/outdoor usage. Furthermore, the OFDMA and SC-FDMA schemes are employed in the system. The number of subcarriers at each sector is 512, 300 of which (25 RBs) are allocated to the MSs and the rest is left

76

as guard band. Accordingly, each MS switches its modulation (BPSK, QPSK, 16QAM and 64QAM) based on the link quality which depends on the received signal power, the power of interference received from surrounding cells and the noise. For HetNet model, an indoor sBS and sMSs are placed inside an apartment. The sMSs and mMSs are co-existing by exploiting the same resources. The system-level simulations are exhausting due to many parameters and calculations that are involved. The rest of the parameters, such as losses (path loss, wall loss, fractional open loop path loss compensation etc.), shadowing (intercell, intracell, correlation etc.), transmit power setting (antenna pattern, gains, limits etc.) can be found in [82].

3.7.2.1 Co-existence for the UL of Homogeneous Deployment

First, co-existence is analyzed in the UL of homogeneous network. In this scenario, 2 users require 8 RBs and the rest have 5 RBs each. Thus, there are a total of 6 RBs overlapping in the system. Two utmost and two closest mMSs are paired for overlapping without any power control. The throughput is calculated based on the symbol error rates. The results are compared to the throughput of interference coordination (IC) and rate-reduction (RR) schemes. The former does not allocate any resources to a user when the number of RBs is not sufficient. For the latter, all users are allocated by sharing available RBs between users without causing interference, i.e. 5 RBs are allocated to the users that need 8 RBs. Then, the throughput CDF of each co-existence scenario is shown in Fig. 3.8. The throughput of the IC technique (Int. Coord.) is the worst since the users that need a number of RBs than the available are not scheduled. The RR approach (Rate Red.) presents better throughput compared to the IC approach. However, all co-existence scenarios have better throughput than RR. It is also known that SC-FDMA and OFDMA signals can be allocated within the same frame. Thus, the overlapping pair is selected by using a look-up-table at each realization for every user which provides the best throughput. Consequently, co-existence with best selection (Best Sel.) approach provides 20% of gain in throughput 90% of the time compared to RR.

3.7.2.2 Co-existence for the UL of HetNet Deployment

Secondly, the performance of the proposed combination of methods (co-existence of different types of signals, ML-SIC receiver and power control) is observed in the UL of the HetNet deployment model. Some modifications are made in the system-level scenario, such as the number of mMSs are randomly
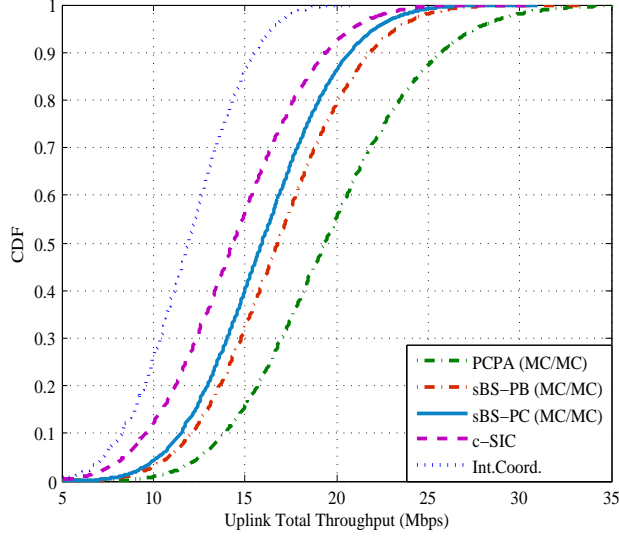
Figure 3.9: Throughput CDFs of power control schemes.

changed at each iteration between 1 and 5, and the RBs are randomly allocated to the MSs. Moreover, the number of indoor sMSs are 1 or 2. Unlike the homogeneous deployment scenario, the users are not forced to co-exist. The co-existence scenarios happen naturally and the overlap ratio between the signals of sMSs and mMSs may vary. The performance is investigated for the proposed power allocation schemes given in Section 3.7. The c-SIC and IC approaches are presented for comparison. First, the throughput of the PCPA, sBS-PB and sBS-PC approaches are observed for MC/MC co-existence for comparison in Fig.3.9. The throughput of the c-SIC is better than the IC approach. The performance of the sBS-PC approach is worse than the sBS-PB approach. The sBS-PC approach allows sMSs to increase their power for successive processing. Increasing the sMS signal power also increases the total interference power in the system and hence, result in worse throughput performance. The PCPA approach provides the best throughput. Because the mMSs are offloaded by the sBS. The overall interference is also increased minimally compared to the other schemes. The throughput CDF of different co-existence cases are presented only for PCPA approach since it performs better than the other schemes in Fig.3.9. In Fig.3.10, the best throughput is obtained by MC/MC co-existence. The reason is that the modulation order is adaptively changed at each RB based on the observed SINR for fair comparison with SC-FDMA signal. The SC/SC co-existence is worse than MC/MC in average. However, at some realizations of the HetNet simulations, SC/SC performs better which is not observable in the curves of SC/SC and MC/MC. For instance, assume that there are two RBs selected

78
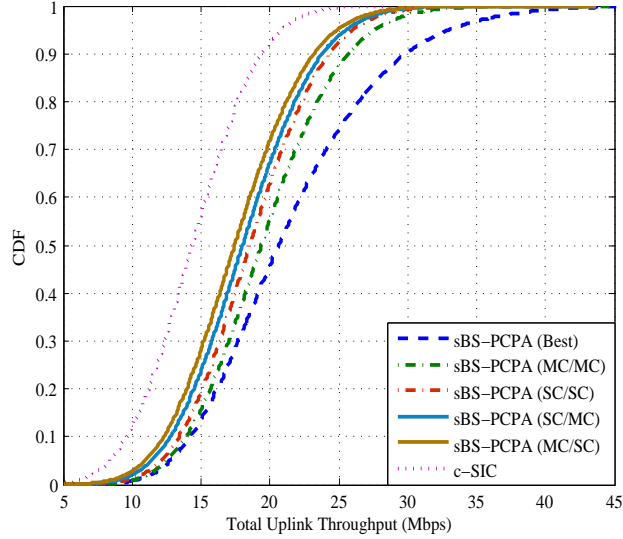
Figure 3.10: The comparison of the throughput CDFs of co-existence w/o frequency offset.

for successive processing. Considering the received SINR of these RBs, 16QAM and 64QAM modulation schemes are assigned when OFDMA signal is employed. However, a single SINR value is calculated when SC-FDMA signal is employed at these RBs. This SINR is calculated by the average interference power observed from these RBs and hence, might allow 16QAM only for the SC-FDMA signal that is transmitted at these RBs. Also, the SINR of the SC-FDMA signal might be large enough to allow 64QAM at these RBs which has a larger throughput compared to the OFDMA signal. To observe this, the co-existing signals are selected based on the observed SINR and the best CDF curve is obtained for PCPA scheme in Fig.3.10, i.e. 90% of the time PCPA scheme with best selection can provide 50% more throughput compared to the c-SIC approach with power control.

CHAPTER 4

IDLE BAND INTEGRATION FOR COOPERATIVE RELAYING IN A COGNITIVE NETWORK AND IMPACT OF BEAM-FORMING ON THE PERFORMANCE

Increasing demand for large throughput requiring wireless services and the lack of available large bandwidth cause difficulties in finding available spectral resources [88].[1] The frequency spectrum that is suitable for wireless mobile communication is already assigned to particular services or licensed to its providers. Therefore, meeting the demand for high data rate requiring services within accessible spectrum range becomes challenging. However, the actual spectrum usage at the licensed and/or dedicated spectrum is under-utilized and some bands are left unused at different frequencies [89]. On the other hand, new bands are expected to be allocated for mobile communication in a non-contiguous manner [90]. In this case, the number of mobile stations (MSs) that supports the existing bands is expected to be larger than the number of MSs that supports the newly allocated bands. This might cause congestion at the existing bands while the newly allocated bands are under-utilized. These idle bands given in the scenarios explained above cannot be used by non-licensed users based on the regulations on the spectrum management. Therefore, spectrum access strategies that exploit the unused bands become important to increase the spectral efficiency.

4.1 Related Work

The spectrum allocation policies are discussed by regulatory authorities and academia, and the idea of spectrum sharing systems is proposed consequently. Accordingly, secondary users (non-licensed users) are allowed to utilize the bands that are licensed to the primary users [91]. To achieve this, secondary user devices perform spectrum sensing and define unused licensed bands to exploit available bands for transmission. Additionally, database approaches can store the geographical spectral occupancy information to for

---

[1]The content of this chapter is under submission process to IEEE Transactions on Vehicular Technology.

spectrum sensing purpose. When primary users are transmitting at a band, secondary users switch-off their transmission or scheduled to the other available bands. This is referred to as interweaved approach where simultaneously co-existence of the licensed and unlicensed users is not allowed [92]. Other approaches, such as underlay and overlay cognition, allow secondary users to exploit the bands that are already occupied by the primary users based on interference limitation or avoidance, respectively [92]. However, due to strict interference constraints, spectrum accessing for secondary users is restricted in both schemes. In this chapter, interweaved spectrum sharing approach is considered. On the other hand, the idle bands may not be large enough to support large throughput requiring wireless services. Another problem might arise in the near future after allocating new spectrum for mobile communication especially for long term evolution-advanced (LTE-A) and beyond [93]. In this case, the existing MSs might not support the non-contiguously allocated new spectrum due to hardware limitations. This causes a bottleneck in the network at some frequencies and inefficient usage of new spectrum. A candidate solution is to collect idle bands from different parts of the spectrum obtain a larger bandwidth. This is a.k.a. spectrum aggregation which requires a transceiver design with multiple radio frequency chains to exploit non-contiguous spectrum [93, 94]. Orthogonal frequency domain multiplexing (OFDM) based schemes can utilize the idle bands by switching the subcarriers on and off based on the availability of the primary bands [95]. However, these solutions are analyzed for direct links between the source and the destination nodes and still obtaining a large bandwidth remains problematic.

Relays can also be utilized to improve the spectrum accessing capabilities of the secondary nodes [96, 97]. The performance of different relaying mechanisms (i.e. amplify and forward (AF) and decode and forward (DF)) are investigated in Rayleigh fading channels when there is no direct link between the source and the destination [98–100]. The exact symbol error rates for both schemes are also analyzed in a non-cooperative relay network [101–103]. On the other hand, the performance of the relays are investigated and different relay selection mechanisms are developed for cooperative relay networks [104–107]. Such relaying mechanisms are also investigated in cognitive networks [108–110]. Additionally, best relay selection approaches are developed for AF and DF schemes in Rayleigh fading channels for cooperative relay networks [111–114]. Aggregating the idle bands to obtain a large spectrum in a cooperative cognitive relay networks is an alternative to the techniques mentioned above for improved spectrum access.

4.2 Contribution

In this chapter, the spectrum aggregation problem is analyzed for indirect links between the source and the destination nodes through multiple relays. The proposed approach allows idle band integration for the secondary nodes. A few relays between the source and the destination collectively aggregate the available bands to facilitate the transmission of a large bandwidth signal as shown in Fig. 4.1. In this framework, the efficient dispersion and the aggregation of the source signal is analyzed based on the probability of finding available bands. Also four different deployment scenarios for the relays are considered in this system to observe the impact of beamforming on the achievable signal-to-noise-ratio (SNR) and the outage probability.

First, the probability of finding a particular number of available bands are analyzed based on different beamforming capabilities of the relays. In the first scenario, the relays are assumed to be deployed with omnidirectional antennas. The source node broadcasts the signal which can be received by a subset of the second hop relays. Then, each relay broadcast a part of the composite signal at every hop, until the composite signal arrives to the destination. The second scheme is an idealized case where the relays are equipped with directional antennas which have perfect beam-forming capabilities. For instance, each relay at the second hop can create a beam to transmit a portion of the composite signal to any band of the relays at the third hop. In the third scheme, each relay at the current hop is associated with only one another relay at the next hop. The source node broadcasts the composite signal and the relays receive a part of it based on their band availability. Then, each part of the composite signal is transmitted towards the destination node through particular paths. The last scheme is more realistic and provides a general model for different deployment schemes. Based on this model, each relay is deployed with directional antennas which have limited beam-forming capabilities. For instance, the signal transmitted by the second hop relay is received by a subset of the third hop relays. A third hop relay can also receive a transmission from multiple second hop relays at different bands.

In Rayleigh fading channels, achieving a particular bandwidth is not sufficient for successful transmission from the source node to the destination node. Therefore, the proposed system is analyzed further to observe the performance metrics such as the maximum achievable SNR and the probability of outage in Rayleigh fading channel. Besides, the source node require a target throughput in practical scenarios for a point-to-point link based on the application requirements running at the source node. Thus, considering the
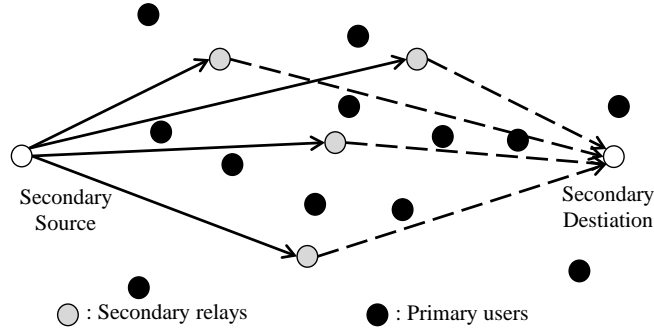
Figure 4.1: Secondary transmission through multiple relays in the presence of primary users.

number of available bands and the impact of the Rayleigh fading channel, the probability of achieving a target SNR is derived and analyzed for the proposed cooperative cognitive relay network.

The remainder of this chapter is arranged as follows. A description of the system model and the mechanism for distributed spectrum aggregation is provided in Section 4.2. The probability of finding a particular number of bands for different deployment schemes are analyzed in Section 4.3. The maximum achievable SNR, the outage probability and the probability of reaching a target SNR for Rayleigh fading channel are analyzed for the proposed system in Section 4.4. Simulation results are presented in Section 4.5.

4.3 System Model

The proposed methodology is analyzed for an OFDM based cognitive network, where the MSs are scattered as primary and secondary users as shown in Fig. 4.1. In this network, the spectrum is licensed to N_P number of primary users. The allocated spectrum is assumed to belong multiple bands and each band is divided into subcarriers. The number of subcarriers in the system is N_L. However, only a fraction of the subcarriers are occupied by the primary users based on their required throughput. In this system, a secondary user S is transmitting a signal to a secondary destination D as shown in Fig. 4.1. It is assumed that a direct link between the source and destination nodes is not available due to the limitations in the secondary user's transmit power. Also finding a required bandwidth as a single chunk is not possible for the source node due to spectral crowd or limitations in the hardware of the secondary user's MS to aggregate a large bandwidth. Therefore, the source, S, seeks for help from the secondary relays that are distributed between S and D.

A traditional two time slots model is adopted for secondary user's transmission through the secondary relays. In the first time slot, the source node performs spectrum sensing over the N_L number of subcarriers for a defined period of time τ which is usually a small fraction of the slot duration T. The spectrum sensing results are collected in a vector $\boldsymbol{\alpha}_s = [\alpha_{s,n} | \alpha_{s,n} \in \{0, 1\}, n = 1, 2, \cdots, N_L]$, by marking the occupied subcarriers with zeros and free bands with ones. The parameter $\alpha_{s,n}$ is assumed to be a random variable. Also, the probability of $\alpha_{s,n}$ to be 0 or 1 are

$$p_0 = \Pr[\alpha_{s,n} = 0] \text{ and } p_1 = \Pr[\alpha_{s,n} = 1] = 1 - p_0. \tag{4.1}$$

which represent the probability of nth subcarrier to be occupied or available in the proximity of the source S respectively. These probabilities are mainly a function of time, location and the considered frequency range; however, many other factors may also be influential. Since the secondary nodes are located in a similar environment, the probability of a subcarrier to be available is assumed to be same within the secondary network. Once $\boldsymbol{\alpha}_s$ is known, the source broadcasts a signal over the available bands in the remaining time slot. Then, $N_R^{(2)}$ number of second hop relays receive this broadcast partially based on the spectral availability in their proximity and forward the signal to the destination.

Assume that the source node requires a throughput of R which is obtained by aggregating a part of the available subcarriers from different bands. A set of subcarriers that are available at the source is defined as $\mathcal{N}_S \triangleq \{n | \forall \alpha_{s,n} = 1\}$. The source node selects a subset of the available subcarriers, $\mathcal{N}_\mathcal{K} \subseteq \mathcal{N}_S$, for transmission.[2] The available subcarriers are modulated by the transmit symbols and the occupied subcarriers are padded by zeros. Note that, the available subcarriers in set $\mathcal{N}_\mathcal{K}$ can be belong to different bands. Therefore, after symbol allocation, inverse discrete Fourier transform (IDFT) operation is performed for each dispersed band. Then, a replica of the desired portion from the end of each time domain signal belonging to the corresponding band is attached to the beginning as cyclic prefix (CP). Then, the composite signal is transmitted through Rayleigh channel and received by multiple relays based on their spectral availability. At the beginning of the second time slot, each second hop relay performs spectrum sensing and generates a spectrum occupancy vector which is $\boldsymbol{\alpha}_r^{(2)} = [\alpha_{r,n}^{(2)} | \alpha_{r,n}^{(2)} \in \{0, 1\}, n = 1, 2, \cdots, N_L], \forall r \in \{1, 2, \cdots, N_R^{(2)}\}$. The common

---

[2]During the subcarrier selection process, the required throughput, availability of the channels at the relays and the usage of the directional antennas are considered in Section 4.3.

available bands between the source and the nth relay at the second hop is obtained by the Hadamard product of spectrum occupancy vectors, which is $\alpha_s \circ \alpha_r^{(2)}$. The operator "$\circ$" represents the Hadamard product. From the result of the product the active secondary bands (free primary bands) are marked with ones and unused bands (occupied primary bands) are marked with zeros. Similarly, the common available bands is obtained for each second hop relay. These spectrum occupancy vectors of the source node and the relays at the second hop are assumed to be mutually independent because they are compiled in two different time slots and at different locations. Each relay removes the CP header from the composite signal and performs discrete Fourier transform (DFT) operation to obtain the received subcarriers at the available bands. The nth subcarrier, $n \in \mathcal{N}_\mathcal{K}$, received by the rth relay at the second hop is

$$y_{r,n}^{(2)} = x_{sr,n}^{(2)} h_{sr,n}^{(2)} + \eta_{r,n}^{(2)}, \tag{4.2}$$

where $x_{sr,n}^{(2)}$ is the nth subcarrier transmitted by the source s to the second hop relay r, $h_{sr,n}^{(2)}$ is the channel frequency response of the nth subcarrier between the source and the relay, and $\eta_{r,n}^{(2)}$ is the complex valued sample of the independent and identically distributed (i.i.d.) AWGN noise in frequency domain observed by the nth subcarrier of the rth relay.

Each relay at the second hop decodes and regenerates the received signal in DF mode. However, the received signal can directly be amplified without decoding in AF mode. The achievable capacity at the second hop relays may not be sufficient due to the spectral occupancy or the variations in the wireless channel. In this case, the relays cannot forward the signal and outage occurs. Otherwise, the relay forwards the source signal based on the desired relaying strategy either in AF or DF mode to the third hop relays. This operation is performed until the source signal reaches the destination node. It is also possible that a subset of the available bands in α_s can be available at multiple relays. If all relays are allowed to forward the received signal without considering band multiplicity, the destination may receive multiple signals from different relays over the same subcarriers which causes collision at the destination. This is avoided by implementing a timer based forwarding approach commonly used in selective relaying [115]. For instance, each relay sets a local timer inversely proportional to the received signal to noise ratio (SNR) that is offered for the $S \rightarrow R_i$ link over a particular band. Note that, some relays that have more than one common free bands with

the source, have more than one activated timers. Eventually, the timer of the relay which has the highest SNR over a particular band expires first and that relay starts forwarding the source signal to the destination. Other relays that have the activated timers for the same band overhear this transmission and refrain from forwarding the source signal at that band. This scheme may be failed under certain circumstances and their detail is beyond the scope of this chapter.[3] In OFDMA systems, timing misalignment of the signals received from different nodes cause interference between subcarriers. However, if the duration of the CP header is chosen based on the timers and the maximum excess delay of the channel, the issues due to timer based approach can be solved easily. The duration of the CP header is assumed to be sufficient and the timers are be short enough. Thus, interference free reception is achieved for the subcarriers that are received from different nodes. These timers can be incorporated in the second time slot by reducing the spectrum sensing period τ to τ_1 and reserving τ_2 for timers such that $\tau = \tau_1 + \tau_2$. This gives the same communication time $T - \tau$ for each relay as in the first slot (or slightly more depending upon how quickly the timer expires within τ_2).

Further assumptions are made for the scenarios explained so far such as the relays at each hop are clustered and the relays have more than one hop distance does not interfere each other. Accordingly, for some of the deployment schemes, a limited feedback channel is assumed between the nodes of consecutive hops. For instance, the current state of the wireless channel can be shared for subcarrier selection.

4.4   Probability of Finding Available Bands

In the proposed system, the relays facilitate the forwarding of the source signal by utilizing the available bands geospatially distributed within the coverage area of the relays. Then, the relays that are involved in forwarding provide an aggregated larger bandwidth collectively. To achieve this, a particular number of bands are required to be available among the nodes at each hop for successful transmission, otherwise outage occurs. Mainly, the outage occur in this system due to spectral unavailability across the secondary nodes and severe conditions of the wireless channel. However, secondary network does not have control on these limitations. Therefore, intelligent adaptation strategies are required. The beamforming capabilities of the source, relay and destination nodes, allow the secondary cooperative network to overcome

---

[3]The readers are referred to [115] and the references therein.

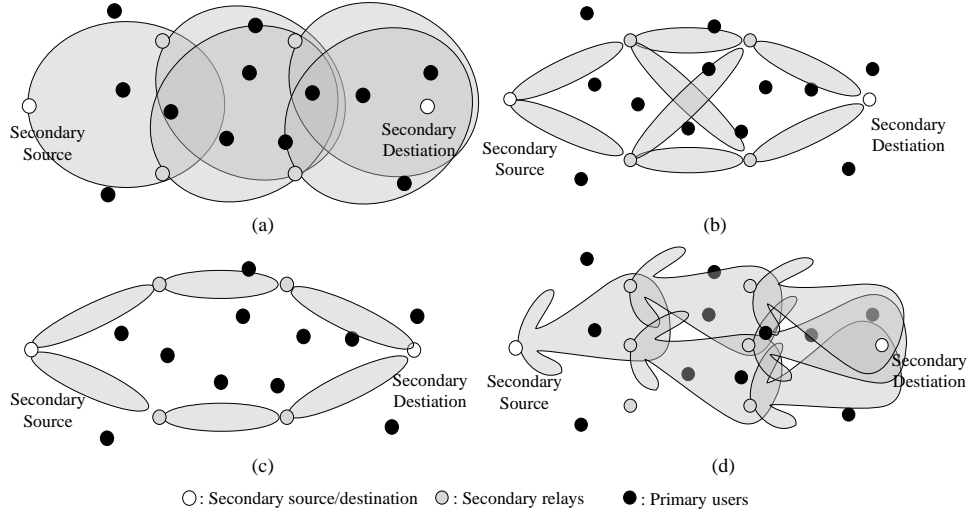○: Secondary source/destination   ◉: Secondary relays   ●: Primary users

Figure 4.2: Secondary transmission through multiple relays with different beam-forming capabilities.

these limitations. To analyze the impact of beamforming, the probability of finding available bands for the source-to-destination link is derived for different deployment schemes. For all deployment schemes, the source detects the available subcarriers among N_L number of total subcarriers. Then, selects K number of available subcarriers by generating a specific combination of K zeros in α_s. The value of K is any number from 0 to N_L. However, $K = 0$ represents no vacant band and the transmission cannot be started. Hence, to analyze the transmission process, we consider that $K = 1, 2, \cdots, N_L$.

4.4.1 Broadcast Mode

In the first scheme, the source node generates parallel streams of the signal and broadcasts over the K unused primary subcarriers through all directions at first hop as shown in Fig. 4.2(a). The signal reaches all second hop relays; however, can be received by those whose corresponding subcarriers are available. Similar strategy applies at each hop until signal arrives to the destination. This scheme is valid for closely deployed nodes that are equipped with omni-directional antennas.

First, the source node requires at least K number of available subcarriers for transmission. Thus, the probability of having any K number of subcarriers to be available and $(N_L - K)$ number of subcarriers to be occupied at the source must be calculated. This probability can be expressed by the probability mass

87

function (PMF) of one of the well-known class of distributions called Binomial distribution which is

$$\Pr[\alpha_s \odot \alpha_s = K] = f(K; N_L, p_1) = \binom{N_L}{K} p_1^K (1 - p_1)^{N_L - K}, \tag{4.3}$$

where operator $\odot$ represents vector dot product and $f(\cdot; \cdot, \cdot)$ represents PMF of the Binomial distribution. Also, having more than K number of available subcarriers after spectrum sensing satisfies the condition for successful transmission. This probability is expressed by the sum of individual PMFs as

$$\sum_{i=0}^{N_L - K} f(K + i; N_L, p_1) = 1 - F(K - 1; N_L, p_1), \tag{4.4}$$

where $F(\cdot; \cdot, \cdot)$ is cumulative distribution function (CDF) of the Binomial distribution that is given for the inputs in (4.4) as

$$F(K - 1; N_L, p_1) = \sum_{i=0}^{K-1} \binom{N_L}{i} p_1^i (1 - p_1)^{N_L - i}. \tag{4.5}$$

When there are $K + i$ number of available subcarriers, $\binom{K+i}{K}$ number of different selections are possible. Hence, the final probability of having any K or more subcarriers to be idle by considering all combinations is

$$\Pr[\alpha_s \odot \alpha_s \geq K] = \sum_{i=0}^{N_L - K} \binom{K + i}{K} f(K + i; N_L, p_1) \tag{4.6}$$

$$= \sum_{i=0}^{N_L - K} \binom{N_L}{K + i} \binom{K + i}{K} p_1^{K+i} p_0^{N_L - K - i}. \tag{4.7}$$

Then, the transmit vector, β_s, is created by selecting the idle subcarriers from α_s. The indices of the selected K number of idle subcarriers are replaced by ones and the remaining indices are replaced by zeros in the vector β_s. Then, the signal is transmitted to the relays at the second hop.

The transmission is not successful if one of the idle subcarriers in the vector β_s is not available across the $N_R^{(2)}$ number of relays at the second hop. The probability of this event is closely related to the outage probability of the system. The idle subcarriers among the relays at the second hop can be determined

by the Hadmard product of the complementary of the spectrum occupancy vectors, $\overline{\alpha}_r^{(2)} \triangleq \mathbf{I}_{N_L \times 1} - \alpha_r^{(2)}$, as

$$\theta = \overline{\alpha}_1^{(2)} \circ \overline{\alpha}_2^{(2)} \circ \ldots \circ \overline{\alpha}_{N_R^{(2)}}^{(2)}, \tag{4.8}$$

where $\mathbf{I}_{N_L \times 1}$ is a vector of ones. If θ preserves the same combination of zeros as $\overline{\beta}_s$, all subcarriers at the source node are available across the participating relays at the second hop and outage will not occur. Note that, the availability of additional free bands does not facilitate the transmission process further. However, these events can still be counted as non-outage events and reduce the outage probability. It is worth to note that having ones in θ is only possible when all elements of that index for all multiplier vectors are equal to one. Therefore, the probability of a subcarrier to be occupied in θ is $(p_0)^{N_R^{(2)}}$. All other combinations of the product in (4.8) result in channel availibility with the probability of $1 - (p_0)^{N_R^{(2)}}$. The probability of finding exactly the same selection of K number of idle subcarriers at the source node and across the second hop relays is

$$\Pr[\overline{\beta}_s = \theta] = (1 - p_0^{N_R^{(2)}})^K (p_0^{N_R^{(2)}})^{N_L - K}. \tag{4.9}$$

The number of idle subcarriers among second hop relays can also be larger than K. For example, if θ is a null vector, it surely covers the selected idle subcarriers in the vector α_s. Therefore, the probability of having the exact same combination of K number of subcarriers in the vector θ and any combination of the remaining $N_L - K$ number of subcarriers to be available is

$$\Pr[\overline{\beta}_s \circ \theta = \overline{\beta}_s] = (1 - p_0^{N_R^{(2)}})^K. \tag{4.10}$$

Accordingly, it is straightforward to observe that $\Pr[\beta_s \circ \overline{\theta} = \overline{\theta}] = \Pr[\overline{\beta}_s \circ \theta = \overline{\beta}_s]$.

When the source node and the destination node are far from each other, the relays at the second hop forward the signal to the relays at the third hop. The number of subcarriers to be forwarded from the rth second hop relay is defined as $K_r^{(2)}$. Thus, it is necessary to find $K_r^{(2)}$ number of available subcarriers $\forall r \in [1, N_R^{(2)}]$ at the rth relay at the second hop. Accordingly, all relays at the second hop has to find $\sum_{r=1}^{N_R^{(2)}} K_r^{(2)} = K$ number of available subcarriers. The selected subcarriers at each relay at the second hop must also have different indices to prevent collisions. Therefore, a control channel is assumed between the

second hop relays which allows the selection of the available subcarriers by each relay sequentially. Based on the sequential selection, the first relay at the second hop selects $K_1^{(2)}$ number of available subcarriers first. The probability of having at least $K_1^{(2)}$ number of idle subcarriers at the first relay at the second hop is

$$\Pr[\alpha_1^{(2)} \odot \alpha_1^{(2)} \geq K_1^{(2)}] = \sum_{i=0}^{N_L - K_1^{(2)}} \binom{N_L}{K_1^{(2)} + i} \binom{K_1^{(2)} + i}{K_1^{(2)}} p_1^{K_1^{(2)} + i} p_0^{N_L - K_1^{(2)} - i} \tag{4.11}$$

$$= \sum_{i=0}^{N_L - K_1^{(2)}} \binom{K_1^{(2)} + i}{K_1^{(2)}} f\left(K_1^{(2)} + i; N_L, p_1^{K_1^{(2)} + i}\right). \tag{4.12}$$

Then, the second relay at the second hop selects $K_2^{(2)}$ number of subcarriers among the available subcarrier which are not overlapping with the selected subcarriers of the first relay. In a generalized form, the probability of finding $K_r^{(2)}$ number of idle subcarriers for the rth relay at the second hop is

$$\Pr[\alpha_r^{(2)} \odot \alpha_r^{(2)} \geq K_r^{(2)}] = \sum_{i=0}^{N_L - K_T} \binom{N_L - K_T}{K_r^{(2)} + i} \binom{K_r^{(2)} + i}{K_r^{(2)}} p_1^{K_r^{(2)} + i} p_0^{N_L - K_T - K_r^{(2)} - i} \tag{4.13}$$

$$= \sum_{i=0}^{N_L - K_T} \binom{K_r^{(2)} + i}{K_r^{(2)}} f\left(K_r^{(2)} + i; N_L, p_1^{K_r^{(2)} + i}\right), \tag{4.14}$$

where the upper limit of the sum term changes as $K_T = \sum_{m=0}^{r-1} K_r^{(2)}$ after the $(r - 1)$ number of relays select subcarriers. The final probability of finding K number of idle subcarriers at the second hop is

$$\Pr[\beta^{(2)} \odot \beta^{(2)} = K] = \prod_{r=1}^{N_R^{(2)}} \sum_{i=0}^{N_L - K_T} \binom{K_r^{(2)} + i}{K_r^{(2)}} f\left(K_r^{(2)} + i; N_L, p_1^{K_r^{(2)} + i}\right). \tag{4.15}$$

Then, the relays at the second hop forward the signal towards the destination. If the destination node is far from the source node, the signal is forwarded through other relays (i.e. third, fourth hop relays etc.). Note that, K number of particular subcarriers must be available at each hop. The probability of finding K number of available subcarriers at the third hop is same as in (4.10). Accordingly, the probability of having K number of available subcarriers across the last hop of relays is as in (4.15). At the last hop of relays, the signal is forwarded to the destination node. The probability of the particular subcarriers to be available at

the destination is

$$\Pr[\boldsymbol{\beta}^{(3)} \odot \boldsymbol{\alpha}_d = K] = p_1^K, \tag{4.16}$$

where $\boldsymbol{\beta}^{(3)}$ is the transmit vector for the group of relays at the last hop (third hop in this case) and $\boldsymbol{\alpha}_d$ is the vector of spectrum sensing results at the destinaion node.

The end-to-end probability of having a successful transmission between the source and destination nodes is obtained by multiplying (4.7), (4.10), (4.15) and (4.16). However, when calculating the outage probability, the K number of subcarriers are assumed to be available and the signal is ready be transmitted at the source. In this case, outage happens if the connection cannot be established across the relays. Thus, the outage is all other possible events of the probability calculated by the multiplication of (4.10) and (4.15).

4.4.2 Ideal-Link Mode

In the second scheme, each transmitting node belonging to a group of relays (i.e. the relays at the second hop) can access any desired subcarrier of the relays at the next hop (i.e. the relays at the third hop) as shown in Fig. 4.2(b). For example, a relay at the second hop is accessing to a subcarrier of a relay at the third hop. In the meantime, another relay at the second hop can also access the same subcarrier of another relay at the third hop without causing any interference. Namely, this scheme is called *ideal-link mode*. To achieve this, the secondary nodes are equipped with directional antennas and assumed to have perfect beamforming capabilities. This assumption might not be applicable for the MSs (the source or destination node) due to the limitations in their hardware. However, relay nodes have more flexibility to implement beamforming techniques. Therefore, we assumed that the source node broadcasts the signal as explained in *broadcast mode*.

The probability of having at least K number of available subcarriers at the source node is same as in (4.7). The probability of the selected subcarriers to be available at the $N_R^{(2)}$ number of second hop relays is also same as in (4.10). Then, the relays at the second hop perform spectrum sensing to forward the signal to the relay at the third hop. The first relay at the second hop has to find at least $K_1^{(2)}$ number of available subcarriers and the second relay has to find at least $K_2^{(2)}$ number of available subcarriers and so on. The

91

probability of selecting $K_1^{(2)}$ number of available subcarriers at the first relay within the second hop relays is

$$\Pr[\beta_1^{(2)} \odot \beta_1^{(2)} = K_1^{(2)}] = \binom{N_L}{K_1^{(2)}} p_1^{K_1^{(2)}}, \tag{4.17}$$

where considering all relays at the second hop, the combined probability becomes

$$\Pr\left[\sum_{r=1}^{N_R^{(2)}} \beta_r^{(2)} \odot \beta_r^{(2)} = K\right] = \prod_{r=1}^{N_R^{(2)}} \binom{N_L}{K_r^{(2)}} p_1^{K_r^{(2)}}. \tag{4.18}$$

Then, the signal is forwarded to the relays at the third hop. At the third hop, the subcarriers at particular indices have to be available across the relays. Thus, the number of idle subcarriers that is required for the same subcarrier index among $N_R^{(3)}$ number of third hop relays must be known. For instance, assume that the nth subcarrier is selected for transmission at $N_n^{(2)}$ number of relays at the second hop. Then, at least the same number of available subcarriers are required for the nth index across the relays at the third hop which is denoted as $\sum_{r=1}^{N_R^{(3)}} \alpha_{r,n}^{(3)} = N_n^{(3)} \geq N_n^{(2)}$. The probability of this event is

$$\Pr\left[N_n^{(3)} \geq N_n^{(3)}\right] = \binom{N_R^{(3)}}{N_n^{(3)}} p_1^{K_r^{(2)}}. \tag{4.19}$$

Then, the probability of having at least K number of available subcarriers is

$$\Pr\left[\sum_{n=1}^{N_L} N_n^{(3)} \geq K\right] = \prod_{n=1}^{N_L} \binom{N_R^{(3)}}{N_n^{(3)}} p_1^{K_r^{(2)}}. \tag{4.20}$$

The signal is forwarded until it reaches to the relays at the last hop similarly. Then, the relays at the last hop finds K number of available subcarriers, which must have different indices for each relay. The probability of this event is same as in (4.15). Finally those particular subcarriers have to be available at the destination node as well whose probability is same as in (4.16).

The end-to-end probability of having connection between the secondary source and the destination node can be calculated by multiplying (4.7), (4.10), (4.18), (4.20), (4.15) and (4.16). The outage probability of this scheme is all other events of the probability obtained by the multiplication of (4.10), (4.18), (4.20) and (4.15).

92

4.4.3 Single-Link Mode

In the third scheme, each relay has connectivity only with one relay at the third hop. For instance, the signal is transmitted from one hop to the next one through multiple paths until it reaches to the relays at the last hop. This scheme is called *single-link mode* and can be applicable in rural areas where the relays are placed lightly within a very large region. In this scheme, the relays are deployed with directional antennas and can create a fixed beam towards one relay at the next hop. Therefore, there is no need for cooperation within the relay at the same hop unlike the sequential selection approach given in *ideal-link mode*.

Finding at least K number of available bands at the source is as in (4.7). Also, the probability of finding particular K number of available bands at the second hop relays is same as in (4.10). After $N_R^{(2)}$ number of relays at the second hop receive the signal, each relay perform spectrum sensing to forward the signal to the relay at the third hop. If the number of required available subcarriers at the first relay of second hop is $K_1^{(2)}$, the probability of having at least K_r number of particular available bands is same as in (4.17). The combined probability to find available subcarriers at each relay at the second hop is also same as in (4.18). The selected subcarriers at a relay at the second hop have to be available at its paired relay at the third hop. Assume that the first relays at the second hop and third hop are paired. Thus, $K_1^{(2)}$ number of subcarriers have to be available at the first relay of the third hop whose probability is $p_1^{K_r^{(2)}}$. For successful transmission of the first relay's signal from the second hop to the third hop, $p_1^{K_r^{(2)}}$ is multiplied by (4.17). Considering all relays, the probability of successful transmission between the relays at the second hop and the relays at the third hop is

$$\Pr\left[\sum_{r=1}^{N_R^{(2)}} \beta_r^{(2)} \odot \alpha_r^{(3)} = K\right] = \prod_{r=1}^{N_R^{(2)}} \binom{N_L}{K_r^{(2)}} p_1^{2K_r^{(2)}}. \tag{4.21}$$

Then, the last hop of relays have to find the same number of available subcarriers with different indices whose probability is as in (4.14). Accordingly, the probability of these subcarriers to be available at the destination node for successful end-to-end transmission is same as in (4.16).

The end-to-end probability of having connection between secondary source towards the destination node is multiplication of (4.7), (4.10), (4.21), (4.14) and (4.16). Accordingly, the outage probability is all other events of the probability obtained by the multiplication of (4.10), (4.21) and (4.14).

4.4.4 Limited-Beamforming Mode

The last scheme is more practical compared to the other schemes and provides a general representation for all deployment schemes. In this scheme, each relay has directional antennas with limited beamforming capabilities. For example, a relay transmits towards a group of relay at the next hop. In the meantime, another relay generates a beam that can transmit for another group of relays at the next hop. These two group of relays at the next hop can also have an intersection as shown in Fig. 4.2(d). This scheme is called *limited-beamforming mode*.

The probability of having K number of available subcarriers at the source is same as in (4.7). Accordingly, the relays at the first hop must have K number of available subcarriers to receive the signal from the source node whose probability is same as in (4.10). In this scheme, the relays are assumed to generate a single beam with some directionality. The relays at the third hop within the coverage of the beam generated by the relay r at the second hop is defined by the set $\mathcal{N}_r^{(2)}$ whose cardinality is $N_r^{(2)}$. A similar set is defined for the beams of each relay at the second hop. These sets intersect based on the coverage of the beams generated by each relay. Each beam is also assumed to reuse all of the N_L number of subcarriers. Therefore, each relay at the second hop must find particular number of subcarriers to broadcast the message to their corresponding relays at the third hop. Considering sequential selection of the subcarriers for the relays at the second hop, the probability of finding $K_1^{(2)}$ number of available subcarriers is as in (4.17).[4] Then, the second relay at the second hop selects $K_2^{(2)}$ number of available subcarriers from the remaining $N_L - K_1^{(2)}$ number of subcarriers. The probability of this event is

$$\Pr[\boldsymbol{\beta}_2^{(2)} \odot \boldsymbol{\beta}_2^{(2)} = K_2^{(2)}] = \binom{N_L}{K_2^{(2)}} p_1^{K_2^{(2)}}. \tag{4.22}$$

The generalized form of the probability of finding K number of idle subcarriers across the relays at the second hop is

$$\Pr[\boldsymbol{\beta}^{(2)} \odot \boldsymbol{\beta}^{(2)} = K] = \prod_{r=1}^{N_R^{(2)}} \binom{N_L - K_{r-1}^{(2)}}{K_r^{(2)}} p_1^{K_r^{(2)}}. \tag{4.23}$$

---

[4]If the created beams do not have an intersection set, there is no need to implement cooperation within the relays at the same hop.

The first relay of the second hop transmits the signal at $K_1^{(2)}$ number of available subcarriers to the relays at the third hop which are in the set $\mathcal{N}_1^{(2)}$. The probability finding $K_1^{(2)}$ number of particular subcarriers to be idle among the relays at this set is

$$\Pr[\overline{\boldsymbol{\beta}}_1^{(2)} \circ \boldsymbol{\theta}_1^{(2)} = \overline{\boldsymbol{\beta}}_1^{(2)}] = (1 - p_0^{N_1^{(2)}})^{K_1^{(2)}}. \tag{4.24}$$

Accordingly, for a successful transmission of the signal between the second hop and the third hop is only possible by receiving K number of subcarriers at the third hop. The probability of this event is

$$\Pr\left[\sum_{r=1}^{N_R^{(2)}} \overline{\boldsymbol{\beta}}_r^{(2)} \odot \boldsymbol{\theta}_r^{(2)} = K\right] = \prod_{r=1}^{N_R^{(2)}} (1 - p_0^{N_r^{(2)}})^{K_r^{(2)}}. \tag{4.25}$$

Similarly, the probability of successful transmission is calculated until the signal arrives to the relays at the last hop. The probability of finding available subcarriers at different indices among the relays at the last hop is same as in (4.15). Finally, the probability of those idle subcarriers to be available at the destination node is as in (4.16).

The probability of having successful transmission is multiplication of (4.7), (4.10), (4.23), (4.25), (4.15) and (4.16). Accordingly, the outage probability is all other events of the probability obtained by the multiplication of (4.10), (4.23), (4.25) and (4.15).

4.5   The Statistics of the Received SNR

Analysis of the probability of finding a particular number of idle subcarriers in different deployment schemes is important to evaluate the performance of the system. However, the wireless channel also affects the end-to-end received SNR and hence, must be considered for performance analysis. Therefore, the statistics of the received SNR is analyzed in Rayleigh channels for two commonly used forwarding schemes; namely, DF and AF.

4.5.1 Decode-and-Forward Relaying

Without any loss of generality, the relays at the second hop demodulate, regenerate and forward the source signal to the next hop in the DF mode. Assume that the relays forward the signal to the destination node at the end of second hop. Then, at the destination node, the SNR of the nth subcarrier is

$$\gamma_{n,d}^{(3)} = \frac{P_r^{(2)}}{\sigma_\eta^2} |h_{n,d}^{(3)}|^2 = \beta_{n,d}^{(3)}, \tag{4.26}$$

where $P_r^{(2)}$ is the transmit power of the rth relay at the second hop, σ_η^2 is the variance of the noise at the destination node and $h_{n,d}^{(3)}$ is the channel coefficient of the link between the rth relay and the destination node over the nth band. Since $|h_{n,d}^{(3)}|$ is Rayleigh distributed, $\gamma_{n,d}^{(3)}$ becomes exponentially distributed, whose PDF and CDF become

$$f_{\gamma_{n,d}^{(3)}}(\gamma) = \frac{1}{\bar{\gamma}_{n,d}^{(3)}} e^{-\frac{\gamma}{\bar{\gamma}_{n,d}^{(3)}}}, \tag{4.27}$$

$$F_{\gamma_{n,d}^{(3)}}(\gamma) = 1 - e^{-\frac{\gamma}{\bar{\gamma}_{n,d}^{(3)}}}, \tag{4.28}$$

respectively, where $\sigma_{n,r} = \bar{\gamma}_{n,d}^{(3)}$ is the general parameter which is the average received SNR of the nth subcarrier at the destination node for DF mode.

4.5.2 Amplify-and-Forward Mode

In AF mode, each relay at the second hop amplifies the source signal based on the instantaneous channel coefficients. Then, the signal is forwarded to the destination node. Since the signal is amplified and forwarded only, the SNR of the received signal at multi-hop relaying schemes is degraded seriously. Thus, only one group of relay is considered in AF mode. The end-to-end SNR in AF mode becomes

$$\gamma_{n,r}^{(2)} = \frac{\alpha_{n,s}^{(1)} \beta_{n,r}^{(2)}}{\alpha_{n,s}^{(1)} + \beta_{n,r}^{(2)} + 1}, \tag{4.29}$$

where $\alpha_{n,s}^{(1)} = \frac{P_s}{\sigma_\eta^2}|h_{n,r}^{(1)}|^2 = \gamma_{n,r}^{(1)}$ is the first hop SNR, P_s is the transmit power of the source node, $h_{n,r}^{(1)}$ is the channel coefficient of the nth subcarrier between the source node and the rth relay and $\beta_{n,r}^{(2)}$ is as defined in (4.26).

A very tight and commonly used upper bound of (4.29) is $\gamma_{n,d}^{(3)} \leq \gamma_{ub} = \min(\alpha_{n,s}^{(1)}, \beta_{n,r}^{(2)})$ which is mathematically more tractable [116]. The term γ_{ub} is an exponentially distributed random variable with parameter $\eta_{n,r} = \frac{\mu_{n,r}\overline{\gamma}_{n,d}^{(3)}}{\mu_{n,r}+\overline{\gamma}_{n,d}^{(3)}}$, where $\mu_{n,r}$ is the average SNR of the signal received by the rth relay over the nth band and $\eta_{n,r}$ represents the average end-to-end SNR of the same link. Thus, γ_{ub} is used instead of $\gamma_{n,r}^{(2)}$ for the analysis. Therefore, the PDF and the CDF of the received signal in AF mode are similar to (4.27) and (4.28) that are given for DF mode. The final form of the PDF and CDF is obtained by defining the general parameter $\sigma_{n,r} = \eta_{n,r}$, in (4.27) and (4.28) for the AF mode.

4.5.3 The Statistics of Maximum Achievable SNR

The received SNR at the second hop offered by the rth relay over the nth subcarrier is denoted as $\gamma_{n,d}^{(3)}$. As discussed above, $\gamma_{n,d}^{(3)}$ is an exponentially distributed random variable with a general parameter $\sigma_{n,r}$ such that $\sigma_{n,r} = \overline{\gamma}_{n,d}^{(3)}$ for the DF mode and $\sigma_{n,r} = \eta_{n,r} = \frac{\mu_{n,r}\lambda_{n,r}}{\mu_{n,r}+\lambda_{n,r}}$ for the AF mode.

Assume that the set $\mathcal{N}_K^{(1)} = \{n_1, n_2, \cdots, n_K\}$ denotes the indices of the K number of subcarriers that are available at the source. Also, the set $\mathcal{I}_{n_k}^{(2)}$ is defined to denote the relays at the second hop whose n_k^{th} subcarrier is available. If the relay that provides the maximum SNR is selected for each available subcarrier, the total SNR at the destination node becomes

$$\gamma_\Sigma = \sum_{n=n_1}^{n_k} \max_{\forall r \in \mathcal{I}_n^{(2)}} \{\gamma_{n,r}^{(2)}\}. \tag{4.30}$$

The CDF of maximum SNR only for one available subcarrier in (4.30), i.e. $\max_{\forall r \in \mathcal{I}_n^{(2)}} \{\gamma_{n,d}^{(3)}\} = \gamma_n^{max}$, is the product of the individual CDFs within $\mathcal{I}_{n_k}$, which is

$$F_{\gamma_n^{max}}(\gamma) = \prod_{\forall r \in \mathcal{I}_n^{(2)}} \left(1 - e^{-\frac{\gamma}{\sigma_{n,r}}}\right), \tag{4.31}$$

97

Then, the PDF of γ_n^{max} is obtained by differentiating (4.31) with respect to γ

$$f_{\gamma_n^{max}}(\gamma) = \sum_{\forall r \in \mathcal{I}_n^{(2)}} \frac{1}{\sigma_{n,r}} e^{-\frac{\gamma}{\sigma_{n,r}}} \prod_{\substack{\forall \hat{r} \in \mathcal{I}_n^{(2)} \\ \hat{r} \neq r}} \left(1 - e^{-\frac{\gamma}{\sigma_{n,\hat{r}}}}\right). \tag{4.32}$$

Assume that the cardinality of $\mathcal{I}_{n_k}$ is M_k, which also means that the n_k^{th} free band at the source is also available at $M_k \leq N_r$ number of relays. Then, the moment generating function (MGF) of γ_n^{max} is obtained as in [106] based on (4.32) as

$$\mathcal{M}_{\gamma_n^{max}}(s) = \sum_{m=1}^{M_k} (-1)^{m+1} \sum_{c_1=1}^{M_k-m+1} \sum_{c_2=1+c_1}^{M_k-m+2} \cdots \sum_{c_m=1+c_{m-1}}^{M_k} \frac{\psi_n}{s + \psi_n}, \tag{4.33}$$

where $\psi_n = \sum_{j=1}^m \frac{1}{\sigma_{n,r}}$. Note that, every value of m generates $\binom{M_k}{m}$ terms in the summation of the form $\frac{\psi_n}{s+\psi_n}$ in (4.33). Every term also has a different ψ_n parameter. Therefore, the number of terms in (4.33) is $\sum_{m=1}^{M_k} \binom{M_k}{m} = 2^{M_k} - 1$. After indexing each term with l, (4.33) can be given in a more concise form as

$$\mathcal{M}_{\gamma_n^{max}}(s) = \sum_{l=1}^{2^{M_k}-1} \frac{\xi_{nl}}{s + \xi_{nl}}, \tag{4.34}$$

where ξ_{nl} represents ψ_n which is evaluated for a particular set of values of $\{m, c_1, c_2, \cdots, c_m\}$ corresponding to the lth term of the summation in (4.33).

The total SNR of the received signal, γ_Σ, at the destination is the sum of the maximum SNRs that are selected among the available subcarriers in $\mathcal{N}_K^{(2)}$ for each subcarrier index. Then, the MGF of the total SNR is the product of MGFs of γ_n^{max} for all $n \in \mathcal{N}_K^{(2)}$, which is

$$\begin{aligned}
\mathcal{M}_{\gamma_\Sigma}(s) &= \prod_{n \in \mathcal{N}_K^{(2)}} \sum_{l=1}^{2^{M_k}-1} \frac{\xi_{nl}}{s + \xi_{nl}}, \\
&= \sum_{l_1=1}^{2^{M_1}-1} \sum_{l_2=1}^{2^{M_2}-1} \cdots \sum_{l_K=1}^{2^{M_K}-1} \frac{\xi_{n_1 l_1} \xi_{n_2 l_2} \cdots \xi_{n_K l_K}}{(s + \xi_{n_1 l_1})(s + \xi_{n_2 l_2}) \cdots (s + \xi_{n_K l_K})}.
\end{aligned} \tag{4.35}$$

98

Then, the CDF of γ_Σ is obtained by utilizing the inverse Laplace transform method [117] as

$$F_{\gamma_\Sigma}(\gamma) = \mathcal{L}^{-1}\left[\frac{\mathcal{M}_{\gamma_\Sigma}(s)}{s}\right]_{s=\gamma}. \tag{4.36}$$

The final form of the CDF is obtained by using partial fractions and solving through [12, (17.13.1) and (13.17.7)] which is

$$F_{\gamma_\Sigma}(\gamma) = \sum_{l_1=1}^{2^{M_1}-1}\sum_{l_2=1}^{2^{M_2}-1}\cdots\sum_{l_K=1}^{2^{M_K}-1}\left[1-\sum_{i=1}^{K}\frac{e^{-\xi_{n_i l_i}\gamma}\prod_{\substack{j=1\\j\neq i}}^{K}\xi_{n_j l_j}}{\prod_{\substack{j=1\\j\neq i}}^{K}(\xi_{n_j l_j}-\xi_{n_i l_i})}\right]. \tag{4.37}$$

By classical definition, the probability of the received SNR being below an SNR threshold is defined as outage probability. If γ_{th} is the threshold for the outage SNR, the outage probability can be found by putting $\gamma = \gamma_{th}$ in (4.37). However, the probability of a successful transmission is also depends on the deployment schemes (based on beamforming) and relaying modes (DF or AF). When there is a source, one group of relay and a destination node for a particular deployment scheme and a preferred relaying mode, the outage probability of system is

$$\Pr_{out} = 1 - \Pr[\mathbf{x}_s \odot \mathbf{y} = \mathbf{y}] + F_{\gamma_\Sigma}(\gamma_{th}). \tag{4.38}$$

At high SNR region, $F_{\gamma_\Sigma}(\gamma_{th}) = 0$ and can be avioded in (4.38). However, the term $1 - \Pr[\mathbf{x}_s \odot \mathbf{y} = \mathbf{y}]$ in (4.38) cannot be avoided and defines the minimum outage probability of the system. Further, if there are more than one group of relays (i.e. $S \to R \to R \to D$), the outage probability is calculated after each hop for DF mode. Therefore, a generalized formula for the overall outage probability is

$$\Pr_{out} = \sum_{l=1}^{N_l}\left(1 - \Pr[\mathbf{x}_s \odot \mathbf{y} = \mathbf{y}] + F_{\gamma_\Sigma}(\gamma_{th})\right), \tag{4.39}$$

where N_l is the number of relay hops in the system.

4.5.4 The Statistics of the Received SNR for Random Selection of the Available Subcarriers

The statistics of the maximum achievable SNR is an important metric for performance evaluation. Timer based approach is employed in the system to utilize the idle bands which have the largest SINR. Such

99

approaches are also prevent collisions by guiding relays to transmit at different bands. If such an approach is not available in the system, the available bands can be selected randomly. The relays within the same group can also cooperate by passing the availability information of the selected bands for transmission to prevent collisions. Thus, the performance of the proposed system for the random selection of the available bands can be compared to maximum achievable SNR.

The target SNR must be achieved at the source node for the a successful transmission of the signal to the relays at the second hop. The probability of achieving the target SNR in Rayleigh fading channel for the link between the first hop and the second hop for K number of available bands is

$$\Pr{}_s[\gamma_\Sigma] = \Pr{}_s\left[\sum_{n \in \mathcal{N}_S} \gamma_{s,n}^{(1)} \geq \gamma_{\text{th}}\right]. \tag{4.40}$$

Note that, the SNR at each band is exponentially distributed random variable for DF and AF relaying modes. Assuming that the received SNR at each subcarrier selected for transmission are mutually independent with distinct values. Thus, the PDF of the sum of SNRs of the available bands given in (4.40) is

$$f_\Sigma(\gamma) = \left[\prod_{i=1}^{K_s} \sigma_{n_j,r}\right] \sum_{j=1}^{K_s} \frac{e^{-\frac{\gamma}{\sigma_{n_j,r}}}}{\prod_{k \neq j k=1}^{K_s} \left(\sigma_{n_k,r} - \sigma_{n_j,r}\right)}, \tag{4.41}$$

where n_j represent the available subcarrier in the set of available subcarriers, $\mathcal{N}_S$. Since each general parameter, $\sigma_{n_j,r}$, is mutually independent and $\sigma_{n_j,r} \neq \sigma_{n_i,r}$ for $j \neq i$, the statistical distribution of the sum of SNRs, f_Σ, is hypoexponential distribution. Although, the CDF of the hypoexponential distribution can be expressed by a special case of phase-type distribution, the actual CDF of sum of SNRs, F_Σ, is mathematically intractable. Thus, the CDF is represented as

$$F_\Sigma(\gamma_{\text{th}}) = \int_0^{\gamma_{\text{th}}} f_\Sigma(\gamma) d\gamma. \tag{4.42}$$

Then, the target SNR is achieved with the probability of $(1 - F_\Sigma(\gamma_{\text{th}}))$. The overall outage probability of system is also same as in (4.38) where $F_{\gamma_\Sigma}(\gamma_{\text{th}})$ is replaced with (4.42).

4.5.5 On the Availability of Particular Number of Subcarriers

Assume that there are K number of common available bands at the source (first hop) and the relays at the second hop. The target SNR can be achieved with a number of available bands less than K if the fading gain of the wireless channel is large. On the other hand, when the number of available bands are larger than K, the total SNR can be less than the target SNR due to the low fading gain at the available subcarriers. Especially in OFDM based systems, a high rate data steam is divided to N number of lower rate streams where N is number of subcarriers. Thus, compensating a subcarrier with the remaining subcarriers is relatively easy since the data at a subcarrier has a low rate. Accordingly, outage might not occur when the condition to find a particular number of available subcarriers is not satisfied. This approach is only possible in DF mode which can decode the signal from K number of subcarriers and then load the same information on the number of subcarriers less than K. In this case, the outage probability expressions are updated by considering the cases when the number of available subcarriers are less than K. The outage probability is performed for each relay separately at the second hop. For instance, assume that the first relay at the second hop received the signal from $K_1^{(2)}$ number of bands. When the signal is forwarded to the relays, there might be $K_1^{(2)} - 1$ available bands. Thus, while calculating the outage probability, the probability of finding $K_1^{(2)} - 1$ number of available bands for the first relay at the second hop is replaced. Also, the CDF, $F_{\gamma_\Sigma}(\gamma_{th})$, is calculated at each hop by considering the number of available bands for each relay. For the selection of the idle subcarriers with maximum SNR and for random selection, $F_{\gamma_\Sigma}(\gamma_{th})$ is replaced with (4.37) and (4.42) respectively.

4.6 Simulation Results

There are three main parameters that affect the performance of the proposed system and result in trade-offs. These parameters are i) number of required required available bands (K) for transmission, ii) number of relays, (N_r), at each hop that facilitates the transmission of large bandwidth signal and iii) probability of a band to be available at each node (p_0). For all simulation scenarios, the x-axis represents the required received average SNR, $\frac{E_s}{N_0}$. There are two group of relays in the system which are clustered for the first hop and the second hop. All relays are also assumed to be scattered between the source and destination. The aim is to achieve the average SNRs to be more than $\frac{E_s}{N_0}$. Also the SNR is kept less than $2\frac{E_s}{N_0}$ to make
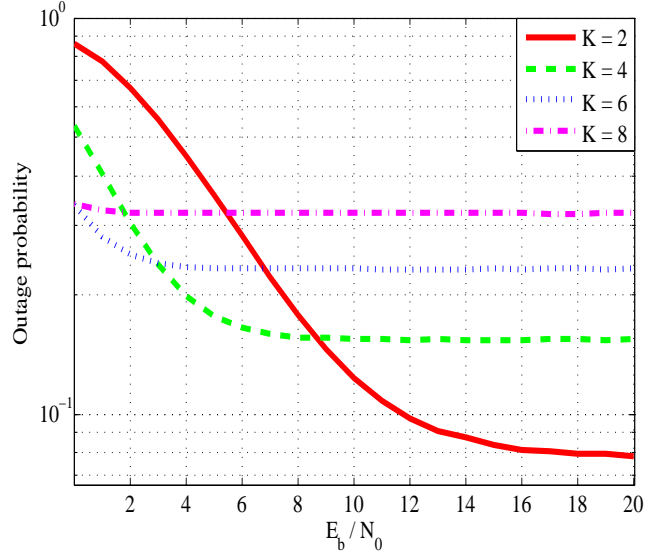
Figure 4.3: Outage probability with different numbers of free primary bands.

sure that signal is not by-passing each hop and to observe the performance of the proposed system. Average SNRs at each hop are also assumed to be different for all bands. Hence, a fixed matrix of order $N_r \times N$ is generated for each hop's average SNRs randomly. The outage threshold SNR for all simulation scenarios is defined as $\gamma_{th} \triangleq 5$.

First, the outage probability of the system is depicted in Fig. 4.3 for different number of required idle bands (varying K) while number of relays ($N_r = 8$) and and the probability of finding an idle band ($p_0 = 0.334$) are fixed. Since the total SNR at the destination is the sum of SNRs received by each band; the required target SNR is less likely to be achieved when $K = 1$ even if finding only 1 idle band in the system is more likely to be achieved. Therefore, the performance floor is defined by the Rayleigh characteristics of the wireless channel. If more idle bands are obtained in the source, the impact of Rayleigh channel becomes less effective. However, the probability of maintaining the same number of idle bands from source to destination is less likely and the outage is defined by the probability of finding the K number of idle bands and outage floor appears at low SNRs.

The performance floor is healed by cooperating more relays in the system. Fig. 4.4 shows the impact of varying N_r and by keeping $N = 16$, $K = 4$ and $p_0 = 0.334$. The probability of finding the required bands increases with more relays in the system. Since the set of number of bands are increasing, the outage
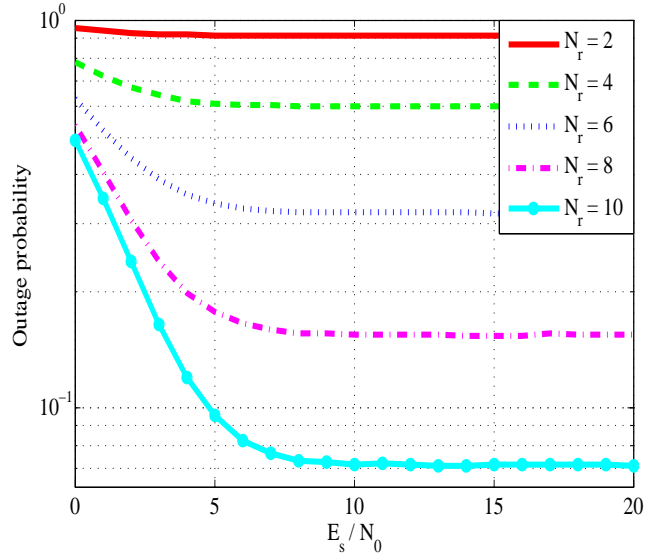
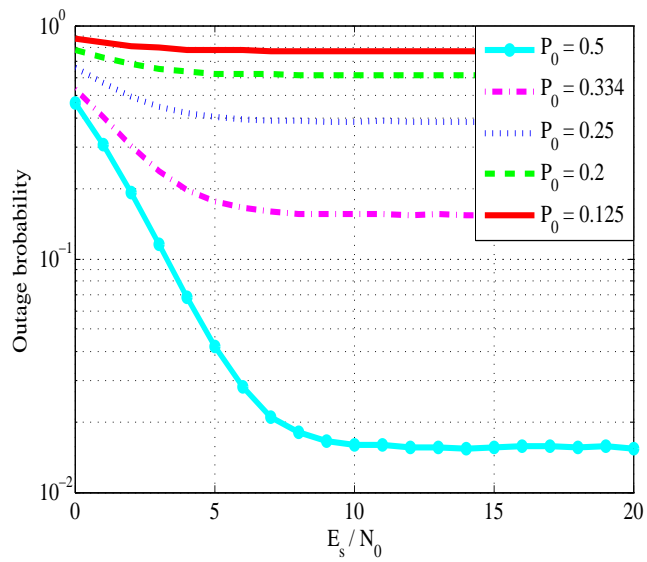Figure 4.4: Outage probability with different numbers of cooperating relays.

Figure 4.5: Outage probability with different probabilities of free primary bands.

probability is decreased eventually. However, the starting point of the floor which is a function of the number of required bands K remains the same in all cases at nearly 15 dB for $K = 4$.

The third parameter is the probability of finding idle bands p_0 which affects the outage probability of the system. As p_0 increases, the outage probability of the system decreases as shown in Fig. 4.5. The probability of finding idle bands is a function of time, location and the considered frequency range. More-
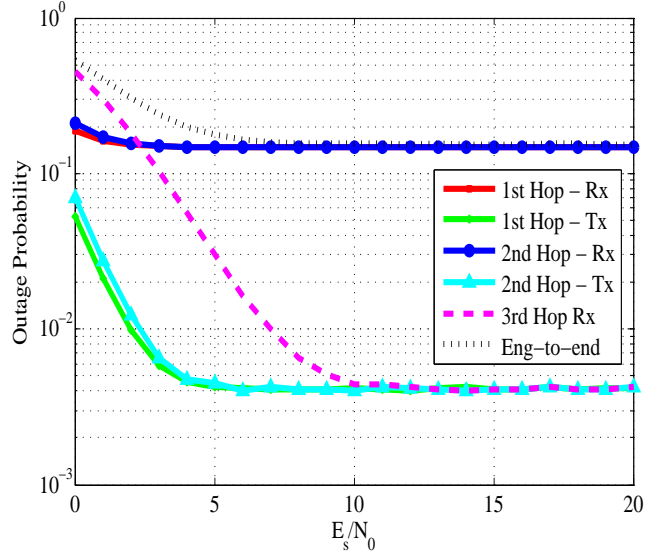
Figure 4.6: The contribution of each hop to the outage probability.

over, the density of the primary user traffic is also effective. At higher values of p_0, the relays can more likely find the required number of bands in the system.

It is also important to show that in this system, 3-hop mechanism is analyzed where $S \rightarrow R \rightarrow R \rightarrow D$ summarizes the three hop transmission. The source node broadcasts towards the first relay group, which performs spectrum sensing to forward the signal towards the second relay group. Then second relay group receives the signal collectively based on band availability. Next, second relay group performs spectrum sensing to forward the signal towards the destination node. In this mechanism, outage can occur when i) the first relay group is receiving, ii) the first relay group is finding idle bands to forward the signal towards second relay group, iii) the second relay group is receiving and iv) second relay group performing spectrum sensing and forwarding the signal towards destination node. At each of these items, outage can occur as explained in the previous sections that due to the unavailability of bands and due to the Rayleigh character-istics of the channel. The contribution of each hop to the outage is depicted in Fig. 4.6. It is obvious that the ent-to-end outage of the system is defined by the hop which has the worst outage probability. Therefore, the lower bound of the end-to-end outage is defined by first and second relay groups while receiving the signal. At low SNR region, the end-to-end outage probability is defined when the destination node is receiving the signal. The best outage is obtained when first relay group and second relay group are transmitting. This is

mainly due to the number of bands that are considered for transmission. For instance, the destination node must have K number of particular bands available among N number of bands. On the other hand, when first and second relay groups are transmitting, those nodes can select any idle bands among $N_r \times N$ bands sequentially.

CHAPTER 5

CONCLUSION

In this dissertation, various approaches are proposed for the capacity limiting problems of the Het-Nets. The proposed approaches are handling the problems from different perspectives. For instance, based-band receiver algorithms are proposed first for interference cancellation purposes. Then, interference problem is handled from another perspective to convert the interference to an advantage by the utilizing MUD approaches. On the other hand, a cooperative relaying approach is proposed for HetNets to facilitate the transmission of large bandwidth signal. All algorithms proposed in Chapter 2, Chapter 3 and Chapter 4 are analyzed by exhaustive system level simulations to observe their practical gains.

First, various filtering approaches are proposed based on blanking which is employed to suppress the DI from the desired signal. In order to take advantage of the proposed methods, there should be a low overlap between the DI signal and the received signal spectrum. Results show that substantial gains can be obtained in the BER performance at low to medium SINR levels.

Then, instead of cancelling the interference, MUD approaches are considered. Alternative to the traditional co-existence of same type of signals and c-SIC processing, the co-existence of OFDMA and SC-FDMA signals is suggested to introduce another degree-of-freedom for successive processing. The proposed co-existence approach not only brings flexibility for signal allocation, but also allows to design an advanced ML-SIC receiver which improves the capability of the HetNets in case of interference.

On the other hand, alternative to the deployment of smallcells in HetNets, relay are considered to obtain a larger spectrum where the proposed approaches so far can also be integrated to this scheme. Spectrum aggregation in a secondary cooperative network is analyzed. A mechanism is proposed to forward the source signal through multiple disjoint bands towards the destination with the help of relays in the absence of a direct link. Metrics such as outage probability of the system and maximum achievable SINR

are analyzed. Also the performance is analyzed based on different beamforming capabilities of the relay nodes.

REFERENCES

[1] V. Chandrasekhar, J. Andrews, and A. Gatherer, "Femtocell networks: a survey," *IEEE Commun. Mag.*, vol. 46, no. 9, pp. 59–67, Sep. 2008.

[2] M. Sahin, I. Guvenc, and H. Arslan, "Iterative interference cancellation for co-channel multicarrier and narrowband systems," in *Proc. IEEE Wireless Commun. Networking Conf. (WCNC)*, vol. 46, Sydney, Australia, Apr. 2010, pp. 1–6.

[3] J. M. Cioffi, *Digital Communications - Signal Processing*, Stanford, 2012. [Online]. Available: http://www.stanford.edu/group/cioffi/book/chap1.pdf

[4] A. Duel-Hallen, J. Holtzman, and Z. Zvonar, "Multiuser detection for cdma systems," *IEEE Personal Communications*, vol. 2, no. 2, pp. 46–58, 1995.

[5] M. Reed, C. Schlegel, P. Alexander, and J. Asenstorfer, "Iterative multiuser detection for cdma with fec: near-single-user performance," *IEEE Transactions on Communications*, vol. 46, no. 12, pp. 1693–1699, 1998.

[6] P. Xia, V. Chandrasekhar, and J. Andrews, "Open vs. closed access femtocells in the uplink," *IEEE Trans. Wireless Commun.*, vol. 9, no. 12, pp. 3798–3809, Dec. 2010.

[7] M. Rahman and H. Yanikomeroglu, "Enhancing cell-edge performance: a downlink dynamic interference avoidance scheme with inter-cell coordination," *IEEE Trans. Wireless Commun.*, vol. 9, no. 4, pp. 1414–1425, Apr. 2010.

[8] J. Andrews, H. Claussen, M. Dohler, S. Rangan, and M. Reed, "Femtocells: Past, present, and future," *IEEE J. Sel. Areas Commun.*, vol. 30, no. 3, pp. 497–508, Apr.

[9] S. Chen and C. Zhu, "Ici and isi analysis and mitigation for OFDM systems with insufficient cyclic prefix in time-varying channels," *IEEE Trans. Consumer Elec.*, vol. 50, no. 1, pp. 78–83, Feb. 2004.

[10] M. Russell and G. Stuber, "Interchannel interference analysis of OFDM in a mobile environment," in *Proc. IEEE Veh. Techn. Conference*, vol. 2, Chicago, IL, Jul. 1995, pp. 820–824.

[11] Y. Li and L. Cimini, "Bounds on the interchannel interference of OFDM in time-varying impairments," *IEEE Trans. Commun.*, vol. 49, no. 3, pp. 401–404, Mar. 2001.

[12] Y. Mostofi and D. Cox, "ICI mitigation for pilot-aided OFDM mobile systems," *IEEE Trans. Wireless Commun.*, vol. 4, no. 2, pp. 765–774, Mar. 2005.

[13] H. Minn, M. Zeng, and V. Bhargava, "On timing offset estimation for OFDM systems," *IEEE Commun. Letters*, vol. 4, no. 7, pp. 242–244, Jul. 2000.

[14] Y. Zhao and S. Haggman, "Intercarrier interference self-cancellation scheme for OFDM mobile communication systems," *IEEE Trans. Commun.*, vol. 49, no. 7, pp. 1185–1191, Jul. 2001.

[15] S. Moshavi, "Multi-user detection for ds-cdma communications," *IEEE Commun. Mag.*, vol. 34, no. 10, pp. 124–136, Oct. 1996.

[16] J. Andrews, "Interference cancellation for cellular systems: a contemporary overview," *IEEE Wireless Communications*, vol. 12, no. 2, pp. 19–29, Apr. 2005.

[17] M. B. Celebi, I. Guvenc, H. Arslan, and K. A. Qaraqe, "Interference suppression based on soft blanking and iterative likelihood test for lte uplink," in *IEEE International Conference on Communications (ICC)*, 2013, pp. 5062–5067.

[18] M. Celebi, I. Guvenc, H. Arslan, and K. Qaraqe, "Interference suppression for the LTE uplink," *Elsevier Pysical Commun.*, vol. 9, no. 0, pp. 1–6, Dec. 2013.

[19] D. Divsalar, M. K. Simon, and D. Raphaeli, "Improved parallel interference cancellation for cdma," *IEEE Transactions on Communications*, vol. 46, no. 2, pp. 258–268, 1998.

[20] M. Varanasi and B. Aazhang, "Multistage detection in asynchronous code-division multiple-access communications," *IEEE Transactions on Communications*, vol. 38, no. 4, pp. 509–519, 1990.

[21] M. Sawahashi, H. Andoh, K. Higuchi, and F. Adachi, "Experiments on coherent multistage interference canceller for ds-cdma mobile radio," in *The Ninth IEEE International Symposium on Personal, Indoor and Mobile Radio Communications*, vol. 2, 1998, pp. 491–496 vol.2.

[22] T. Giallorenzi and S. Wilson, "Suboptimum multiuser receivers for convolutionally coded asynchronous ds-cdma systems," *IEEE Transactions on Communications*, vol. 44, no. 9, pp. 1183–1196, 1996.

[23] A. Viterbi, "Very low rate convolution codes for maximum theoretical performance of spread-spectrum multiple-access channels," *IEEE Journal on Selected Areas in Communications*, vol. 8, no. 4, pp. 641–649, 1990.

[24] P. Patel and J. Holtzman, "Analysis of a simple successive interference cancellation scheme in a ds/cdma system," *IEEE Journal on Selected Areas in Communications*, vol. 12, no. 5, pp. 796–807, 1994.

[25] P. Frenger, P. Orten, and T. Ottosson, "Code-spread cdma with interference cancellation," *IEEE Journal on Selected Areas in Communications*, vol. 17, no. 12, pp. 2090–2095, 1999.

[26] M. Varanasi, "Group detection for synchronous gaussian code-division multiple-access channels," *IEEE Transactions on Information Theory*, vol. 41, no. 4, pp. 1083–1096, 1995.

[27] F. van der Wijk, G. Janssen, and R. Prasad, "Groupwise successive interference cancellation in a ds/cdma system," in *Sixth IEEE International Symposium on Personal, Indoor and Mobile Radio Communications*, vol. 2, 1995, pp. 742–746 vol.2.

[28] C. Berrou, A. Glavieux, and P. Thitimajshima, "Near shannon limit error-correcting coding and decoding turbo-codes," in *IEEE International Conference on Communications Technical Program*, vol. 2, Geneva, Italy, 1993, pp. 1064–1070 vol.2.

[29] P. Jung and M. Nasshan, "Results on turbo-codes for speech transmission in a joint detection cdma mobile radio system with coherent receiver antenna diversity," *IEEE Transactions on Vehicular Technology*, vol. 46, no. 4, pp. 862–870, 1997.

[30] P. Alexander, M. Reed, J. Asenstorfer, and C. Schlegel, "Iterative multiuser interference reduction: turbo cdma," *IEEE Transactions on Communications*, vol. 47, no. 7, pp. 1008–1014, 1999.

[31] X. Wang and H. Poor, "Iterative (turbo) soft interference cancellation and decoding for coded cdma," *IEEE Transactions on Communications*, vol. 47, no. 7, pp. 1046–1061, 1999.

[32] T. Cover, "Broadcast channels," *IEEE Trans. on Inf. Theory*, vol. 18, no. 1, pp. 2–14, Jan. 1972.

[33] W. van Etten, "Maximum likelihood receiver for multiple channel transmission systems," *IEEE Transactions on Communications*, vol. 24, no. 2, pp. 276–283, 1976.

[34] S. Verdu, "Minimum probability of error for asynchronous gaussian multiple-access channels," *IEEE Transactions on Information Theory*, vol. 32, no. 1, pp. 85–96, 1986.

[35] S. Moshavi, "Multi-user detection for ds-cdma communications," *IEEE Communications Magazine*, vol. 34, no. 10, pp. 124–136, 1996.

[36] G. Caire, R. Muller, and T. Tanaka, "Iterative multiuser joint decoding: optimal power allocation and low-complexity implementation," *IEEE Transactions on Information Theory*, vol. 50, no. 9, pp. 1950–1973, 2004.

[37] S. Verdu, "Adaptive multiuser detection," in *IEEE Third International Symposium on Spread Spectrum Techniques and Applications*, 1994, pp. 43–50 vol.1.

[38] R. Yates, "A framework for uplink power control in cellular radio systems," *IEEE Journal on Selected Areas in Communications*, vol. 13, no. 7, pp. 1341–1347, 1995.

[39] J. Herdtner and E. Chong, "Analysis of a class of distributed asynchronous power control algorithms for cellular wireless systems," *IEEE Journal on Selected Areas in Communications*, vol. 18, no. 3, pp. 436–446, 2000.

[40] D. Kim, "On the convergence of fixed-step power control algorithms with binary feedback for mobile communication systems," *IEEE Transactions on Communications*, vol. 49, no. 2, pp. 249–252, 2001.

[41] A. Agrawal, J. Andrews, J. Cioffi, and T. Meng, "Iterative power control for imperfect successive interference cancellation," *IEEE Transactions on Wireless Communications,*, vol. 4, no. 3, pp. 878–884, 2005.

[42] P. Hatrack and J. Holtzman, "Reduction of other-cell interference with integrated interference cancellation/power control," in *IEEE 47th Vehicular Technology Conference*, vol. 3, 1997, pp. 1842–1846.

[43] J. Andrews and T. Meng, "Optimum power control for successive interference cancellation with imperfect channel estimation," *IEEE Transactions on Wireless Communications*, vol. 2, no. 2, pp. 375–383, 2003.

[44] G. Boudreau, J. Panicker, N. Guo, R. Chang, N. Wang, and S. Vrzic, "Interference coordination and cancellation for 4g networks," *IEEE Communications Magazine*, vol. 47, no. 4, pp. 74 –81, Apr. 2009.

[45] M. Necker, "Interference coordination in cellular OFDMA networks," *IEEE Network*, vol. 22, no. 6, pp. 12–19, Dec. 2008.

[46] D. Lopez-Perez, İ. Güvenç, G. Roche, M. Kountouris, T. Quek, and J. Zhang, "Enhancing inter-cell interference coordination challanges in heterogeneous networks," *IEEE Wireless Commun. Mag.*, vol. 18, no. 3, pp. 22–30, Jun. 2011.

[47] H. YuNan, C. YongYu, C. Jie, and Y. DaCheng, "A novel inter-cell interference coordination scheme based on dynamic resource allocation in lte-tdd systems," in *IEEE Vehicular Technology Conference (VTC-Spring)*, Taipei, May. 2010, pp. 1 –5.

[48] X. Mao, A. Maaref, and K. Teo, "Adaptive soft frequency reuse for inter-cell interference coordination in sc-fdma based 3gpp lte uplinks," in *IEEE Global Telecommunications Conference (GLOBECOM)*, New Orleans, LA, Nov. 2008, pp. 1–6.

[49] Y. Yu, E. Dutkiewicz, X. Huang, M. Mueck, and G. Fang, "Performance analysis of soft frequency reuse for inter-cell interference coordination in lte networks," in *International Symposium on Communications and Information Technologies (ISCIT)*, Tokyo, Japan, Oct. 2010, pp. 504–509.

[50] X. Zhang, C. He, L. Jiang, and J. Xu, "Inter-cell interference coordination based on softer frequency reuse in ofdma cellular systems," in *Proc. IEEE International Conference on Neural Networks and Signal Processing*, Nanjing, China, Jun. 2008, pp. 270–275.

[51] W.-J. Choi, K.-W. Cheong, and J. Cioffi, "Iterative soft interference cancellation for multiple antenna systems," in *IEEE Wireless Communications and Networking Confernce (WCNC)*, vol. 1, 2000, pp. 304–309 vol.1.

[52] D. Warrier and U. Madhow, "On the capacity of cellular cdma with successive decoding and controlled power disparities," in *IEEE Vehicular Technology Conference (VTC)*, vol. 3, 1998, pp. 1873–1877 vol.3.

[53] N. Hadaschik and G. Ascheid, "Deriving a joint interference detection and channel estimation for WB-OFDM from EM-MAP theory," in *IEEE International Conference on Communications (ICC)*, May 2008, pp. 1322 –1327.

[54] M. Kopbayashi, J. Boutros, and G. Caire, "Successive interference cancellation with siso decoding and em channel estimation," *IEEE Journal on Selected Areas in Communications*, vol. 19, no. 8, pp. 1450–1460, 2001.

[55] R. R. Muller and J. B. Huber, "Capacity of cellular cdma systems applying interference cancellation and channel coding," in *In Proc. of Communication Theory Mini Conference (CTMC) at IEEE Globecom*, 1997, pp. 179–184.

[56] R. Buehrer, "Equal ber performance in linear successive interference cancellation for cdma systems," *IEEE Transactions on Communications*, vol. 49, no. 7, pp. 1250–1258, 2001.

[57] P. Alexander and A. Grant, "Iterative channel and information sequence estimation in cdma," in *Sixth IEEE International Symposium on Spread Spectrum Techniques and Applications*, vol. 2, 2000, pp. 593–597 vol.2.

[58] M. Celebi, I. Guvenc, and H. Arslan, "Interference mitigation for LTE through iterative blanking," in *IEEE Global Telecommun. Conf. (GLOBECOM)*, Houston, TX, Dec. 2011, pp. 1–6.

[59] 3rd Generation Partnership Project, "FDD home eNodeB (HeNB), radio frequency (RF) requirement analysis (Release 9)," in *3GPP TR 36.921*, Mar. 2010, pp. 12–28.

[60] M. Husso, Z. Zheng, J. Hamalainen, and E. Mutafungwa, "Dominant interferer mitigation in closed femtocell deployment," in *Proc. IEEE Int. Symp. Personal, Indoor, Mobile Radio Conf. (PIMRC)*, Istanbul, Turkey, Sept. 2010, pp. 169–174.

[61] K. Yamamoto, H. Murata, and S. Yoshida, "Management of dominant interference in cognitive radio networks," in *Proc. IEEE Int. Symp. Personal, Indoor, Mobile Radio Conf. (PIMRC)*, Istanbul, Turkey, Sep. 2010, pp. 451–455.

[62] J. V. Andrews, "Interference cancellation for cellular systems: A contemporary overview," *IEEE Wireless Commun. Mag.*, vol. 12, no. 2, pp. 19–29, Apr. 2005.

[63] H. Arslan and K. Molnar, "Cochannel interference suppression with successive cancellation in narrow-band systems," *IEEE Commun. Lett.*, vol. 5, no. 2, pp. 37–39, 2001.

[64] H. Schoeneich and P. Hoeher, "Iterative semi-blind single-antenna cochannel interference cancellation and tight lower bound for joint maximum-likelihood sequence estimation," *Elsevier Signal Process.*, vol. 84, no. 11, pp. 1991–2004, 2004.

[65] B. Kaufman, E. Erkip, J. Lilleberg, and B. Aazhang, "Femtocells in cellular radio networks with successive interference cancellation," in *Proc. IEEE Int. Conf. Commun. (ICC)*, Kyoto, Japan, Jun. 2011, pp. 1–5.

[66] J. Stott, "Detection and removal of clipping in multi-carrier receivers," European Patent EP 1 043 874, Oct. 11, 2000.

[67] T. Zogakis, P. Chow, J. Aslanis, and J. Cioffi, "Impulse noise mitigation strategies for multicarrier modulation," in *Proc. IEEE Int. Conf. Commun. (ICC)*, Geneva, Switzerland, May 1993, pp. 784–788.

[68] H. Suraweera, C. Chai, J. Shentu, and J. Armstrong, "Analysis of impulse noise mitigation techniques for digital television systems," in *Proc. International OFDM Workshop*, Hamburg, Germany, Sept. 2003, pp. 172–176.

[69] T. Li, W. H. Mow, V. Lau, M. Siu, R. Cheng, and R. Murch, "Robust joint interference detection and decoding for OFDM-based cognitive radio systems with unknown interference," *IEEE J. Sel. Areas Commun.*, vol. 25, no. 3, pp. 566–575, Apr. 2007.

[70] M. Marey and H. Steendam, "Analysis of the narrowband interference effect on OFDM timing synchronization," *IEEE Trans. Signal Process.*, vol. 55, no. 9, p. 45584566, Sep. 2007.

[71] A. Coulson, "Narrowband interference in pilot symbol assisted OFDM systems," *IEEE Trans. Wireless Commun.*, vol. 3, no. 6, pp. 2277–2287, Nov. 2004.

[72] P. Sun and L. Zhang, "Timing synchronization for OFDM based spectrum sharing system," in *Proc. International Symposium on Wireless Communication Systems (ISWCS)*, York, U.K., Sep. 2010, pp. 951 –955.

[73] S. Zhidkov, "Performance analysis and optimization of OFDM receiver with blanking nonlinearity in impulsive noise environment," *IEEE Trans. Veh. Technol.*, vol. 55, no. 1, pp. 234–242, Jan. 2006.

[74] H. Yoo, F. Guilloud, and R. Pyndiah, "Probability distribution analysis of M-QAM-modulated OFDM symbol and reconstruction of distorted data," *EURASIP J. on Adv. in Signal Process.*, vol. 2011, no. 1, p. 135, Dec. 2011.

[75] K. Bae, J. Andrews, and E. Powers, "Quantifying an iterative clipping and filtering technique for reducing PAR in OFDM," *IEEE Trans. Wireless Commun.*, vol. 9, no. 5, pp. 1558–1563, May 2010.

[76] C. Yih, "Iterative interference cancellation for OFDM signals with blanking nonlinearity in impulsive noise channels," *IEEE Signal Process. Lett.*, vol. 19, no. 3, pp. 147–150, Mar. 2012.

[77] D. Hao and P. A. Hoeher, "Iterative estimation and cancellation of clipping noise for multi-layer IDMA systems," *Proc. IEEE Int. Conf. Service Computing*, Jan. 2008.

[78] A. Molisch, M. Toeltsch, and S. Vermani, "Iterative methods for cancellation of intercarrier interference in OFDM systems," *IEEE Trans. Veh. Technol.*, vol. 56, no. 4, pp. 2158 –2167, Jul. 2007.

[79] S. Sesia, I. Toufik, and M. Baker, *LTE The UMTS Long Term Evolution from Theory to Practice*. UK: John Wiley and Sons, 2009.

[80] J. G. Proakis, *Digital Commun.*, 4th ed.   New York: McGraw-Hill, 2001.

[81] R1-104968, "Summary of the description of candidate eICIC solutions," in *3GPP Std.*, Madrid,Spain, Aug. 2010.

[82] 3GPP, "Further advancements for E-UTRA physical layer aspects," in *3GPP TR 36.814 V9.0.0*, Mar. 2010.

[83] M. B. Celebi and H. Arslan, "Interference suppression based on soft blanking and iterative likelihood test for lte uplink," in *reviev process by IEEE Trans. on Wireless Commun.*, 2014, p. N/A.

[84] J. Andrews and T. Meng, "Optimum power control for successive interference cancellation with imperfect channel estimation," *IEEE Trans. Wireless Commun.*, vol. 2, no. 2, pp. 375–383, Mar. 2003.

[85] J. Andrews and T. H. Meng, "Performance of multicarrier CDMA with successive interference cancellation in a multipath fading channel," *IEEE Trans. Commun.*, vol. 52, no. 5, pp. 811–822, May 2004.

[86] N. Otao, Y. Kishiyama, and K. Higuchi, "Performance of non-orthogonal access with SIC in cellular downlink using proportional fair-based resource allocation," in *Proc. IEEE Int. Symp. on Wireless Commun. Systems (ISWCS)*, Paris, France, Aug. 2012, pp. 476–480.

[87] H. Holma and A. Toskala, *LTE for UMTS-OFDMA and SC-FDMA Based Radio Access*, 1st ed. West Sussex: John Wiley and Sons, 2009.

[88] M. C. V. I. F. Akyildiz, W.-Y. Lee and S. Mohanty, "Next generation/dynamic spectrum access/cognitive radio wireless networks: a survey," *Elsevier Computer Networks Journal*, vol. 50, no. 13, pp. 2127–2159, Sep. 2006.

[89] FCC, "Notice of proposed rule making and order," in *Federal Communication Commission, Document No. 03-222*, Dec. 2003.

[90] ——, "Spectrum table, online available," in *http://transition.fcc.gov/oet/spectrum/table/fcctable.pdf*.

[91] J. Mitola and J. Maguire, G.Q., "Cognitive radio: making software radios more personal," *IEEE Personal Communications*, vol. 6, no. 4, pp. 201–220, Aug. 1999.

[92] S. Haykin, "Cognitive radio: Brain-empowered wireless communications," *IEEE Journal on Selected Areas in Communications*, vol. 23, no. 2, pp. 201–220, Feb. 2005.

[93] 3rd Generation Partnership Project, "Evolved universal terrestrial radio access (e-utra); carrier aggregation; base station (bs) radio transmission and reception," in *3GPP TR 36.808*, Jun. 2012, pp. 1–31.

[94] J. B. E. B. A. T. A. Shukla, B. Willamson and D. Robinson, "A study for the provision of aggregation of frequency to provide wider bandwidth services: Final report," in *QINETIQ/06/01773*, Aug. 2006, pp. 1–188.

[95] Q. Z. D. Chen and W. Jia, "Aggregation aware spectrum assignment in cognitive ad-hoc networks," in *Proceedings of Cognitive Radio Oriented Wireless Networks and Communications, (CrownCom)*, Sigapore, Singapore 2008, pp. 1–6.

[96] J. N. Laneman and G. W. Wornell, "Distributed space-time-coded protocols for exploiting cooperative diversity in wireless networks," *IEEE Trans. on Infor. Theory*, vol. 49, no. 10, p. 24152425, Nov. 2003.

[97] S. Ikki and M. Ahmed, "Performance analysis of adaptive decode-and-forward cooperative diversity networks with best-relay selection," *IEEE Trans. on Commun.*, vol. 58, no. 1, pp. 68–72, Jan. 2010.

[98] T. M. Cover and A. A. El-Gamal, "Capacity theorems for the relay channel," *IEEE Trans. on Info. Theo.*, vol. 25, no. 5, pp. 572–584, Sep. 1979.

[99] M. O. Hasna and M.-S. Alouini, "A performance study of dual-hop transmissions with fixed gain relays," *IEEE Trans. on Wireless Commun.*, vol. 3, no. 6, pp. 1963–1968, Nov. 2004.

[100] R. A. Y. Zhao and T. J. Lim, "Symbol error rate of selection amplify-and-forward relay systems," *IEEE Commun. Letters*, vol. 10, no. 11, pp. 757–759, Nov. 2006.

[101] R. T. J. L. Yi Zhao; Adve, "Improving amplify-and-forward relay networks: Optimal power allocation versus selection," in *IEEE International Symposium on Information Theory*, Seattle, WA, Jul. 2006, pp. 1234–1238.

[102] M.-S. Hasna, M.O.; Alouini, "End-to-end performance of transmission systems with relays over rayleigh-fading channels," *IEEE Trans. On Wireless Commun*, vol. 2, no. 6, pp. 1126–1131, Nov. 2003.

[103] P. A. Anghel and M. Kaveh, "Exact symbol error probability of a cooperative network in a rayleigh fading environment," *IEEE Trans. on Wireless Commun.*, vol. 3, no. 5, pp. 1416–1421, Sep. 2004.

[104] X. C. A. Ribiero and G. B. Giannakis, "Symbol error probabilities for general cooperative links," *IEEE Trans. on Wireless Commun.*, vol. 4, no. 3, pp. 1264–1273, May 2005.

[105] W. S. A. S. Ibrahim, A. K. Sadek, K. J., and R. Liu, "Cooperative communications with relay selection: When to cooperate and whom to cooperate with ?" *IEEE Trans. Wireless. Commun.*, vol. 7, no. 7, pp. 2814–2827, Jul. 2008.

[106] S. Ikki and M. H. Ahmed, "Performance of multiple-relay cooperative diversity systems with best relay selection over rayleigh fading channels," *EURASIP Journal on Advances in Signal Processing*, vol. 2008, no. 580368, pp. 1–7, Mar. 2008.

[107] M.-S. A. M. O. H. K. Q. S. I. Hussain, M. M. Abdallah, "Performance analysis of selective cooperation in underlay cognitive networks over rayleigh channels," in *EEE Int. Workshop on Sig. Proc. Advances in Wireless Comm. (SPAWC)*, San Francisco, CA, Jun. 2011, pp. 111–115.

[108] J. Z. J. Jia and Q. Zhang, "Cooperative relay for cognitive radio networks," in *IEEE International Conference on Computer Communications (INFOCOM)*, Rio de Janeiro, Brazil, Apr. 2009, pp. 2304–2312.

[109] Q. Z. J. J. J. Zhang, "Cooperative relay to improve diversity in cognitive radio networks," *IEEE Commun. Mag.*, vol. 47, no. 49, pp. 111–117, Feb. 2009.

[110] D. N. C. T. J. N. Laneman and G. W. Wornell, "Cooperative diversity in wireless networks: Efficient protocols and outage behaviour," *IEEE Trans. on Info. Theo.*, vol. 50, no. 12, pp. 3062–3080, Dec. 2004.

[111] H. X. G. Y. L. D. W. L. Li, X. Zhou and A. Soong, "Simplified relay selection and power allocation in cooperative cognitive radio systems," *IEEE Trans. on Wireless Commun.*, vol. 10, no. 1, pp. 33–36, Jan. 2011.

[112] J. G. A. J. Lee, H. Wang and D. Hong, "Outage probability of cognitive relay networks with interference constraints," *IEEE Trans. on Wireless Commun.*, vol. 10, no. 2, pp. 390–395, Feb. 2011.

[113] L. Ruan and V. K. N. Lau, "Decentralized dynamic hop selection and power control in cognitive multi-hop relay systems," *IEEE Trans. on Wireless Commun.*, vol. 9, no. 10, pp. 3024–3030, Oct. 2010.

[114] D. B. da Costa and S. Aïssa, "Performance analysis of relay selection techniques with clustered fixed-gain relays," *IEEE Signal Process. Letters*, vol. 17, no. 2, pp. 201–204, Feb. 2010.

[115] D. P. R. A. Bletsas, A. Khisti and A. Lippman, "A simple cooperative diversity method based on netwrok path selection," *IEEE Jour. On Sel. Areas Commun.*, vol. 24, no. 3, pp. 659–672, Mar. 2006.

[116] S. Ikki and M. H. Ahmed, "Performance analysis of cooperative diversity wireless networks over Nakagami-m fading channel," *IEEE Commun. Lett.*, vol. 11, no. 4, pp. 334–336, Apr. 2007.

[117] M. Simon and M.-S. Alouini, *Digital Communication over Fading Channels*, 1st ed.   Ney York, NY, USA: John Wiley and Sons, 2000.

APPENDICES

Appendix A : Impact of Soft-Windowing on the Desired SC-FDMA Signal

Proof 1 (Proof of Theorem 1) *The frequency-domain soft filtered signal, $\widehat{S}[k]$, was given in (2.15) as a piecewise function as*

$$
\widehat{S}[k] = \begin{cases}
\frac{1}{\sqrt{N}} \sum\limits_{n=0}^{N-1} s[n]e_{n,k} & , 0 \leq k < k_1 - \frac{M}{2}L, \\[2em]
W[k]\frac{1}{\sqrt{N}} \sum\limits_{n=0}^{N-1} s[n]e_{n,k} & , k_1 + \frac{M}{2} \leq k < k_2 - \frac{M}{2}L, \\[2em]
\frac{1}{\sqrt{N}} \sum\limits_{n=0}^{N-1} s[n]e_{n,k} & , k_2 + \frac{M}{2} \leq k < NL.
\end{cases}
\tag{A.1}
$$

Soft filtered signal in time-domain can be given as

$$
\hat{s}[m] = \frac{1}{\sqrt{N}} \sum_{k=0}^{N-1} \widehat{S}[k]e_{m,k}^{-1}.
\tag{A.2}
$$

The impact of soft filtering to the time-domain signal can be represented by substituting $\widehat{S}[k]$ in (A.1) into $\hat{s}[m]$ after fixing the bounds of the sum terms as

$$
\hat{s}[m] = \begin{cases}
\frac{1}{\sqrt{N}} \sum\limits_{k=0}^{k_1-\frac{M}{2}-1} \left(\frac{1}{\sqrt{N}} \sum\limits_{n=0}^{N-1} s[n]e_{n,k} \right) e_{m,k}^{-1}, \\[2em]
\frac{1}{\sqrt{N}} \sum\limits_{k=k_1-\frac{M}{2}}^{k_1+\frac{M}{2}-1} \left(W_{\mathrm{L}}\left[k - k_1 + \frac{M}{2}\right] \frac{1}{\sqrt{N}} \sum\limits_{n=0}^{N-1} s[n]e_{n,k} \right) e_{m,k}^{-1}, \\[2em]
\frac{1}{\sqrt{N}} \sum\limits_{k=k_2-\frac{M}{2}}^{k_2+\frac{M}{2}-1} \left(W_{\mathrm{R}}\left[k - k_2 + \frac{M}{2}\right] \frac{1}{\sqrt{N}} \sum\limits_{n=0}^{N-1} s[n]e_{n,k} \right) e_{m,k}^{-1}, \\[2em]
\frac{1}{\sqrt{N}} \sum\limits_{k=k_2+\frac{M}{2}}^{N-1} \left(\frac{1}{\sqrt{N}} \sum\limits_{n=0}^{N-1} s[n]e_{n,k} \right) e_{m,k}^{-1}.
\end{cases}
\tag{A.3}
$$

Appendix A (Continued)

After collecting the common terms together, soft filtered signal can be obtained as a single function as

$$\hat{s}[m] = \frac{1}{N} \sum_{n=0}^{N-1} s[n] \left(\sum_{k=0}^{k_1-\frac{M}{2}-1} c_{m,n}{}^k + \sum_{k=k_1-\frac{M}{2}}^{k_1+\frac{M}{2}-1} W_L\left[k - k_1 + \frac{M}{2}\right] c_{m,n}{}^k \right.$$
$$\left. + \sum_{k=k_2-\frac{M}{2}}^{k_2+\frac{M}{2}-1} W_R\left[k - k_2 + \frac{M}{2}\right] c_{m,n}{}^k + \sum_{k=k_2+\frac{M}{2}}^{N-1} c_{m,n}{}^k \right). \tag{A.4}$$

First, we distribute the window functions given is (2.12) and (2.13) as

$$\hat{s}[m] = \frac{1}{N} \sum_{n=0}^{N-1} s[n] \left(\sum_{k=0}^{k_1-\frac{M}{2}-1} c_{m,n}{}^k + \sum_{k=k_2+\frac{M}{2}}^{N-1} c_{m,n}{}^k + \sum_{k=k_1-\frac{M}{2}}^{k_1+\frac{M}{2}-1} \frac{c_{m,n}{}^k}{2} + \sum_{k=k_2-\frac{M}{2}}^{k_2+\frac{M}{2}-1} \frac{c_{m,n}{}^k}{2} \right.$$
$$\left. + \sum_{k=k_1-\frac{M}{2}}^{k_1+\frac{M}{2}-1} \left[\frac{c_{m,n}{}^k}{2} \cos\left(\frac{\pi\left[k - \left(k_1 - \frac{M}{2}\right)\right]}{M} \right) \right] + \sum_{k_2-\frac{M}{2}}^{k_2+\frac{M}{2}-1} \left[\frac{c_{m,n}{}^k}{2} \cos\left(\pi + \frac{\pi\left[k - \left(k_2 - \frac{M}{2}\right)\right]}{M} \right) \right] \right). \tag{A.5}$$

For the cases where $(m = n)$ and $(m \neq)$, (A.5) is split into two followed by exploiting exponential sum formulas as in (2.10) and obtained in (A.6).

$$\hat{s}[m] = \begin{cases} \frac{1}{N} \sum_{n=0}^{N-1} s[n] \left[\sum_{k=k_1-\frac{M}{2}}^{k_1+\frac{M}{2}} \cos\left(\frac{\pi\left[k - \left(k_1 - \frac{M}{2}\right)\right]}{M} \right) \frac{c_{m,n}{}^k}{2} + \sum_{k=k_2-\frac{M}{2}}^{k_2+\frac{M}{2}} \cos\left(\pi + \frac{\pi\left[k - \left(k_2 - \frac{M}{2}\right)\right]}{M} \right) \frac{c_{m,n}{}^k}{2} \right. \\ \left. + \frac{c_{m,n}{}^{k_1-\frac{M}{2}} - c_{m,n}{}^{k_2+\frac{M}{2}}}{1 - c_{m,n}} + \frac{1}{2}\left(\frac{c_{m,n}{}^{k_1-\frac{M}{2}} - c_{m,n}{}^{k_1+\frac{M}{2}}}{1 - c_{m,n}} + \frac{c_{m,n}{}^{k_2-\frac{M}{2}} - c_{m,n}{}^{k_2+\frac{M}{2}}}{1 - c_{m,n}} \right) \right] & , m \neq n \\ \frac{1}{N} \sum_{n=0}^{N-1} s[n] \left[k_1 + (N - k_2) + \frac{1}{2} \sum_{k=k_1-\frac{M}{2}}^{k_1+\frac{M}{2}} \cos\left(\frac{\pi\left[k - \left(k_1 - \frac{M}{2}\right)\right]}{M} \right) \right. \\ \left. + \frac{1}{2} \sum_{k=k_2-\frac{M}{2}}^{k_2+\frac{M}{2}} \cos\left(\pi + \frac{\pi\left[k - \left(k_2 - \frac{M}{2}\right)\right]}{M} \right) \right] & , m = n. \end{cases}$$
$$\tag{A.6}$$

The last two cosine sum terms of (A.6) shown to be constants, i.e.

$$\sum_{k=k_1-\frac{M}{2}}^{k_1+\frac{M}{2}} \cos\left(\frac{\pi\left[k - \left(k_1 - \frac{M}{2}\right)\right]}{M} \right) = 1, \tag{A.7}$$

Appendix A (Continued)

$$\sum_{k=k_2-\frac{M}{2}}^{k_2+\frac{M}{2}} \cos\left(\pi + \frac{\pi\left[k - \left(k_2 - \frac{M}{2}\right)\right]}{M}\right) = -1. \tag{A.8}$$

Therefore, the desired part of $\hat{s}[m]$ (where $m = n$) becomes $\frac{N-k_2+k_1}{N} s[m]$ in (A.6). Thus, from the remaining terms in (A.6), the ISI part, $\xi[m]$, (where $(m-n)eqn$) can be simplified further. For the ease of representation, definitions are made as: $\beta \triangleq (m-n), \gamma \triangleq \left(k - k_1 + \frac{M}{2}\right), \kappa \triangleq \left(k - k_2 + \frac{M}{2}\right)$, and are substituted from the second line of (A.6). These terms are congregated under the factors of $e^{\frac{M}{2}}$ and $e^{-\frac{M}{2}}$ from the third line of (A.6) as

$$\xi[m] = \frac{1}{N} \sum_{\substack{n=0 \\ n\neq m}}^{N-1} s[n] \left[\frac{c_{m,n}^{k_1-\frac{M}{2}} - c_{m,n}^{k_2+\frac{M}{2}}}{1 - c_{m,n}} + \frac{1}{2}\left(\left[c_{m,n}^{-\frac{M}{2}} + c_{m,n}^{\frac{M}{2}}\right]\left[c_{m,n}^{k_1} + c_{m,n}^{k_2}\right]\right) \right.$$
$$\left. + \frac{1}{2}\left[\sum_{\gamma=0}^{M-1}\left(\cos\left(\frac{\pi\gamma}{M}\right)c_{\gamma,\left(\frac{M}{2}-k_1\right)}^{\beta}\right) + \sum_{\kappa=0}^{M-1}\left(\cos\left(\frac{\pi\kappa}{M}\right)c_{\kappa,\left(\frac{M}{2}-k_2\right)}^{\beta}\right)\right] \right]. \tag{A.9}$$

After utilizing Euler's formula and taking constant terms out of the sums, (A.9) becomes

$$\xi[m] = \frac{1}{N} \sum_{\substack{n=0 \\ n\neq m}}^{N-1} s[n] \left[\frac{c_{m,n}^{k_1-\frac{M}{2}} - c_{m,n}^{k_2+\frac{M}{2}} - j\sin\left(\frac{\pi(n-m)M}{N}\right)\left[c_{m,n}^{k_1} + c_{m,n}^{k_2}\right]}{1 - c_{m,n}} \right.$$
$$\left. + \frac{1}{2}\left[e_{\left(k_1-\frac{M}{2}\right),\beta}\sum_{\gamma=0}^{M-1}\left(\cos\left(\frac{\pi\gamma}{M}\right)e_{\gamma,\beta}\right) + e_{\left(k_2-\frac{M}{2}\right),\beta}\sum_{\kappa=0}^{M-1}\left(\cos\left(\frac{\pi\kappa}{M}\right)e_{\kappa,\beta}\right)\right] \right]. \tag{A.10}$$

Euler's formula can be employed in (A.10) to obtain

$$\sum_{\gamma=0}^{M-1}\left(\cos\left(\frac{\pi\gamma}{M}\right)e_{\gamma,\beta}\right) = \frac{1}{2}\left(\frac{1 + e^{j\left(\frac{2\pi\beta M}{N}\right)}}{1 - e^{j\left(\frac{\pi}{M}+\frac{2\pi\beta}{N}\right)}} + \frac{1 + e^{j\left(\frac{2\pi\beta M}{N}\right)}}{1 - e^{-j\left(\frac{\pi}{M}-\frac{2\pi\beta}{N}\right)}}\right). \tag{A.11}$$

Appendix A (Continued)

Thus, the terms γ and κ are disappeared from (A.11). *The final form of ξ[m] can be obtained by replacing* (A.11) *in* (A.10) *as*

$$
\xi[m] = \frac{1}{N} \sum_{\substack{n=0 \\ n \neq m}}^{N-1} s[n] \left[\frac{c_{m,n}^{\,k_1 - \frac{M}{2}} - c_{m,n}^{\,k_2 + \frac{M}{2}} - j \sin\left(\frac{\pi(n-m)M}{N} \right) \left[c_{m,n}^{\,k_1} + c_{m,n}^{\,k_2} \right]}{1 - c_{m,n}} \right.
$$
$$
\left. + \frac{1}{4} \left(\frac{1 + e^{j\left(\frac{2\pi\beta M}{N} \right)}}{1 - e^{j\left(\frac{\pi}{M} + \frac{2\pi\beta}{N} \right)}} + \frac{1 + e^{j\left(\frac{2\pi\beta M}{N} \right)}}{1 - e^{-j\left(\frac{\pi}{M} - \frac{2\pi\beta}{N} \right)}} \right) \left[c_{m,n}^{\,k_1 - \frac{M}{2}} + c_{m,n}^{\,k_2 - \frac{M}{2}} \right] \right]. \tag{A.12}
$$

$$
\hat{s}[m] = \frac{1}{N} \sum_{\substack{n=0 \\ n \neq m}}^{N-1} s[n] \left[\frac{1}{4} \left(\frac{1 + e^{j\left(\frac{2\pi\beta M}{N} \right)}}{1 - e^{j\left(\frac{\pi}{M} + \frac{2\pi\beta}{N} \right)}} + \frac{1 + e^{j\left(\frac{2\pi\beta M}{N} \right)}}{1 - e^{-j\left(\frac{\pi}{M} - \frac{2\pi\beta}{N} \right)}} \right) \left[c_{m,n}^{\,k_1 - \frac{M}{2}} + c_{m,n}^{\,k_2 - \frac{M}{2}} \right] \right.
$$
$$
\left. + \frac{c_{m,n}^{\,k_1 - \frac{M}{2}} - c_{m,n}^{\,k_2 + \frac{M}{2}} - j \sin\left(\frac{\pi(n-m)M}{N} \right) \left[c_{m,n}^{\,k_1} + c_{m,n}^{\,k_2} \right]}{1 - c_{m,n}} \right] + \frac{N - k_2 + k_1}{N} s[m]. \tag{A.13}
$$

Finally, after combining desired and ISI terms and replacing β, γ and κ back, blanked signal through the use of a raised cosine windowed becomes as in (A.13), *which is shown in* (2.16).

Appendix B : Copyright Notice for Chapter 2

Appendix C : Copyright Notice for Chapter 2

Copyright Clearance Center

RightsLink®

Home   Create Account   Help   Live Chat

IEEE
Requesting permission to reuse content from an IEEE publication

Title:	Interference suppression based on soft blanking and iterative likelihood test for LTE uplink
Conference Proceedings:	Communications (ICC), 2013 IEEE International Conference on
Author:	Celebi, M.B.; Guvenc, I.; Arslan, H.; Qaraqe, K.A.
Publisher:	IEEE
Date:	9-13 June 2013
Copyright © 2013, IEEE	

Welcome to RightsLink

IEEE has partnered with Copyright Clearance Center's RightsLink service to offer a variety of options for reusing IEEE content. Select the "I would like to ..." drop-down menu to view the many reuse options available to you.

I would like to... ❓   make a selection   ▼

Appendix D : Copyright Notice for Chapter 2

Copyright Clearance Center

RightsLink®

Home | Create Account | Help | Live Chat

Title: Interference suppression for the LTE uplink

Author: Mehmet Bahadır Çelebi,İsmail Güvenç,Hüseyin Arslan,Khalid A. Qaraqe

Publication: Physical Communication

Publisher: Elsevier

Date: December 2013

Copyright © 2013 Elsevier B.V. Published by Elsevier B.V. All rights reserved.

User ID

Password

☐ Enable Auto Login

LOGIN

Forgot Password/User ID?

If you're a copyright.com user, you can login to RightsLink using your copyright.com credentials. Already **a RightsLink user** or want to learn more?

Welcome to RightsLink

Elsevier has partnered with Copyright Clearance Center's RightsLink service to offer a variety of options for reusing Elsevier content. Select the "I would like to ..." drop-down menu to view the many reuse options available to you.

I would like to... ❓ | make a selection ▼ |

To request permission for a type of use not listed, please contact Elsevier Global Rights Department.

Are you the author of this Elsevier journal article?

Appendix E : Copyright Notice for Chapter 3

IEEE COPYRIGHT AND CONSENT FORM

To ensure uniformity of treatment among all contributors, other forms may not be substituted for this form, nor may any wording of the form be changed. This form is intended for original material submitted to the IEEE and must accompany any such material in order to be published by the IEEE.Please read the form carefully and keep a copy for your files.

TITLE OF PAPER/ARTICLE/REPORT, INCLUDING ALL CONTENT IN ANY FORM, FORMAT, OR MEDIA (hereinafter, "The Work"):**Theoretical Analysis of the Co-existence of LTE-A Signals and Design of an ML-SIC Receiver**

COMPLETE LIST OF AUTHORS:**Celebi, Mehmet; Arslan, Huseyin**

IEEE PUBLICATION TITLE (Journal, Magazine, Conference, Book):**IEEE Transactions on Wireless Communications**

COPYRIGHT TRANSFER

1. The undersigned hereby assigns to The Institute of Electrical and Electronics Engineers,Incorporated (the "IEEE") all rights under copyright that may exist in and to: (a) the above Work,including any revised or expanded derivative works submitted to the IEEE by the undersigned based on the Work; and (b) any associated written or multimedia components or other enhancements accompanying the Work.

CONSENT AND RELEASE

2. ln the event the undersigned makes a presentation based upon the Work at a conference hosted or sponsored in whole or in part by the IEEE, the undersigned, in consideration for his/her participation in the conference, hereby grants the IEEE the unlimited, worldwide, irrevocable permission to use, distribute, publish, license, exhibit, record, digitize, broadcast, reproduce and archive, in any format or medium, whether now known or hereafter developed: (a) his/her presentation and comments at the conference; (b) any written materials or multimedia files used in connection with his/her presentation; and (c) any recorded interviews of him/her (collectively, the "Presentation"). The permission granted includes the transcription and reproduction ofthe Presentation for inclusion in products sold or distributed by IEEE and live or recorded broadcast ofthe Presentation during or after the conference.

3. In connection with the permission granted in Section 2, the undersigned hereby grants IEEE the unlimited, worldwide, irrevocable right to use his/her name, picture, likeness, voice and biographical information as part of the advertisement, distribution and sale ofproducts incorporating the Work or Presentation, and releases IEEE from any claim based on right of privacy or publicity.

4. The undersigned hereby warrants that the Work and Presentation (collectively, the "Materials") are original and that he/she is the author of the Materials. To the extent the Materials incorporate text passages, figures, data or other material from the works of others, the undersigned has obtained any necessary permissions. Where necessary, the undersigned has obtained all third party permissions and consents to grant the license above and has provided copies of such permissions and consents to IEEE.

[X] Please check this box if you do not wish to have video/audio recordings made of your conference presentation.

See below for Retained Rights/Terms and Conditions, and Author Responsibilities.

AUTHOR RESPONSIBILITIES

The IEEE distributes its technical publications throughout the world and wants to ensure that the material submitted to its publications is properly available to the readership of those publications. Authors must ensure that their Work meets the requirements as stated in section 8.2.1 of the IEEE PSPB Operations Manual, including provisions covering originality, authorship, author responsibilities and author misconduct. More information on

ABOUT THE AUTHOR

Mehmet Bahadır Çelebi received his B.S. degree in Electrical and Communications Engineering from Istanbul Technical University, Istanbul, Turkey in 2006 and his M.S. degree in Electrical and Electronics Engineering from Middle East Technical University, Ankara, Turkey in 2009. He also worked as a research engineer at ASELSAN and The Scientific and Technological Research Council of Turkey (TÜBİTAK) both in research and development teams in 2006 till 2010. He was with Texas A&M University in 2011. Since January 2010, he has been a member of the Wireless Communication and Signal Processing Group at University of South Florida and he has been working towards his Ph.D. degree. During his Ph.D. study he has been collaborating with researchers in DOCOMO Labs USA Inc. and Texas A&M University. His primary areas of research interest are heterogeneous networks, baseband algorithm design, system-level integration, interference coordination, cancellation, power control and cognitive radios.